UNIVERSITÉ DE STRASBOURG

ECOLE DOCTORALE pcp

ÉCOLE DOCTORALE DE PHYSIQUE ET CHIMIE-PHYSIQUE

Institut Charles Sadron

THÈSE présentée par :

Laurence JENNINGS

soutenue le : **23 Novembre 2015**

pour obtenir le grade de : **Docteur de l'université de Strasbourg**

Discipline/ Spécialité : Physique et Chimie-Physique

Micelles figées de copolymères séquencés: de l'auto-assemblage hors-équilibre aux comportements in vitro et in vivo

THÈSE dirigée par :

M. SCHOSSELER François	Directeur de thèse, Université de Strasbourg
M. MENDES Eduardo	Codirecteur de thèse, TUDelft

RAPPORTEURS :

M. DURAND Alain	Rapporteur externe, Université de Lorraine
M. JANIER Marc	Rapporteur externe, Université Claude Bernard

AUTRES MEMBRES DU JURY :

M. MAALOUM Mounir	Examinateur interne, Université de Strasbourg

Kinetically Frozen Copolymer Nanocarriers: From Non-Equilibrium Self-Assembly to *in vitro* and *in vivo* Evaluation

Laurence Jennings

Institut Charles Sadron, Strasbourg

November 2015

Dissertation submitted to the University of Strasbourg

For the degree of Doctor of Philosophy

The research leading to these results has received funding from the People Programme (Marie Curie Actions) of the European Union's Seventh Framework Programme (FP7/2007-2013) under REA grant agreement no. PITN-GA-2012-317019 'TRACE 'n TREAT'.

Table of Contents

1 Introduction

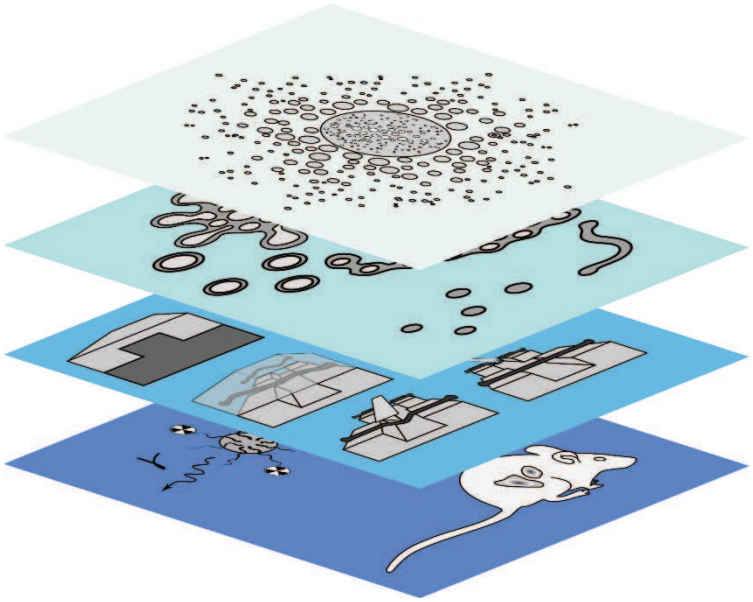

This introductory chapter serves the function of guiding the reader through this thesis. In the initial part there will be an overview of the consortium which this PhD project was part of. This will include a description of all the members of the consortium as well as an overview of the workflow between partners. Subsequently the motivation and scope for the formation of the consortium and specifically behind this thesis will be given. Due to the interdisciplinary nature of this project, each chapter covers a different topic, all of which belong to different fields of research. In order to facilitate the reader, each chapter begins with its own introductory section which is focused on presenting the basic scientific knowledge and references required for a comprehension of the experimental part.

1.1 Trace ‘n Treat Consortium

Trace ‘n Treat is a Marie Curie Initial Training Network, funded by the European Commission within the 7th Framework Programme that has started on October 1, 2012. The aim of the consortium is the development of molecular and supramolecular technology for nuclear imaging and radionuclide therapy that will contribute to the fight against cancer.

The consortium is composed of 8 early stage researchers (ESR), PhD students, located in four different European countries: Belgium, France, Germany and The Netherlands. The academic and commercial partners of the consortium, with a brief description of their role and the number of appointed researchers are listed below:

- **Erasmus Medial Center**; Rotterdam, The Netherlands – **1 appointed ESR**
    - The Erasmus University Medical Center, Erasmus MC, is one of the largest University Medical Center in Europe. The development of Somatostatin Receptor-Targeted Radionuclide therapy of tumors is one of the major achievements in radiomedicine developed at Erasmus MC.[1] The fellow appointed at Erasmus MC, under the supervision of Prof. Marion de Jong, had the task of performing in-vivo studies using the micelles produced by the other fellows of the consortium.
- **IDB Holland** *from atom to image*; Baarle Nassau, The Netherlands
    - Private company offering a full range of radiopharmaceuticals and preparation kits for radiopharmaceuticals. IDB Holland works both as a manufacturer and distributor of radioactive sources, radiopharmaceuticals and preparation kits for labelling and detection purposes.
- **Institut Charles Sadron**, University of Strasbourg; Strasbourg, France – **2 appointed ESR**
    - The Institut Charles Sadron is a research center of the French national research organization, the Centre National de Recherche Scientifique (CNRS). It is located in Strasbourg and associated with the city’s university. The institute was created in 1954 to develop a center specialized in fundamental research in the field of polymer science. The two appointed researchers of the Institut Charles Sadron, under the supervision of Dr. Gilles Waton, Dr. François Schosseler and Dr. Eduardo Mendes, had the tasks of developing and characterizing the molecular and supramolecular nanocarriers.

- **Institute for Transuranium Elements**; Karlsruhe, Germany
    - ITU is a research nuclear research institute located in Karlsruhe, Germany. The main research focus of ITU lie in the research of actinides, to contribute to an effective safety for the nuclear fuel cycle and to study the technological and medical applications of radionuclides with a particular focus on actinides and alpha therapy.[2] They also manage the various versions and editions of the Karlsruhe Nuclide Chart.
- **Johannes Gutenbeg University** of Mainz; Mainz, Germany – **1 appointed ESR**
    - Located in Germany, the JoGu Mainz is among the ten largest universities in Germany. It was established in 1477 and re-established in 1946. The Institute for Nuclear Chemistry is equipped with a TRIGA Mark II reactor. These reactors are highly safe thanks to the use of uranium zirconium hydride (UZrH) fuel. This has a large negative fuel temperature coefficient of reactivity which means that as the temperature of the core increases the reactivity rapidly decreases. This drastically hinders the possibility of nuclear meltdown. The special feature of this reactor is that it can be safely pulsed at a power of 250 MW.[3] Thanks to these facilities, the appointed researcher at JoGu, under the supervision of Prof. Frank Roesch, had the task of developing new strategies for the radiolabeling of the micelles.
- **Medizinische Hochschule Hannover**; Hannover, Germany – **1 appointed ESR**
    - The MHH is a university medical center founded in 1965. The MHH established one of the first centers for Positron Emission Tomography (PET) in Germany in 1976. This thanks to the installation of a medical cyclotron (Scanditronix MC35) allowing on site production of short lived radioisotopes such as ^{18}F. Since then the institute became specialized in the production and application of PET isotopes.[4] The fellow appointed at the MHH, under the supervision of Prof. Tobias Ross, had the task of developing new techniques to radiolabel the micelles with PET isotopes, mainly ^{18}F.
- **MILabs**; Utrecht, The Netherlands – **1 appointed ESR**
    - MiLabs was founded in 2006 as a spin-off company from the University Medical Center. It is specialized in the development of clinical and preclinical imaging devices. Thanks to the development of their first commercially successful devices, the U-SPECT and U-SPECT/CT, they were able to provide unmatched resolutions for preclinical imaging. Their focus covers both highest resolution and highest sensitivity imaging devices.[5–7] The appointed fellow at MILabs, under the supervision of Prof. Dr. Frederik Beekman, had the task of improving the reconstruction algorithms for their preclinical SPECT systems.

- **TUDelft**; Delft, The Netherlands – **1 appointed ESR**
    - The Technical University of Delft, TUDelft, is the largest and oldest public technical university in The Netherlands. It was established in 1842 as a Royal Academy. The university hosts the nuclear research institute Reactor Institute Delft (RID). The institute features the Hoger Onderwijs Reactor (HOR) which is a 2 MW pool type research reactor which was completed in 1963. The research performed at RID covers a vast range of fields, from environmental sciences to material characterization.[8,9] The fellow appointed at RID, under the supervision of Dr. Antonia Denkova, had the task of developing new methods of production of ^{99}Mo.
- **University of Gent**; Gent, Belgium – **1 appointed ESR**
    - Established in 1817 the University of Gent, is one of the largest Flemish universities and became in 1930 the first Dutch-speaking university of Belgium. UGent played a major role in the foundation of modern organic chemistry thanks to the unraveling of the structure of benzene by Friedrich August Kekulé. The university has a strong polymer synthesis group and the appointed fellow, under the supervision of Prof. Peter Dubruel, had the task of developing chemically modified copolymers for the development of functionalized micelles.
- **Urenco Nederland**; Almelo, The Netherlands
    - Urenco is a nuclear fuel company operating several uranium enrichment plants in Germany, The Netherlands, United States and United Kingdom. It is one of the largest companies in this business having the 29% of global market share of enriched uranium. The enrichment of uranium by Urenco is performed using centrifuge enrichment technology.

The scheme in Figure 1 provides an overview of the various roles of the fellows in the collaboration.

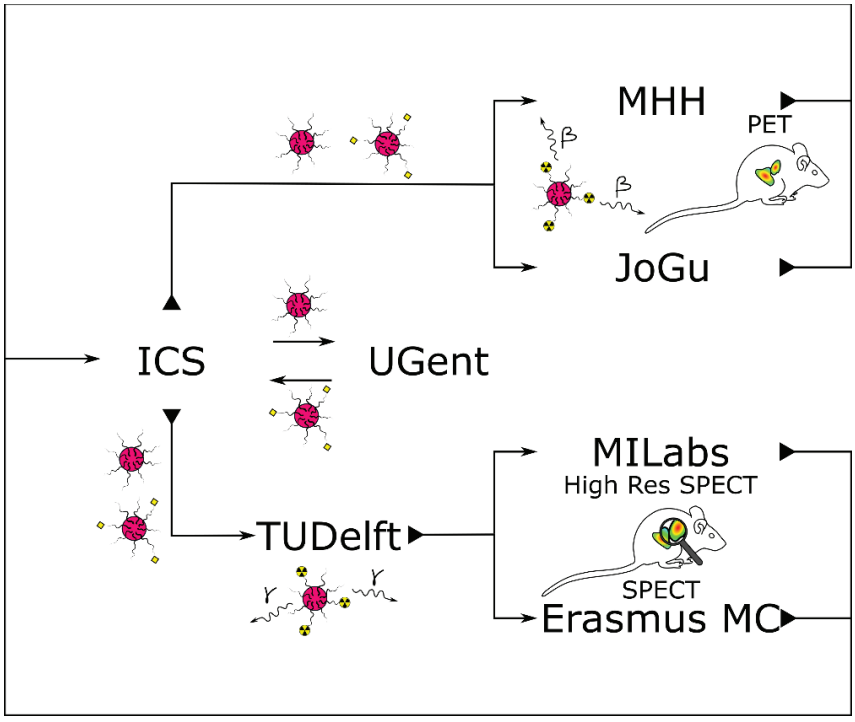

Figure 1 Schematic overview of the Trace 'n Treat collaboration

The project starts with the two institutes specialized in polymers: the ICS and UGent. The two fellows appointed at the ICS will prepare micelles and characterize their physicochemical properties. The polymer chemist in UGent then modifies the polymers to obtain micelles which can be labelled thanks to the attachment of functional groups or chelators. The micelles are then returned to the ICS to further verify if the modifications have altered the micellization behavior or the micelle properties. Subsequently the functionalized micelles are sent to the collaborators in MHH and JoGu who will develop new labelling strategies for beta emitting radio isotopes and to perform preclinical PET scans. In parallel to this, through a collaboration with the reactor institute in Delft, the fellows of the ICS will provide Erasmus MC and MILabs with gamma emitter labelled micelles for high resolution SPECT evaluation. The output of the in-vivo experiments is then returned to the ICS as a feedback loop in order to further optimize the physicochemical properties of the micelles knowing the initial in-vivo performance.

As one of the two fellows working in the Institut Charles Sadron, my thesis will document the work done to develop supramolecular nanocarriers of different morphologies and to characterize their physicochemical properties and their behavior in-vitro and in-vivo.

1.2 Motivation and Scope

The motivation behind the creation of the Trace ‘n Treat consortium is the fight against cancer. Cancer is defined as the group of diseases characterized by uncontrolled growth and spread of abnormal cells. This behavior is caused by external factors, such as unhealthy diet, infections and tobacco, but also by internal factors such as hormonal unbalances, immune conditions and inherited genetic mutations. The projected amount of cancer cases for year 2030 is of 21.7 million and 13 million cancer deaths worldwide. The major bottleneck for the development of cancer treatments is in the vast amount of different types of cancer. The most frequently occurring cancers are those located in the lungs, bronchi, trachea, prostate and breast, colon-rectum, stomach and cervix uteri. These are the types of cancer which have the highest occurrence, however the total number of cancer types is larger than 100. In order to simplify the distinction of different cancers, a classification system has been made which is based on the type of cell that the tumor originated. These include:

- Carcinoma, cancers derived from epithelial cells
- Sarcoma arising from bone, cartilage, fat or nerves
- Lymphoma and leukemia arising from blood cells
- Germ cell tumor arising mostly from the testicles or ovaries
- Blastoma, cancers derived from embryonic tissue

To this already huge number of diseases it has to be added the genetic variance between patients which alters the behavior of the cancer itself and the effectiveness of the different treatments or drugs. The main treatments for cancer include surgery, radiation therapy, chemotherapy, hormone therapy, immune therapy and targeted therapy.[10] One particularly promising approach for the treatment of solid tumors is their passive targeting via nanoparticles of well-defined size and shape. This approach is based on the Enhanced Permeability and Retention (EPR) effect.[11–15] This effect is based on the characteristic leaky vasculature of solid tumors which makes it possible for nanocarriers to extravasate from circulation and to be retained within the core of the tumor. The advantage of such a passive targeting strategy is that it could be applicable to a wide range of cancer types due to the unspecific interaction with the solid tumors.

The EPR effect is the main strategy that is going to be exploited throughout the Trace ‘n Treat project in order to develop targeted radionuclide therapy. This consists in the combination of internal radiotherapy with the use of a targeting vector (i.e. nanoparticles, liposomes, polymers, dendrimers, peptides) which delivers the radioactive material directly to the cancerous site. This approach requires knowledge of physical chemistry, chemical synthesis, radiochemistry, biology and nuclear imaging

techniques. Because of this wide range of scientific domains, a multidisciplinary collaboration with experts on each field is the most effective way to develop and put in practice new ideas.

The scope of the Trace ‘n Treat consortium can therefore be divided into two parts: the core scientific objective and the educational objective. The scientific goal of Trace ‘n Treat is the development of molecular and supramolecular nanocarriers for targeted radionuclide therapy, through this clearly defined objective lies the educational scope which is the formation of a young group of researchers with the multidisciplinary knowledge who will be able to start their scientific career in this important field.

Moving from the more general consortium to the specifics of this project, this thesis is concerned with studying the effects of morphology of nanocarriers on their performances in-vivo and in-vitro. This is a complex aspect of nanocarrier behavior. Few studies have brought non spherical micelles from the physicochemical characterization stage up until the in-vivo characterization. The few who did, however, reported positive or arguably astonishing results.[16–18] The complexity of the formation and characterization of elongated nanoparticles has been a bottleneck for the proliferation of similar studies. This leads to the motivation of this thesis which is the development of the knowledge and the tools required to bridge the gap between spherical and non-spherical block copolymer micelles for biological applications.

Due to the vast choice of nanocarriers available it was necessary to make a choice and to focus on one specific domain. We chose to work on kinetically frozen block copolymer micelles. These are micelles which present several preparation obstacles but that have multiple intrinsic advantages over the classical dynamic micelles. The most important advantages are the resistance of the micelles against dilution without crosslinking and the wide range of possible morphologies. The main technique used for the formation of kinetically frozen micelles of different morphologies is the emulsion evaporation method which is based on the confinement of block copolymer in evaporating emulsion droplets of an organic solvent in water.[19–21] This method in particular has been shown to have a large degree of freedom in the morphology of the final assemblies, although the phenomena which make this possible haven’t been clearly understood. The initial scope of this thesis was therefore to break down and to understand the emulsion evaporation method and the formation of kinetically frozen micelles, and through this to understand and control what causes the characteristic polymorphism of kinetically frozen micelles.

In parallel to this first objective, another main focus of this research was centered on the differences between spherical and elongated micelles. Because of this it was natural to be concerned with the physical differences between these nanoparticles. The main one which comes to mind of course is the

aspect ratio, which can be extended to the concept of flexibility and elastic modulus. The persistence length and elastic modulus of elongated micelles is undeniably an important parameter for any possible application of these micelles. So within the scope of bridging the characterization gap between spherical and elongated micelles we developed a versatile technique to determine the mechanical modulus of elongated micelles.

In conclusion, fulfilling the objective of the Trace 'n Treat consortium, a full comparison of the behavior of radiolabeled spherical and elongated micelles was performed in-vivo using Single Photon Emission Computed Tomography.

Throughout this thesis the importance of controlling the morphology of self-assembled nanoparticles is the recurring theme. It is also important to keep in mind that this is not only related with the applications tackled through the Trace 'n Treat consortium, but that the findings of this thesis could be beneficial for people working in very different fields than the one of targeted radionuclide therapy. Indeed, having the capability of creating self-assembled nanoparticles of finely controlled morphologies would open the doors to a very vast range of applications.

To give some examples, focusing our attention on elongated micelles, we can think of their applications as conducting nanowires, nano-filters for water purification, scaffolds for tissue engineering, additives which act as viscosity enhancers or even as reinforcement for composite materials.

The interest of different industries in high aspect ratio nanomaterials is very clear when looking at the number of publications and patents. In 2006 alone approximately 500 patents, of which half biomedical, and 2200 scientific publications were filed.[22] The largest part, more than 50%, of the US patents for nanofibers, is for medical prosthesis. This is followed by filtration devices, whose market has a projected value of US $700b by the year 2020.[23] Then come the fields of composite materials, tissue templates, liquid crystal devices and electromagnetic shielding. With respect to the biomedical field one can imagine, together with drug delivery carriers, nanoscale wound dressing.[23]

All the fields of application listed above represent possible opportunities for the development of high value nanomaterials. The ability to form in high quantities and low costs, very reproducible nanowires of specific surface functionality would then open the doors to possible industrial applications which could benefit the lives and comfort of many people.

1.3 Structure and Contents of the Chapters

Each chapter of this thesis begins with an abstract describing in a few lines the topics covered. For the experimental chapters this will briefly contain the research question, the results obtained, the methods used to obtain such results and finally some conclusive remarks or prospect for future research.

The field of nanoparticles for targeted therapy is very multidisciplinary and the topics covered in each chapter of this thesis are different from one another so it is likely that the reader is not acquainted with all the topics. Because of this, each abstract is followed by a general scientific introduction which serves the function of introducing the reader to the main topic of the chapter.

In the second chapter the spontaneous emulsification behavior of the ternary system PS-PEO/chloroform/water is studied. This phenomenon is at the foundation of the formation of kinetically frozen micelles of different morphologies through the emulsion evaporation method. The novelty in this chapter is the finding that the presence of PEO in chloroform induces the formation of water in chloroform micro and nano emulsions which are of fundamental importance for the understanding of the morphologies resulting from the emulsion evaporation method.

The third chapter describes a new method for the formation of kinetically frozen micelles of controlled morphology. This method was developed, in part, thanks to the findings described in chapter 2. In this chapter, one of the main open questions regarding the emulsion evaporation method is answered. That is the effect of the evaporation rate of the organic solvent on the morphology of the micelles. As will be described in this chapter, by increasing the evaporation rate of the organic solvent, it is possible to obtain micelle morphologies of lower curvature: from spherical to elongated and finally to vesicles.

In the fourth chapter the mechanical modulus of elongated micelles is determined. This was done by developing a universal method that could be applied to different (bio)polymeric elongated structures. The micelles were suspended on substrates with micrometer sized pillars and their modulus was determined by nano three-point bending tests using an atomic force microscope. Thanks to the sensitivity of this method it was possible to determine the subtle effect of the crystalline PEO corona on the modulus of the micelles. The results obtained offer also an approach on how to tune the diameter and stiffness of the micelles.

The fifth chapter will conclude this thesis showing a full characterization of the micelles, combined with their radio-labelling technique and in-vitro and in-vivo evaluation. The *in vivo* evaluation was done using Single Photon Emission Computed Tomography. A particular focus was given to the

different circulation time of spherical and elongated micelles and to their different biodistribution in healthy mice.

As a final remark, in order to aid the reader, the chapters of this thesis have been ordered in a logical way, however this does not respect the chronological way in which the experiments were performed. This was due to the tight schedule given by the collaborations and the unpredictable nature of scientific research. Because of this some experimental procedures performed in the later chapters might seem like a step back from the achievements obtained in the initial chapters.

1.4 References

[1] M. De Jong, R. Valkema, F. Jamar, L. K. Kvols, D. J. Kwekkeboom, W. a P. Breeman, W. H. Bakker, C. Smith, S. Pauwels, E. P. Krenning, Semin. Nucl. Med. 2002, 32, 133–140.

[2] C. Apostolidis, R. Molinet, J. McGinley, K. Abbas, J. Möllenbeck, A. Morgenstern, Appl. Radiat. Isot. 2005, 62, 383–387.

[3] D. M. Fouquet, J. Razvi, W. L. Whittemore, Nucl. News 2003, 46, 46–56.

[4] H. J. Helmeke, T. Harms, W. H. Knapp, Appl. Radiat. Isot. 2001, 54, 753–759.

[5] O. Ivashchenko, F. Van Der Have, J. L. Villena, H. C. Groen, R. M. Ramakers, H. H. Weinans, J. Freek, S. Radiation, M. Imaging, R. Magnus, Mol. Imaging 2014, 31, 1–27.

[6] O. Ivashchenko, F. van der Have, M. Goorden, R. M. Ramakers, F. J. Beekman, J. Nucl. Med. 2015, 56, 470–476.

[7] F. van der Have, B. Vastenhouw, R. M. Ramakers, W. Branderhorst, J. O. Krah, C. Ji, S. G. Staelens, F. J. Beekman, J. Nucl. Med. 2009, 50, 599–605.

[8] J. E. Sloof, B. T. Wolterbeek, J. Environ. Radioact. 1992, 16, 229–242.

[9] N. H. Van Dijk, S. G. E. Te Velthuis, M. T. Rekveldt, J. Sietsma, S. Van Der Zwaag, Phys. B Condens. Matter 1999, 267-268, 88–91.

[10] American Cancer Society, Global Cancer Facts & Figures 3rd Edition, 2015.

[11] Y. Matsumura, H. Maeda, Cancer Res. 1986, 46, 6387– 6392.

[12] J. Fang, H. Nakamura, H. Maeda, Adv. Drug Deliv. Rev. 2011, 63, 136–151.

[13] H. Maeda, J. Wu, T. Sawa, Y. Matsumura, K. Hori, J. Control. Release 2000, 65, 271–284.

[14] H. Maeda, Adv. Enzyme Regul. 2001, 41, 189–207.

[15] U. Prabhakar, H. Maeda, R. K. Jain, E. M. Sevick-Muraca, W. Zamboni, O. C. Farokhzad, S. T. Barry, A. Gabizon, P. Grodzinski, D. C. Blakey, Cancer Res. 2013, 73, 2412–2417.

[16] Y. Geng, P. Dalhaimer, S. Cai, R. Tsai, M. Tewari, T. Minko, D. E. Discher, Nat. Nanotechnol. 2007, 2, 249–255.

[17] D. a. Christian, S. Cai, O. B. Garbuzenko, T. Harada, A. L. Zajac, T. Minko, D. E. Discher, Mol. Pharm. 2009, 6, 1343–1352.

[18] P. Kolhar, A. C. Anselmo, V. Gupta, K. Pant, B. Prabhakarpandian, E. Ruoslahti, S. Mitragotri, Proc. Natl. Acad. Sci. U. S. A. 2013, 110, 10753–8.

[19] J. Zhu, R. C. Hayward, J. Am. Chem. Soc. 2008, 130, 7496–7502.

[20] J. Zhu, N. Ferrer, R. C. Hayward, Soft Matter 2009, 5, 2471.

[21] J. Zhu, R. C. Hayward, Angew. Chemie - Int. Ed. 2008, 47, 2113–2116.

[22] C. T. Laurencin, S. G. Kumbar, S. P. Nukavarapu, R. James, M. V Hogan, Recent Pat. Biomed. Eng. 2008, 1, 68–78.

[23] Z. M. Huang, Y. Z. Zhang, M. Kotaki, S. Ramakrishna, Compos. Sci. Technol. 2003, 63, 2223–2253.

2 Spontaneous Emulsification

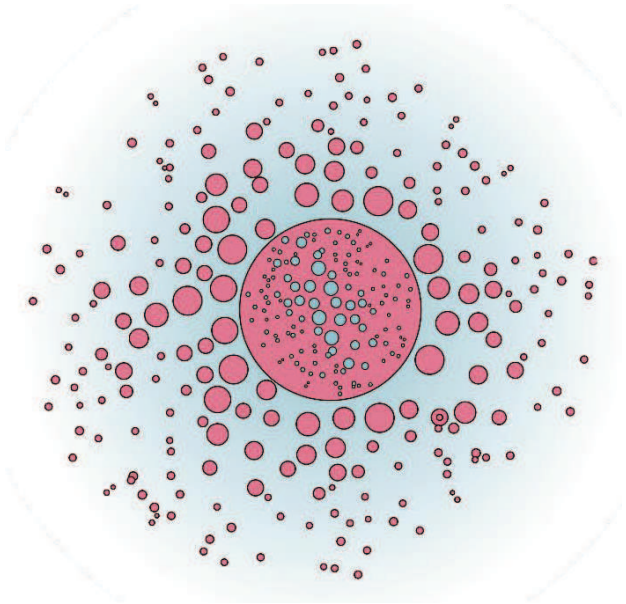

Kinetically frozen micelles can be formed by confining copolymers into emulsions of volatile organic solvents in water. The intrinsic advantages of kinetically frozen micelles over dynamic ones lie in their stability against dilution and in the large variety of morphologies attainable. Until now, the process of self-assembly through emulsion evaporation has been treated like a black box. Here we have broken down the emulsion evaporation process to understand how the morphology of self-assembled block copolymer structures is related to the spontaneous emulsification between the two emulsion solvents. We show how PEO based block copolymers spontaneously induce the formation of a water in chloroform emulsion. The results presented in this chapter make it possible to explain the formation of complex morphologies, such as strings of vesicles, and provide a first step towards a rational control of the morphology of kinetically frozen micelles.

2.1 Introduction

An emulsion is, in general, a mixture of two solvents, usually immiscible, where one of the two is dispersed as fine droplets within a continuous matrix formed by the second solvent. From this definition derive the two terms dispersed and continuous phase which are respectively used to describe the two components of an emulsion. Emulsions are generally unstable due to the high surface area which can be reduced by phase separation. Microemulsions are a sub-group of emulsions which are made thermodynamically stable thanks to the use of surfactant molecules. Emulsions and microemulsions belong to the larger domain of colloids. These are all the systems comprised of a fine dispersion within a continuous matrix, with the main constraint that the dispersed objects are moving by Brownian motion and are therefore not sedimenting. Although all emulsions are colloids, for clarity it is preferable to refer to liquid in liquid colloids as emulsions and to limit the word colloid for solid in liquid dispersions.

The applications that have been found for emulsions are endless, they span from the food[1] and pharmaceutical industry,[2] to the fabrication of asphalt[3,4] and building materials.[5] The applications of emulsions can be divided into two classes: those in which an emulsion is used to solubilize a compound into a non-solvent and those in which a compound has to be confined within a small volume. An example for the first case can be the dissolution of a hydrophobic drug within the oily dispersed phase of a water-based injectable solution.[6] An example for the second case can be the emulsion polymerization, which consists in confining monomers within the dispersed phase of an emulsion, to form spherical polymer beads such as latex.[7] The combination of these two aspects, solubilization and confinement, is what makes the crossover between emulsions and self-assembly a very powerful tool. Such principles can be used for self-assembly driven by confinement effects on the block copolymers, with the ability to load the cores of the assembled particles.

Block copolymers of sufficiently high molecular weight, undergo phase separation between the two incompatible blocks when at sufficiently high concentrations. This leads to the formation of specific bulk patterns which depend on the block length ratio and the number of the copolymer blocks. These are shown schematically in Figure 1 for diblock copolymers.

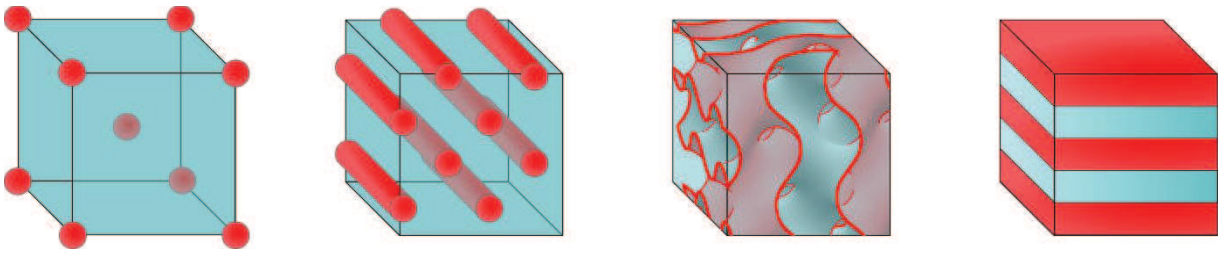

Figure 1 Possible bulk phase separation patterns of block copolymers with immiscible blocks when confined. From left to right the block length ratio is shifting towards more symmetric values.

More complex patterns become possible when increasing the number of blocks of the copolymers used, however only diblock copolymers will be treated throughout this thesis. The combination of confinement within shrinking emulsions has been used to form internally structured micro and nanoparticles.[8–12] A schematic example of the cross-section of possible morphologies obtained by this approach is shown in Figure 2.

Figure 2 Examples of nanostructured microparticles formed by bulk confinement of block copolymers in shrinking emulsions. In blue are, for example, hydrophilic domains and in red are the hydrophobic ones of an amphiphilic block copolymer.

When emulsions are used to confine copolymers which preferentially distribute along the interface between the two solvents it is important to consider the microphase separation which occurs in two dimensions. In this case the number of possible conformations is smaller than those available in bulk and are generally either circular islands or elongated cylinders as shown in Figure 3. This has been exploited to form micro and nanoparticles which have a patterned surface.[13,14]

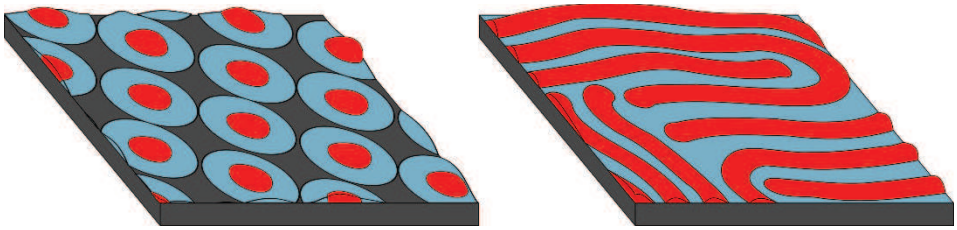

Figure 3 Possible conformations of block copolymers of immiscible blocks when confined on a surface. On the left the copolymers form circular islands while on the right they form cylindrical domains. In red are the hydrophobic domains and in blue are the hydrophilic ones.

In the examples given above, each emulsion droplet is converted into a single, spherical, particle. In 2008 Zhu et al. introduced a method which made it possible to form several nano-sized block copolymer micelles from the destabilization of each micro-emulsion droplet.[15] The advantage of this

method lies in the possibility to form core-loaded micellar nanoparticles whose size and morphology are determined by the block copolymers used. Moreover, this technique makes it possible to form kinetically frozen micelles. These are micelles formed using relatively high molecular weight copolymers and, specifically for water solutions, pronouncedly hydrophobic blocks such as polystyrene or polybutadiene.[16,17] Pioneering work on these micelles was done by Adi Eisenberg showing that they lacked the dynamic features of surfactant micelles, such as unimer exchange, and could therefore be trapped under conditions far from thermodynamic equilibrium.[18] This allowed great freedom in the possible morphologies formed.[19–22] The stability against dilution and vast range of morphologies of kinetically frozen micelles make them particularly interesting, for example, for the development of long circulating drug delivery nanoparticles.[23–25]

The emulsion evaporation method developed by Zhu et al. is based on the accumulation of amphiphilic block copolymers at the interfaces between a volatile dispersed phase and a continuous aqueous phase. The evaporation of the droplets induces a local surface concentration increase which lowers the surface tension between the droplets and the aqueous bulk phase.[26] The authors ascribe the underlying mechanisms of this method to the phenomenon of spontaneous emulsification. A theoretical model of this phenomenon has been proposed by Granek et al.[27] These authors describe a system in which a surfactant rich continuous aqueous phase induces spontaneous emulsification of the dispersed phase oil droplets. This behavior is caused by the accumulation of surfactant molecules at the water-oil interfaces. This lowers the surface tension between the two solvents. At sufficiently high surfactant concentrations, null or even transiently negative surface tensions are reached and small surfactant coated oil droplets are spontaneously emulsified from the larger oil droplets. A scheme of this theory transposed to the experimental conditions investigated by Zhu et al. (oil droplets containing amphiphilic molecules and dispersed in an aqueous continuous phase) is shown in Figure 4.

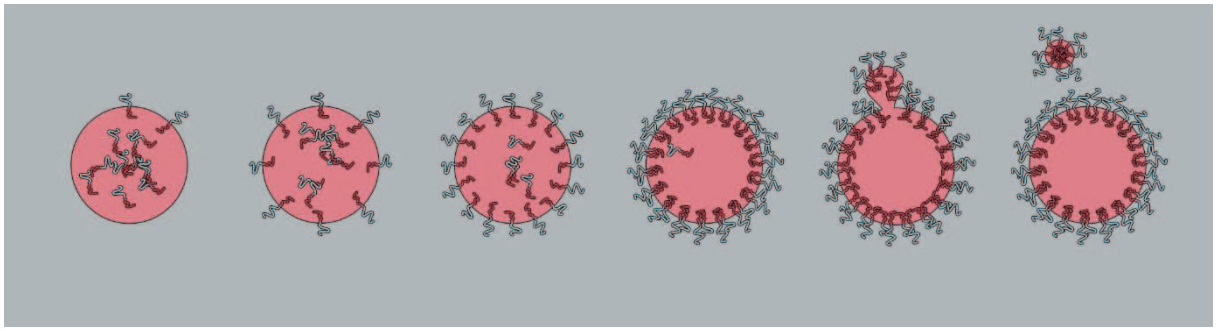

Figure 4 Schematic representation of the micelle formation through the theory of spontaneous emulsification. From left to right are the various stages of the micelle formation. The starting point is an oil droplet containing amphiphilic molecules within a water matrix. The amphiphilic molecules accumulate on the interface between the two solvents. This lowers the surface tension between the two solvents until null or transiently negative values are reached and new surface area is generated by spontaneous emulsification. The final result is the formation of copolymer micelles from the solvent-solvent interface.

In first approximation, this description fits well with the experimental observations by Zhu et al. However it must be noticed that the experimental situation corresponds to a more complex situation in which the "surfactant" (i.e. amphiphilic block copolymers) is found in the dispersed phase and undergoes confinement effects. Moreover, the dispersed phase becomes progressively more viscous with the evaporation of this solvent and this will gradually limit the mobility of these amphiphilic molecules. This feature introduces additional kinetic effects that are not considered in the theory by Granek et al. Although micelles formed through this technique have been employed for various applications,[24,28–31] there are still open questions regarding the mechanisms and the parameters which control the assembly and morphology of the copolymers.

Several works have shown how the morphology of kinetically frozen micelles does not depend in a trivial way on the copolymer block length ratio, but can be tuned by altering the process of preparation.[32] This includes the addition of salts, co-surfactants[33–35] and the use of different co-solvents.[36] Zhu et al. showed how an increasing amount of Sodium Dodecyl Sulfate as co-surfactant causes the transition from low to high curvature micelle morphology (i.e. microparticles – multi-vesicle – vesicle – vesicle string – elongated – spherical).[33] According to the theory of spontaneous emulsification, upon surface instability, the copolymer monolayer at the emulsion interface is deformed into the micelle morphologies which are more energetically favorable with respect to the block length of the copolymer. From purely topological considerations, this is coherent with the formation of smaller monolayers (elongated or spherical micelles), while the formation of single or interconnected bilayers (vesicles and strings of vesicles) is questionable. One way to explain the formation of such morphologies would be by the presence of bilayers within the chloroform droplets prior to surface instability. This would require the presence of a double emulsion (water/chloroform/water). In Figure 5 is a scheme showing the possible continuous deformations.

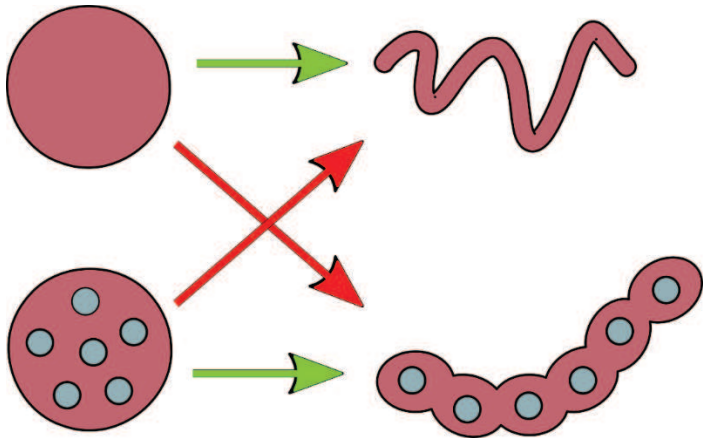

Figure 5 Scheme showing the possible morphologies obtained by continuous deformation and confinement upon solvent evaporation, starting either from a plain droplet or a double emulsion droplet. Green (resp. red) arrows denote transformations that are consistent (resp. inconsistent) with continuous transformations preserving the topology.

These considerations undermine the credibility of the hypothesis that micelle formation through the emulsion evaporation method is happening simply due to low interfacial tensions between the dispersed phase and the continuous one. From the experimental results available in the literature, the situation appears to be more complex than what is described in the theoretical model by Granek et al. As a result, the state of art in this field is still a matter of empirical know-how with very few theoretical or even phenomenological guidelines. So far, the processes leading to the formation of such micelles have been treated like a black box: the results of different formulations were studied only after the micelles had formed. Through this approach two different hypotheses have been presented: the one previously described and supported by Zhu et al. which states that the formation of the micelles is driven by low or transiently negative surface tensions between the solvents,[26] and the one supported by Su et al.[36] stating that the micelles are formed due to the spontaneous curvature that the copolymer induces at the solvent-solvent interface. Herein we approached the problem bottom up trying to simplify it and to shed light on the validity of these two hypotheses.

2.2 Results and Discussion

We observed the phenomenon of micelle formation through the emulsion evaporation system in order to verify whether this occurs by low interfacial tensions, by the spontaneous curvature the solvent-solvent interface assumes in the presence of amphiphilic copolymers, or by a totally different mechanism.

To do this we started by observing the behavior of a planar interface between water and chloroform in the presence of PS-PEO of different block length ratios. This initial experiment was done in the absence of solvent evaporation to avoid confinement effect on the copolymers. The interface behavior was observed using a horizontal microscope. The results of this initial experiment are therefore only caused by the solvent-solvent interactions mediated by the amphiphilic copolymer. We then increased the complexity of the system by studying the behavior of single emulsion droplets in presence of solvent evaporation. This added two extra features: the effects of confinement caused by the solvent evaporation, the steady increase in copolymer concentration in each chloroform droplet, and the presence of interfaces with different radii of curvature due to the unavoidably polydisperse emulsion. The emulsions were observed by placing them in an imaging chamber and using an inverted microscope. The most notable curvature difference was between the chloroform droplets which were adsorbed on the bottom of the imaging chamber and those which were floating in solution. The three situations we analyzed are shown schematically in Figure 6.

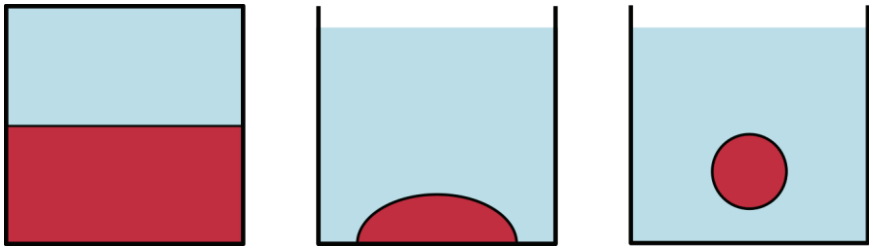

Figure 6 Overview of the three experimental conditions. On the left is a macroscopically flat interface in the absence of evaporation. In the center and on the right are respectively the adsorbed and floating microemulsion droplets, observed in the presence of solvent evaporation.

Two PS-PEO copolymers of different molecular weight were used: $PS_{9.5k}$-PEO_{18k} and PS_{16k}-$PEO_{7.5k}$. These are respectively known to form spherical and elongated micelles through the emulsion evaporation method.[15,31] From the molecular weight of the blocks, and the length of the monomers, we can estimate the ratio between the hydrophobic and the hydrophilic backbone length. This is of 0.2 and 0.8 respectively for the two copolymers. This quantity can provide a rough idea of the spontaneous curvature of a solvent-solvent interface in the presence of a very dense copolymer brush. The smaller the ratio, the more pronounced is the strain on the interface towards the formation of convex curvature in the direction of the hydrophilic chains. A scheme showing how the copolymer block length ratio affects the curvature of the interface is shown in Figure 7. The central image represents the situation in which the copolymer's blocks are equally long. Since we are only focused on water soluble micelles, and considering the block lengths of the copolymers we used, we will focus on the left hand side of this scheme.

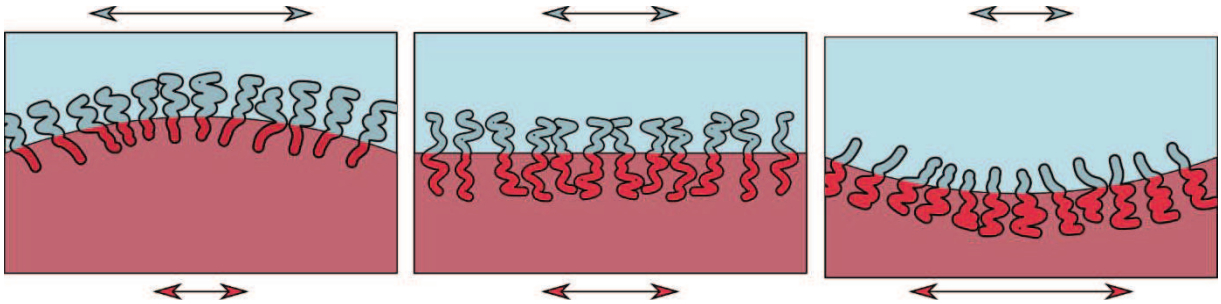

Figure 7 Effect of copolymer block length ratio on the curvature assumed by a copolymer coated solvent-solvent interface. From the left the hydrophobic to hydrophilic block length ratio is increasing resulting in an inversion of the preferred curvature. The arrows indicate the strain applied by a copolymer brush on the two sides of the solvent-solvent interface.

Using both the hypothesis of low surface tensions and that of spontaneous curvature as starting points we expected the two copolymers to respectively stabilize spherical and finger-like surface instabilities growing from the chloroform into the water phase. This would occur when both copolymers reached the same critical bulk concentration.[26]

To verify this, we placed the chloroform PS-PEO solution on the bottom of a cuvette, added water above it, sealed the cuvette and observed the behavior of the newly formed interface with a horizontal microscope. A schematic view of the setup is shown in Figure 8.

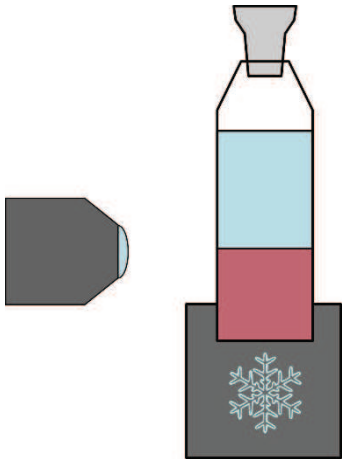

Figure 8 Schematic representation of the experiments performed to observe the evolution of a flat macroscopic interface between the two solvents. The cuvettes were placed on a thermostated stage to keep the temperature constant. The PS-PEO chloroform solution is in red and the water in blue.

In Figure 9 are shown the two cuvettes 24 hours after the formation of the interface. Below the photographs of the cuvettes, are shown the microscope images of each phase.

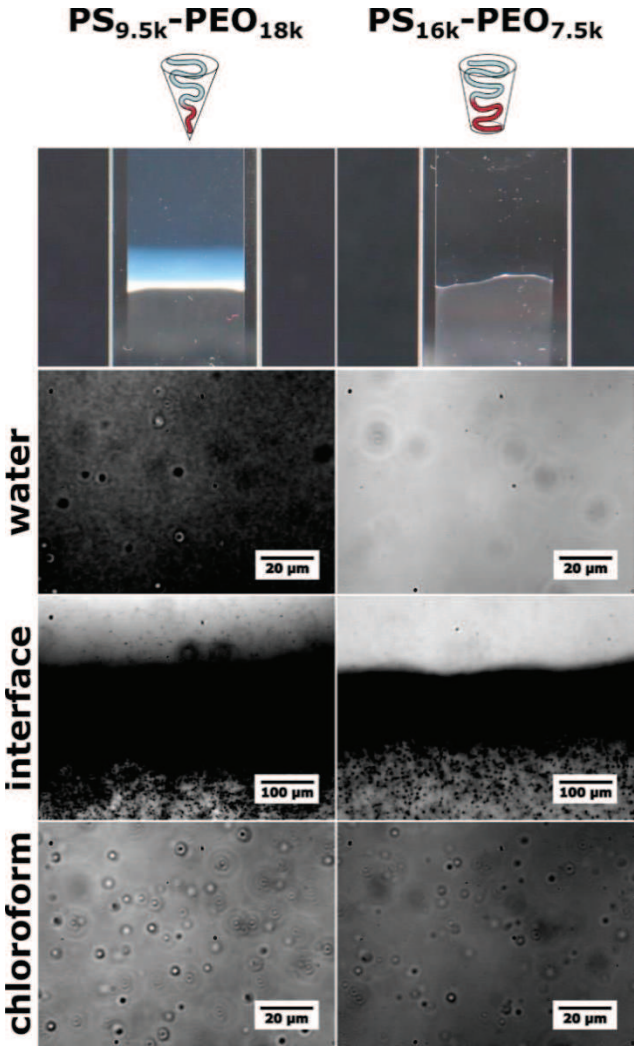

Figure 9 Overview of the spontaneous emulsification processes in a chloroform, PS-PEO, water system. All images were taken 24 hours after the formation of the solvent-solvent interface. In the top row are shown the two cuvettes. In the following rows, microscopy images detail the state of the three regions.

As soon as the interface between the two solvents was formed, it was possible to see the spontaneous formation of a water in chloroform emulsion, which is clearly visible for both copolymers in the bottom row of Figure 9. The size of the droplets was of the order of the micrometer. This result was very surprising because the formation of a water in chloroform emulsion didn't fall within either of the two hypotheses previously described. Particularly interesting was the fact that this spontaneous emulsification was going against the spontaneous interface curvature induced by the copolymers, This is especially clear for the more hydrophilic $PS_{9.5k}$-PEO_{18k}.

To explain this behavior it is necessary to understand the solubility of poly(ethylene oxide). PEO is generally considered a hydrophilic polymer due to its water solubility, however it has also been shown that water is one of the worse solvents for PEO.[37] With an increasing M_w of the PEO, the quality of water as a solvent decreases. It was found that for $M_w > 2000$ the contribution of the OH termination of the PEO is negligible for the solubility of the copolymer.[38] The peculiar solubility properties of PEO

are due to the combined presence of the CH_2 groups which contribute to the polymer's hydrophobicity while the oxygen contributes to the water solubility. It is believed that the water solubility is given by the formation of hydrogen bonds between water molecules and the oxygen atoms.[39] This combination causes high M_w PEO to be a weakly amphiphilic polymer on its own.

An organic solvent capable of donating H-bond, like chloroform, can accommodate both CH_2 and O moieties in the PEO backbone. Therefore, pure chloroform is a better solvent for PEO than pure water.[38] Nevertheless, because the strength of the H-bond donated by chloroform is weaker than the one associated with water,[40] the preferred dissolution condition for the PEO block is along any interface between chloroform and water. There both the CH_2 groups and the oxygen atoms have their preferred environment. Because of this the copolymers could assume a brush configuration, where the whole PEO block is extended into the water phase, only under surface confinement. This makes the scheme shown in Figure 7 only valid for high copolymer surface concentrations. The spontaneous curvature induced by the copolymer at the chloroform-water interfaces is therefore a very complex parameter that strongly depends on the surface concentration of amphiphilic molecules. Since we observe the formation of water droplets in chloroform as soon as the interface between the two solvents is made, we deduce that these are formed at the lowest surface coverage. In order to fully verify this hypothesis, a full study including a detailed dynamic investigation of the evolution of such interface at a molecular level is required, however, this goes beyond the goal of this thesis.

Previous works did not consider the very specific solubility behavior of PEO in water or chloroform or realize its consequences on the mechanisms of spontaneous emulsification. Taking into account these aspects, the conformation of the copolymers sitting at the interface can be likened to a large floating PEO raft with a dangling PS tail extended in the chloroform phase. In this conformation, while the PEO favors a flat interface, the PS block promotes a convex curvature towards the chloroform phase. It becomes then clear that at low surface coverage, the spontaneous curvature induced by our copolymers sitting at the interface favors water in oil emulsion. The formation of water droplets in chloroform occurs as soon as the interface between the two solvents is made. This confirms that these are formed at the lowest surface coverage and that this surprising spontaneous emulsification can be explained by the above features.

The pathway through which the droplets of water are formed in chloroform remains an open question. In fact water has a small but finite solubility in chloroform, 0.065 mass fraction at 22°C.[41] The presence of both water molecules and PS-PEO in the chloroform phase could favor the nucleation of small water domains. These would contribute to the formation of water droplets coated by copolymers which would alternatively be in excess in the bulk chloroform phase. This would decrease

the amount of dissolved water in the chloroform phase and would drive the diffusion of new water molecules from the outer water phase to restore the water equilibrium concentration in the chloroform phase. In this way, water would be progressively pumped from the water phase into the chloroform phase. One could also imagine the invagination of entire water droplets from the interface, a process which is no longer forbidden with this new picture for the conformation of the copolymers at the interface. This point was not investigated in this thesis and should be part of a specific study.

This observation is of fundamental importance, as mentioned previously, since the presence of a water in chloroform emulsion could potentially be the key for the explanation of the formation of bilayer morphologies.

Some hours after the formation of the initial interface, we observed the formation of a colloidal suspension in the water phase of the sample containing the $PS_{9.5k}$-PEO_{18k}. The presence of a sub micrometer suspension was detected thanks to the blueish tint of the solution (Figure 9, 1st row, left). The size of the particles forming this suspension was too small to be clearly distinguished by optical microscopy, however some tiny dots were visible by closer inspection of the interface (Figure 9, 2nd and 3rd row, left). The presence of this colloidal suspension in water was only visible for the $PS_{9.5k}$-PEO_{18k} sample.

We verified the nature of this colloidal suspension by scanning electron microscopy revealing the presence of spherical micelles in the water phase of the cuvette containing $PS_{9.5k}$-PEO_{18k} (Figure 10).

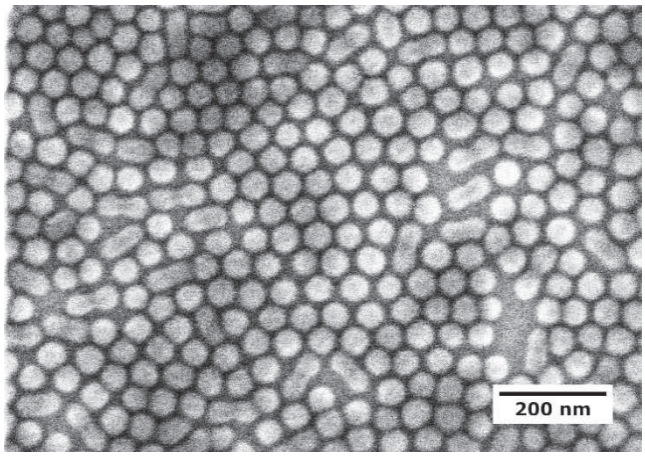

Figure 10 Scanning Electron Microscopy image of spherical micelles spontaneously formed at a chloroform water interface in presence of $PS_{9.5k}$-PEO_{18k}. A fraction of the micelles appears to have a 1:2 aspect ratio.

Scanning electron microscopy of the water phase of the PS_{16k}-$PEO_{7.5k}$ didn't show any micelles. Since both copolymers have been shown to form micelles at the same bulk copolymer concentration, we were expecting both to form micelles in the water phase.[26] However, without evaporation, and therefore confinement, only spherical micelles of the more hydrophilic copolymer were formed. This

suggested a fundamental difference between the mechanisms of formation of spherical and elongated PS-PEO micelles through the emulsion evaporation method.

Summarizing the results of these first experiments, based on the theory of spontaneous emulsification we were expecting the formation of spherical or finger-like surface instabilities, depending on the copolymer used. These instabilities would grow from the chloroform phase into the water phase resulting in a solution of micelles in water. This scenario was only true for the $PS_{9.5k}$-PEO_{18k} spherical micelles. We did not observe the formation of elongated micelles from the PS_{16k}-$PEO_{7.5k}$ samples. Moreover, we observed the formation of a water in chloroform emulsion for both samples. This is very counterintuitive if we consider the block length ratio of the copolymers, especially for the more hydrophilic $PS_{9.5k}$-PEO_{18k}. We therefore believe that the presence of water in chloroform is mediated by the presence of PEO chains and their preferred solubility at the interface between chloroform and water. The presence of the water in chloroform emulsion will play an important role in the understanding of the micelle formation in presence of solvent evaporation.

In view of these findings, we moved on to study the micelle formation from evaporating emulsion droplets. By mechanical stirring it was possible to stabilize droplets with a diameter below 20 microns. As previously mentioned, we observe the evaporating emulsions from imaging chambers and using an inverted microscope. The imaging chambers are not sealed and allow solvent evaporation. A schematic view of the setup is shown in Figure 11.

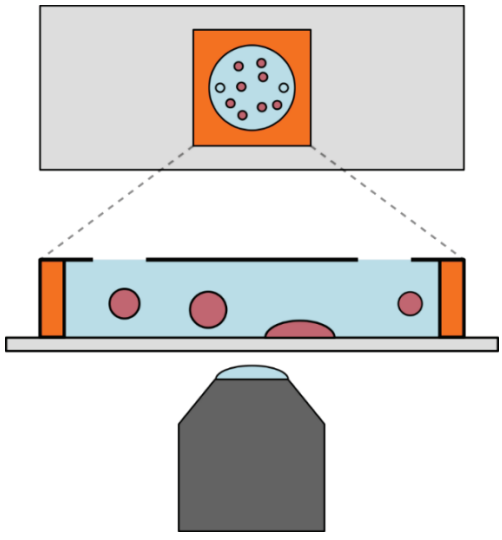

Figure 11 Schematic view of the experimental setup to observe the formation of micelles through the evaporating emulsion droplets. In the top is a top view of the glass slide and imaging chamber. Below this is close-up scheme showing, from the side, the emulsion droplets in the chamber and the position of the inverted microscope objective.

This experiment was aided by the addition of the fluorescent dye DiI to the chloroform-copolymer solution. Upon micelle formation the dye was encapsulated within the micelle core, making it possible to visualize them using a fluorescence microscope. This is particularly useful to view and follow the growth of elongated micelles.

The chloroform droplets visualized during these experiments were of two kinds: the ones which were floating in solution and the ones which were adsorbed on the glass slide. Since the average volumes of the droplets were similar, the adsorbed droplets always had a much larger radius of curvature than that of the floating ones. We will start from the description of the floating droplets and then focus on the adsorbed ones.

Figure 12 shows the evolution of floating droplets containing the two copolymers. In the case of $PS_{9.5k}$-PEO_{18k}, on the left, the fluorescent droplet decreased in size steadily until it disappeared completely. When the droplets contained the copolymer PS_{16k}-$PEO_{7.5k}$, the behavior was different. These would undergo a catastrophic destabilization: they would proceed by splitting into several smaller droplets while forming elongated filaments. The process continued until only a cloud of elongated structures was visible. These results are in agreement with previous results from the literature and with both hypotheses used to explain them.

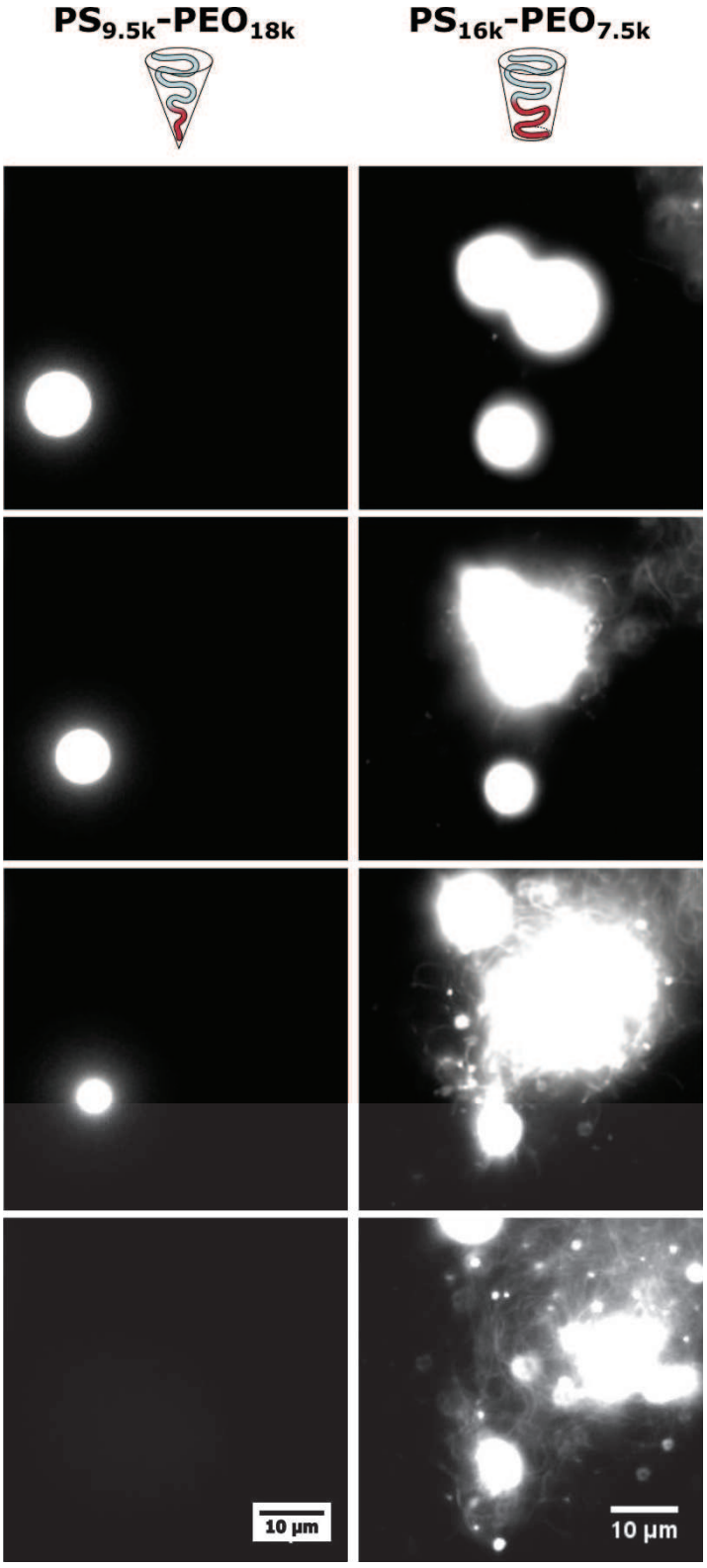

Figure 12 Fluorescence microscopy images of the time evolution of typical chloroform droplets containing DiI and PS-PEO copolymers. The droplet containing $PS_{9.5k}$-PEO_{18k} (left) reduces progressively its size corresponding with the formation of spherical micelles from the interface. In the case of PS_{16k}-$PEO_{7.5k}$ (right) the droplet's evolution is catastrophic and proceeds through the division of the initial drops into several smaller ones interconnected by filaments. Finally a series of elongated micelles are left in a water solution.

When observing the floating chloroform droplets, however, we didn't observe the spontaneous formation of a water in chloroform emulsion as we did from the previous experiments performed on the flat chloroform-water interfaces. However, differently from the planar interfaces, the small radius of curvature of the floating droplets observed would require an energetically expensive deformation to accommodate the invagination of a micrometer sized water droplet. Therefore, any spontaneous emulsification could only result in water in oil droplets with a size much below the optical microscopy resolution.

To verify the presence of submicrometer water domains in the floating oil droplets, we vacuum dried the emulsions within the imaging chambers prior micelle formation. By removing the chloroform sufficiently fast, and subsequently drying the water, the droplets would be "frozen" in an aspect which would represent their morphology in solution prior destabilization and micelle formation. The samples were then imaged using SEM. Figure 13 shows one of such particles for the PS_{16k}-$PEO_{7.5k}$.

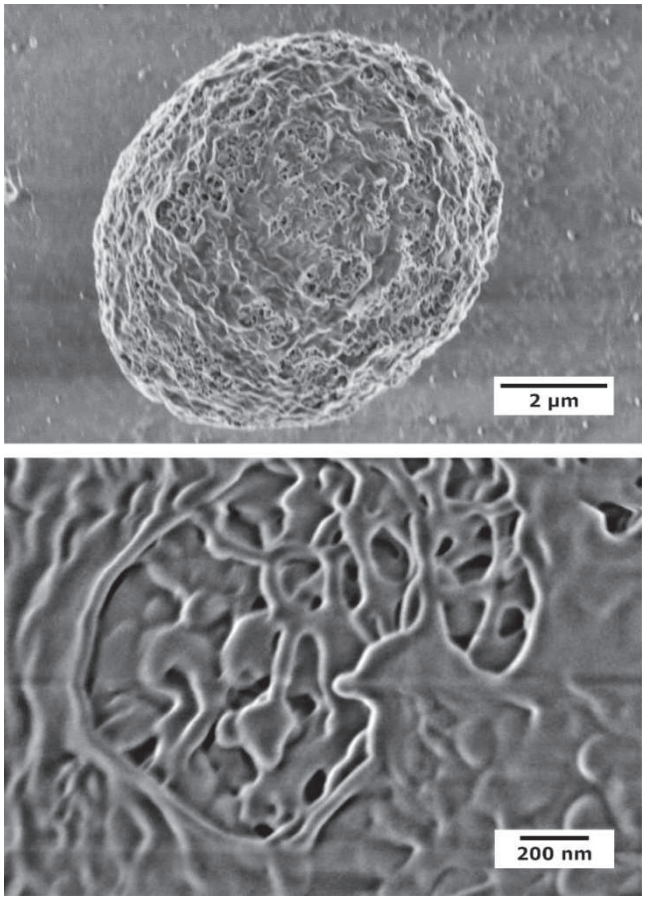

Figure 13 Scanning Electron microscopy image of a dry emulsion droplet of chloroform containing PS_{16k}-$PEO_{7.5k}$. It can be seen that within the spherical dry droplet the copolymer is already arranged into a network of filaments suggesting the presence of water domains prior solvent evaporation. The bottom image shows a detail of the particle.

The solidified droplet appeared as a very porous network of block copolymer filaments. The porous structure suggested the presence of water prior evaporating the solvent under vacuum. The size of the water domains is too small to be visualized by optical microscopy.

Similar structures were not found when performing the same sample preparation with the $PS_{9.5k}$-PEO_{18k}. The possibility to entrap the chloroform droplets into a conformation which precedes micelle formation relies on the fact that the solvent can be removed faster than the micelles are formed. This is likely not the case for $PS_{9.5k}$-PEO_{18k} since, as we have seen from the observations with the planar interface, this copolymer formed spontaneously spherical micelles even without evaporation. On the other hand, the PS_{16k}-$PEO_{7.5k}$ required the solvent evaporation and confinement, to destabilize the chloroform droplets and form micelles. Therefore, only the droplets containing PS_{16k}-$PEO_{7.5k}$ can be captured in an intermediate conformation which occurs before the micelles are formed.

From these observations we provide a hypothesis on the mechanism by which the elongated micelles of PS_{16k}-$PEO_{7.5k}$ are formed. We have shown that this block copolymer does not form micelles without solvent evaporation, and we have shown that prior micelle formation the block copolymer is already arranged in a network which resembles a “ball of yarn”.

We have also shown that as soon as the chloroform containing PS-PEO is placed in contact with water, and an interface between the two solvents is formed, there is the spontaneous formation of water droplets in the chloroform phase mediated by the PEO blocks. To explain the evolution of the water in chloroform emulsion it is useful to imagine an ideal case in which the copolymer concentration is constant and no solvent evaporation is taking place.

Under these conditions, below a certain copolymer concentration, all the PS-PEO will be located at the interface between the large chloroform drop and the outer water phase. In this case no spontaneous emulsification will occur (Figure 14). For Simplicity we imagine an ideal system with only one chloroform droplet to avoid issues of coalescence at low copolymer concentrations.

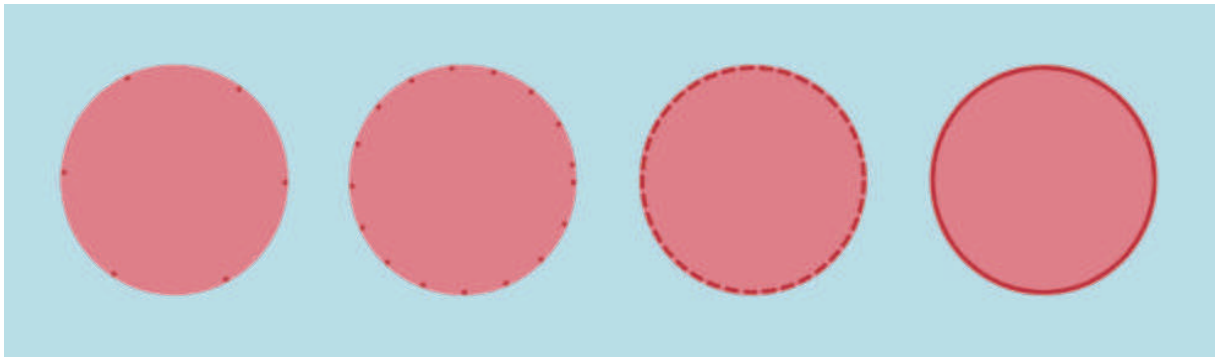

Figure 14 Schematic representation of the arrangement of PS-PEO molecules at the interface between water and chloroform. The copolymer concentration in the droplet is increasing from left to right. The dark red represents the presence of PS-PEO molecules. At the lowest PS-PEO concentrations the block copolymers will arrange at the interface between the two solvents. A critical concentration will correspond to the complete coating of the interface.

Increasing the PS-PEO concentration creates a driving force for the formation of additional water-chloroform interface. This happens through the formation of droplets of water in chloroform and proceeds until a sufficient amount of surface has been created to accommodate the excess copolymer. Further increasing the PS-PEO concentration will lead to a situation in which the water droplets will saturate the chloroform drop. Under these conditions the water droplets are confined against each other forming a liquid foam phase (Figure 15).

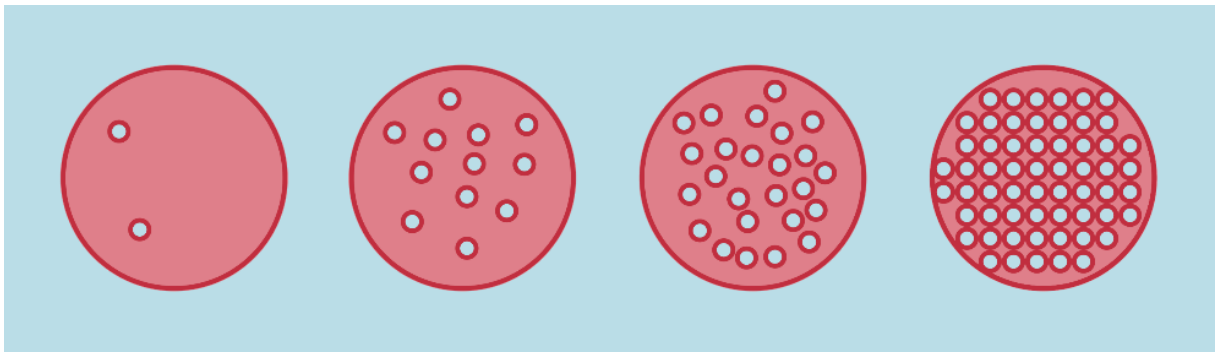

Figure 15 Schematic representation of the arrangement of PS-PEO molecules at the interface between water and chloroform. The copolymer concentration in the droplet is increasing from left to right. The dark red represents the presence of PS-PEO molecules. Higher copolymer concentrations than those shown in Figure 14 require the formation of additional water-chloroform interfaces. This is achieved by the formation of water in chloroform droplets. By increasing the copolymer concentration, the number of droplets required to accommodate all the copolymer is increased until saturation of the chloroform.

A pathway to further increase the total water-chloroform surface, with the constraint of maintaining the volume of water constant, is to transition to elongated water domains. The separate water droplets are turned into cylindrical domains increasing the surface to volume ratio of water. Such cylinders are formed only at high PS-PEO surface concentration (Figure 16). Ultimately, the morphology with the highest surface area would be a sponge phase with very low chloroform content. This phase is achieved only if no emulsion inversion has occurred before.

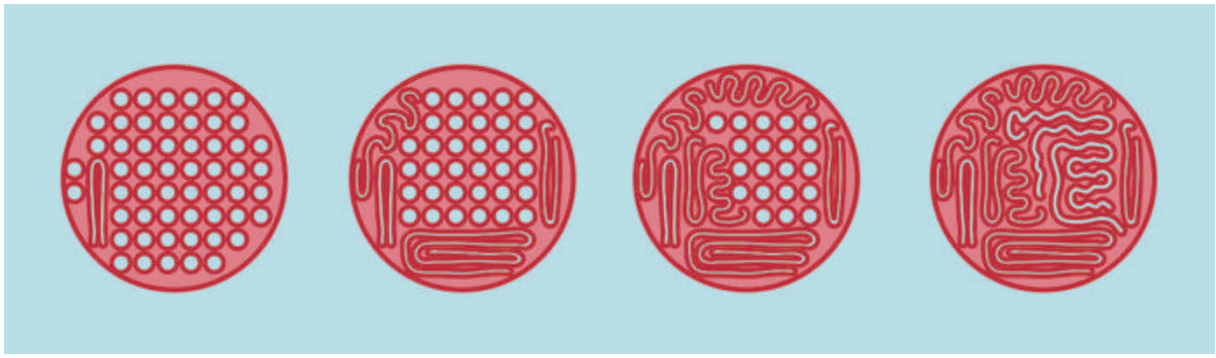

Figure 16 Schematic representation of the arrangement of PS-PEO molecules at the interface between water and chloroform. The copolymer concentration in the droplet is increasing from left to right. The dark red represents the presence of PS-PEO molecules. Once the chloroform is saturated with spherical water droplets the only way to achieve more water-chloroform surface is to stabilize elongated water domains. The different surface to volume ratio between the spherical and elongated morphology allows to accommodate more copolymer at the water-chloroform interface.

In the experimental situation there is a local increase in copolymer concentration in each droplet due to the chloroform evaporation. Provided the copolymers have enough time to rearrange at the solvent-solvent interface, all of the previously described stages are reached. This proceeds with until the formation of the sponge phase. This makes it possible for the copolymer to form the "ball of yarn" conformation shown in Figure 13. By further evaporating the chloroform, at a certain moment, the cores of these cylindrical structures will be the only regions to still be swollen in chloroform. Finally, after sufficient chloroform has evaporated, the emulsion water in chloroform emulsion is inverted resulting in the formation of elongated PS-PEO micelles in water (Figure 17).[42]

This emulsion inversion happens without a significant loss of contour length, the newly formed elongated micelles are swollen with chloroform for the initial stage, however, the removal of this solvent will cause the PS blocks to rearrange within the newly formed micelle core. This has the tendency to rearrange to stretch out and stiffen the micelles which gives the impression that the micelles are being ejected from the evaporating chloroform droplet.

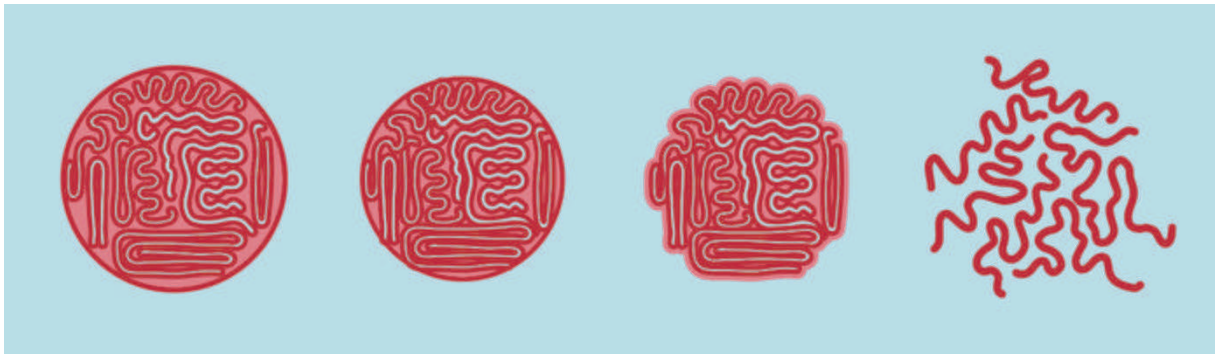

Figure 17 Schematic representation of the formation of elongated PS-PEO micelles. The solvent is evaporating from left to right. The dark red represents the PS blocks. Evaporation of the chloroform will cause the confinement of the elongated water domains. This continues until a sponge phase is formed. Finally reducing the solvent even more will cause an emulsion inversion which results in the formation of PS-PEO cylinders in water.

After this, we observed the behavior of the adsorbed emulsion droplets. These have naturally a larger curvature radius than the floating ones. The first thing we observed was that they systematically contained visible water droplets within them, the sizes of which were similar to those we observed from the initial planar interface experiments. The radius of curvature of the adsorbed droplets is much larger than that of those in suspension, however the formation of the water in chloroform emulsion was never visualized directly as in the case of the planar interfaces. Because of this, it remains uncertain whether the water in chloroform emulsion is due to the larger radius of curvature of the adsorbed droplet or to the adsorption itself. An example of adsorbed double emulsion is shown for each copolymer in Figure 18.

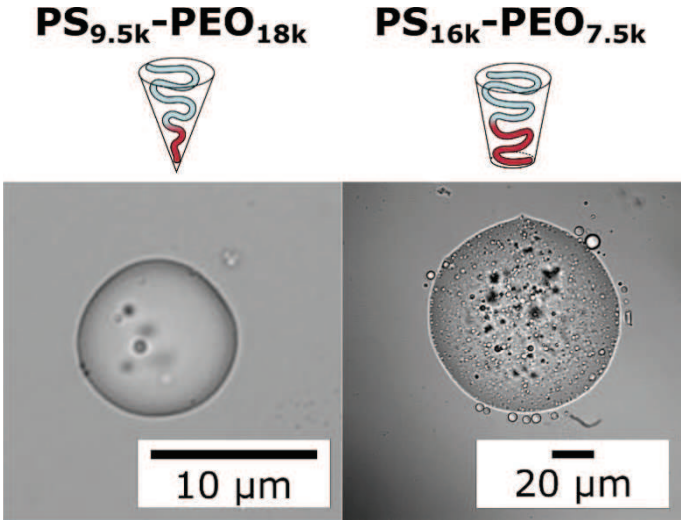

Figure 18 Adsorbed chloroform droplets showing the presence of an inner water emulsion.

We observed that upon surface destabilization these adsorbed droplets were generating morphologies of lower curvature than those expected: elongated micelles for the $PS_{9.5k}$-PEO_{18k} and vesicles or budding vesicles for the PS_{16k}-$PEO_{7.5k}$ (Figure 19).

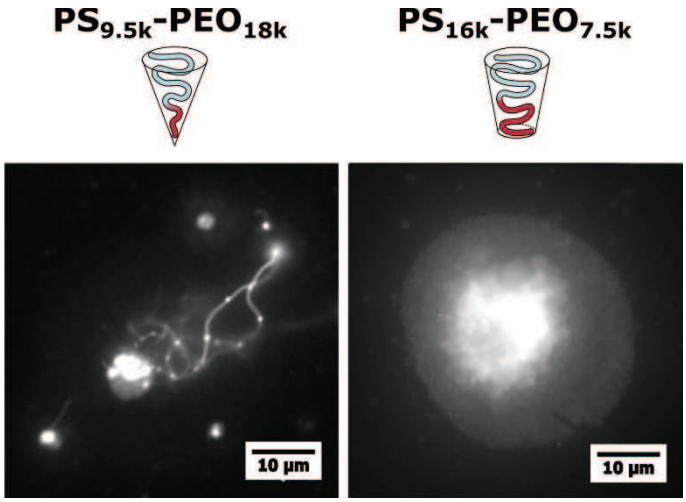

Figure 19 Fluorescence microscopy of the micelles formed from adsorbed double emulsions. On the left are elongated micelles formed with $PS_{9.5k}$-PEO_{18k}. On the right are vesicles and a budding vesicle formed with PS_{16k}-$PEO_{7.5k}$.

This result was very surprising since it provided a direct observation of the formation of micelles of different morphologies from the same formulations. In order to further characterize the various morphologies obtained we performed scanning electron microscopy after having allowed full chloroform evaporation and having dried the water phase by vacuum.

The $PS_{9.5k}$-PEO_{18k} samples showed the presence of both spherical and elongated micelles confirming the observations performed by fluorescence microscopy. The diameter of the micelles was measured by SEM and was of 44 ± 6 nm and 32 ± 4 nm for the spherical and the elongated ones respectively (Figure 20).

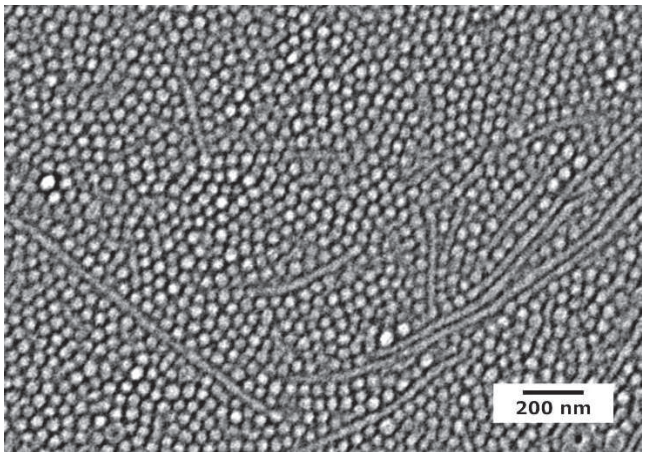

Figure 20 Spherical and Elongated micelles formed by the floating and adsorbed droplets of chloroform containing $PS_{9.5k}$-PEO_{18k}

The PS_{16k}-$PEO_{7.5k}$ samples showed the presence of elongated micelles, vesicles and budding vesicles. This was also in agreement with the observations performed by fluorescence microscopy confirming the stability of such morphologies. The diameter of the elongated micelles was measured from SEM

images and was of 56 ± 6 nm. In Figure 21 is shown a mixture of elongated micelles and spherical vesicles.

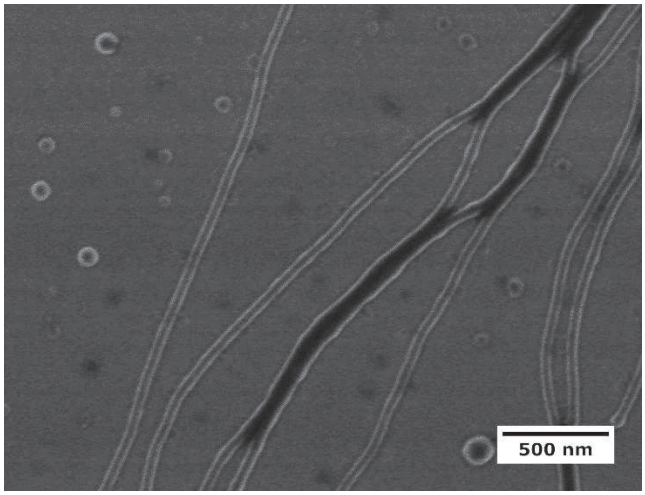

Figure 21 Elongated micelles and vesicles formed by emulsions of chloroform containing PS_{16k}-$PEO_{7.5k}$.

In Figure 22 are shown three images of an adsorbed budding vesicle, each performed using a different imaging technique. Both the optical and the confocal images were performed while the structure was still in water. The SEM image was done on a dry sample.

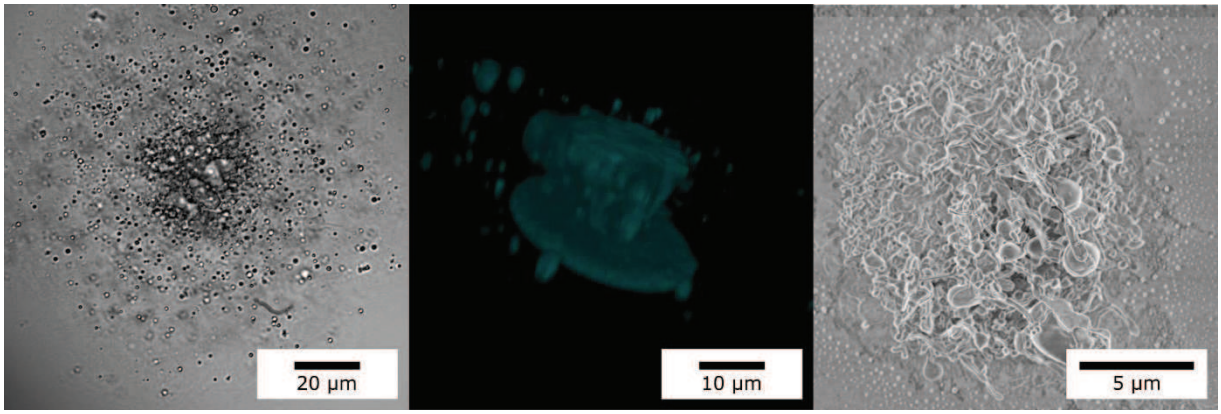

Figure 22 Images of an adsorbed budding vesicle formed from a droplet containing PS_{16k}-$PEO_{7.5k}$. On the left is an optical microscopy image. In the center is a Side view done by confocal microscopy Z-stack. The flat top of the image is due to the total height of the structure to be larger than the possible range of the Z-stack. On the right is an SEM image.

We also observed the presence of elongated structures which appeared to have a pearl necklace morphology. We performed transmission electron microscopy (TEM) on these samples and found that these structures were series of interconnected vesicles. Such strings of vesicles have been observed by Zhu et al. previously.[33] The formation of this morphology can be explained by the presence of water droplets in the chloroform prior surface destabilization. The strings of vesicles are shown in Figure 23.

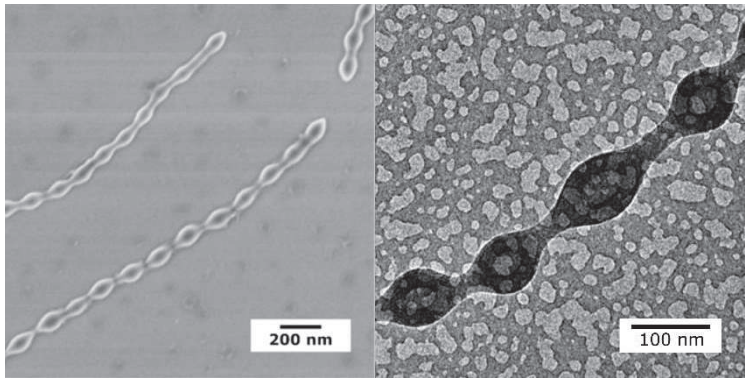

Figure 23 String of vesicles formed from adsorbed droplets containing PS_{16k}-$PEO_{7.5k}$. On the left is an SEM image while on the right is a TEM image showing the vesicular nature of these structures.

Before discussing the results as a whole, in Figure 24 is an overview of the experiments performed for both copolymers and the resulting morphologies.

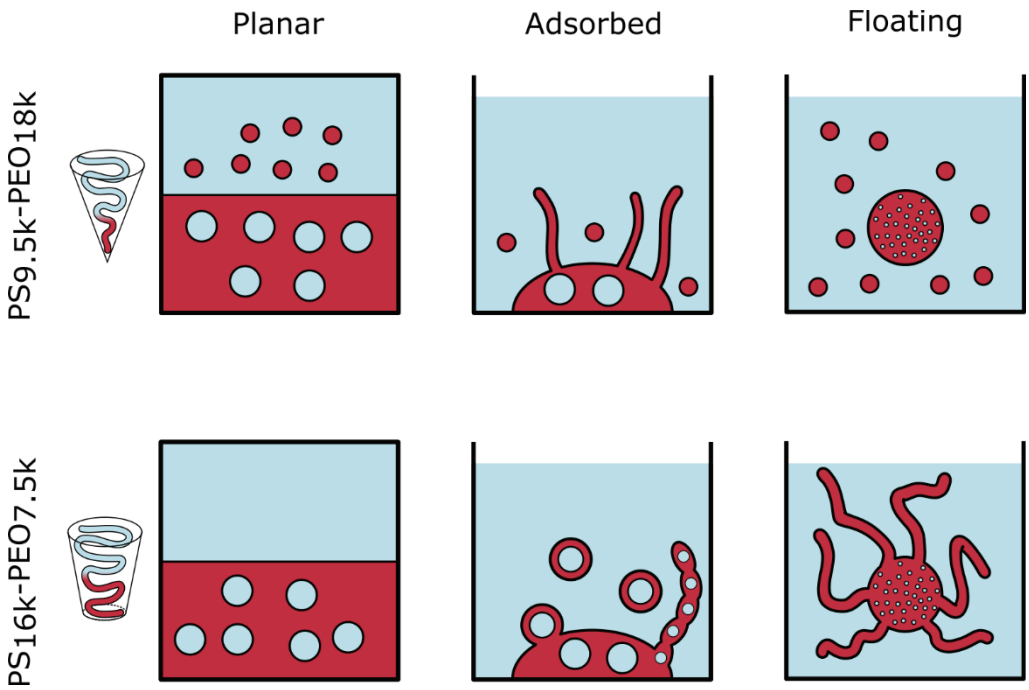

Figure 24 Overview of the three different interfaces studied and of the different micelles morphologies formed.

Three aspects arose from these experiments: the spontaneous formation of water in chloroform emulsions which is independent of the block copolymer composition, the formation of elongated PS_{16k}-$PEO_{7.5k}$ micelles which, unlike the $PS_{9.5k}$-PEO_{18k}, only occurs under confinement, and the fact that adsorbed droplets cause the copolymers to form micelles of different morphologies than those formed from floating droplets.

We can exclude the curvature of the interface as being the direct cause for the formation of the different morphologies. This is especially clear when looking at the behavior of the $PS_{9.5k}$-PEO_{18k} which

goes from spherical micelles to elongated and back to spherical when increasing the curvature of the interface. Therefore we suspect the water in chloroform emulsions induced by PEO of being the key point for the interpretation of all these results. The formation of the elongated $PS_{9.5k}$-PEO_{18k} micelles from adsorbed chloroform droplets is suspected to occur only in correspondence with the confinement of the water in chloroform emulsion. These results suggest a pathway for controlling the morphology of the micelles which will be described in Chapter 3.

2.3 Conclusions

We studied the phenomenon of micelle formation through emulsion evaporation by a series of direct observations. We started by observing a planar interface in the absence of solvent evaporation and found that, regardless of the block length ratio of the PS-PEO used, an emulsion of water in chloroform would be spontaneously formed. This behavior, which goes against the spontaneous interfacial curvature deduced from simple considerations on the block lengths of the PS-PEO copolymers used, has been explained thanks to the weakly amphiphilic nature of PEO and its preferred dissolution at the interface between chloroform and water. This aspect, which had not been considered previously in conjunction with kinetically frozen micelle formation, is of fundamental importance. This is because the presence of a water in chloroform emulsion alters completely the picture of the formation of micelles through emulsion evaporation and it also makes it possible to explain how micelles of bilayer morphology can be formed. Moreover, we observed that in the absence of solvent evaporation only the spherical micelles of $PS_{9.5k}$-PEO_{18k} are formed.

In view of these finding, we studied the behavior of evaporating microemulsions of chloroform in water. Doing this, we confirmed that elongated micelles of PS_{16k}-$PEO_{7.5k}$ are only formed in presence of solvent evaporation. Moreover, these micelles are not growing like fingers from the chloroform-water interface, as suggested by the spontaneous emulsification hypothesis supported by Zhu et al., instead they are formed prior surface instability within the chloroform droplets. This is explained thanks to the presence of the water in the chloroform emulsion. Through our observations, we have proposed a hypothesis to explain the formation of elongated PS_{16k}-$PEO_{7.5k}$ micelles though emulsion inversion caused by the evaporation of the chloroform phase.

Finally, we have observed that the chloroform emulsion droplets behaved differently when adsorbed or when floating in suspension. The first difference was in the size of the water in chloroform emulsion which was larger for the adsorbed droplets. This was likely to be related to the curvature of the interfaces being much larger for the adsorbed droplets than for the floating ones. The second, more

striking, difference was that the adsorbed droplets would cause the formation of micelles of different morphology than the droplets in suspension. We hypothesize that this phenomenon is linked to the visibly different size of the water in chloroform emulsions. This final point suggested a possible, formulation independent, pathway to control the morphology of micelles formed by emulsion evaporation. This gave rise to the technique which will be described in the next chapter.

2.4 Experimental Section

Observation of the Spontaneous Emulsification

A horizontal microscope setup was used to observe the evolution of the chloroform/water interface. A 10x objective was used in transmission and connected to an Infinity2 camera (Lumenera) to capture the images.

Emulsion destabilization observation

A stock solution of 10 mg/mL PS-PEO in chloroform was prepared for these experiments. To this solution 0.02% wt of the fluorescent dye DiI were added. From this solution, 10 µL were placed in a vial containing 1 mL of MilliQ water. An emulsion was formed using a Vortex for 30 seconds. The emulsion was then transferred using a glass syringe into a 20 mm circular CoverWell™ Perfusion Chamber stuck onto a glass coverslip. The total volume added to fill up the chamber was 180 µL. The emulsion is then observed using a Nikon Eclipse TE2000E inverted fluorescence microscope. Instability of the droplets occurs within a few minutes from the preparation of the perfusion chamber.

Scanning Electron Microscopy

5x5 mm silicon chips were treated with plasma and coated with 5 µL of 0.1 mg/mL micelle solution. These were imaged using a SU8000 UHR Cold-Emission FE-SEM Scanning Electron Microscope (Hitachi, Japan). The samples were imaged at 1kV acceleration voltage. The micelle samples were imaged without the addition of a conductive coating. The larger aggregates were sputtered with gold using a Bal-Tec SCF 050 Sputter Coater. A coating of approximately 10 nm was applied using a current of 40 mA and a sputtering time of 30 seconds at a working distance of 50 mm.

2.5 References

[1] S. Friberg, K. Larsson, J. Sjoblom, Food Emulsions, CRC Press, 2003.

[2] R. J. Prankerd, V. J. Stella, PDA J. Pharm. Sci. Technol. 1990, 44, 139–149.

[3] J. Read, The Shell Bitumen Handbook, Shell Bitumen, 1991.

[4] D. Needham, Developments in Bitumen Emulsion Mixtures for Roads, University of Nottingham, 1996.

[5] I. Terada, T. Yamada, M. Nishi, M. Uchida, N. Sugiyama, M. Kaneko, N. Takeda, Water Repellent Gypsum Composition, 1977, US 4042409 A.

[6] S. Benita, M. Y. Levy, J. Pharm. Sci. 1993, 82, 1069–1079.

[7] R. G. Gilbert, Emulsion Polymerization: A Mechanistic Approach, Academic Pr, 1995.

[8] Z. Lu, G. Liu, F. Liu, Macromolecules 2001, 34, 8814–8817.

[9] Z. Lu, G. Liu, F. Liu, J. Appl. Polym. Sci. 2003, 90, 2785–2793.

[10] M. Okubo, N. Saito, R. Takekoh, H. Kobayashi, Polymer (Guildf). 2005, 46, 1151–1156.

[11] T. Tanaka, N. Saito, M. Okubo, Macromolecules 2009, 42, 7423–7429.

[12] S. Jeon, G. Yi, C. M. Koo, S. Yang, Macromolecules 2007, 40, 8430–8439.

[13] R. Zheng, G. Liu, X. Yan, J. Am. Chem. Soc. 2005, 127, 15358–15359.

[14] J. Hu, G. Liu, G. Nijkang, J. Am. Chem. Soc. 2008, 130, 3236–3237.

[15] J. Zhu, R. C. Hayward, J. Am. Chem. Soc. 2008, 130, 7496–7502.

[16] T. Nicolai, O. Colombani, C. Chassenieux, Soft Matter 2010, 6, 3111–3118.

[17] S. Jain, F. S. Bates, Macromolecules 2004, 37, 1511–1523.

[18] Z. Gao, S. K. Varshney, S. Wong, A. Eisenberg, Macromolecules 1994, 27, 7923–7927.

[19] L. Zhang, A. Eisenberg, Science 1995, 268, 1728–1731.

[20] L. Zhang, A. Eisenberg, J. Am. Chem. Soc. 1996, 118, 3168–3181.

[21] H. Shen, L. Zhang, A. Eisenberg, J. Am. Chem. Soc. 1999, 121, 2728–2740.

[22] K. Yu, A. Eisenberg, Macromolecules 1996, 29, 6359–6361.

[23] S. M. D'Addio, W. Saad, S. M. Ansell, J. J. Squiers, D. H. Adamson, M. Herrera-Alonso, A. R. Wohl, T. R. Hoye, C. W. MacOsko, L. D. Mayer, et al., J. Control. Release 2012, 162, 208–217.

[24] Y. Geng, P. Dalhaimer, S. Cai, R. Tsai, M. Tewari, T. Minko, D. E. Discher, Nat. Nanotechnol. 2007, 2, 249–255.

[25] T. Miller, G. Van Colen, B. Sander, M. M. Golas, S. Uezguen, M. Weigandt, A. Goepferich, Pharm. Res. 2013, 30, 584–595.

[26] J. Zhu, R. C. Hayward, J. Colloid Interface Sci. 2012, 365, 275–279.

[27] R. Granek, R. C. Ball, M. E. Cates, J. Phys. II 1993, 3, 829–849.

[28] H. M. Aliabadi, S. Elhasi, A. Mahmud, R. Gulamhusein, P. Mahdipoor, A. Lavasanifar, Int. J. Pharm. 2007, 329, 158–165.

[29] D. a. Christian, S. Cai, O. B. Garbuzenko, T. Harada, A. L. Zajac, T. Minko, D. E. Discher, Mol. Pharm. 2009, 6, 1343–1352.

[30] V. V. Shuvaev, M. A. Ilies, E. Simone, S. Zaitsev, Y. Kim, S. Cai, A. Mahmud, T. Dziubla, S. Muro, D. E. Discher, et al., ACS Nano 2011, 5, 6991–6999.

[31] P. J. Glazer, L. Bergen, L. Jennings, A. J. Houtepen, E. Mendes, P. E. Boukany, Small 2014, 10, 1729–1734.

[32] R. C. Hayward, D. J. Pochan, Macromolecules 2010, 43, 3577–3584.

[33] J. Zhu, N. Ferrer, R. C. Hayward, Soft Matter 2009, 5, 2471.

[34] A. Nordskog, T. Futterer, H. Von Berlepsch, C. Boutcher, A. Heinemann, H. Schlaad, Phys. Chem. Chem. Phys. 2004, 6, 3123–3129.

[35] L. M. Bronstein, D. M. Chernyshov, E. Vorontsov, G. I. Timofeeva, L. V. Dubrovina, P. M. Valetsky, S. Kazakov, A. R. Khokhlov, J. Phys. Chem. B 2001, 105, 9077–9082.

[36] M. Su, Z. Su, Macromolecules 2014, 47, 1428–1432.

[37] C. Ö. Dinç, G. Kibarer, A. Güner, J. Appl. Polym. Sci. 2010, 117, 1100–1119.

[38] M. Spitzer, E. Sabadini, W. Loh, J. Braz. Chem. Soc. 2002, 13, 7–9.

[39] J. Israelachvili, Proc. Natl. Acad. Sci. U. S. A. 1997, 94, 8378–8379.

[40] J. March, Advanced Organic Chemistry: Reactions, Mechanisms, and Structure, McGraw-Hill, 1977.

[41] N. S. Zefirov, Chemical Encyclopedia, 1995.

[42] J. L. Salager, A. Forgiarini, L. Márquez, A. Peña, A. Pizzino, M. P. Rodriguez, M. Rondón-González, Adv. Colloid Interface Sci. 2004, 108-109, 259–272.

3 Morphology of kinetically frozen micelles

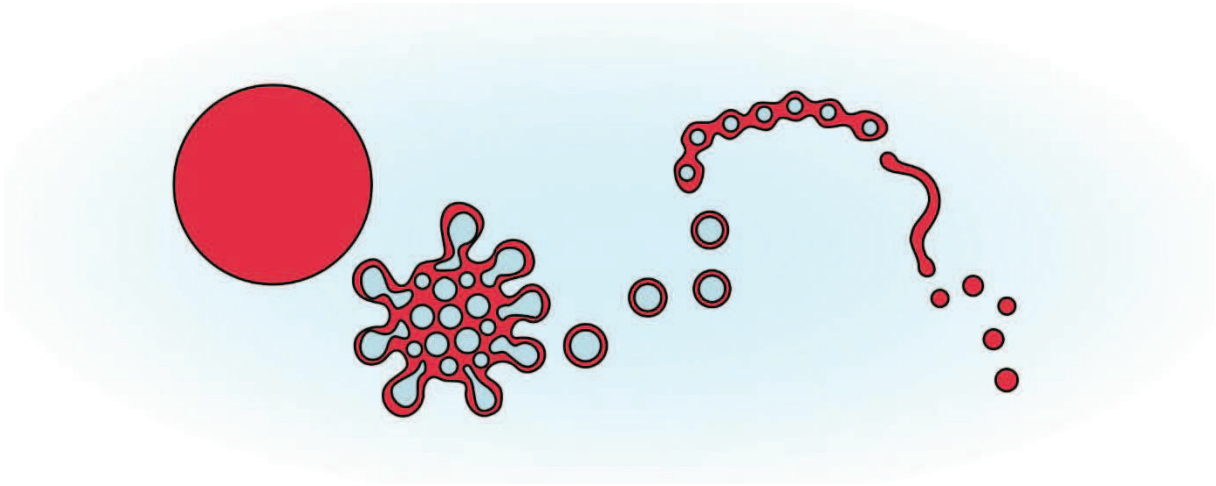

In this chapter we describe a technique we developed to control the morphology of poly(styrene)-poly(ethylene oxide) micelles formed through the emulsion evaporation method. A block copolymer solution in chloroform is deposited at the water-air interface of a water volume. Evaporation of the chloroform causes the copolymers to self-assemble into kinetically frozen micelles. It was found that the rate of evaporation of the organic solvent influences the morphology of the final self-assembled structures. Using two copolymers with different block length ratios we show how increasing the evaporation rate leads to the formation of lower curvature structures: from spherical to elongated and finally to vesicular morphology. As well as providing a valid method for the formation of morphology controlled micelles, the results presented in this chapter answers the question of the effect of solvent removal rate on the formation of micelles by emulsion evaporation.

3.1 Introduction

The concept of micelle formation through co-solvent evaporation, and topics on micelle morphology were introduced in the previous chapter. This chapter will cover more thoroughly the concept of kinetically frozen micelle morphology. We will do this in the introduction by providing an overview of the various techniques which were developed over the years. This will be presented through the chronological development of this field and the pros and cons of the different techniques will be highlighted.

Before discussing the aspect of far from equilibrium micelle morphology, it is useful to begin with the more familiar concept of equilibrium micelle morphology. The most simple and most used concept for the explanation of the packing of long linear (bio)molecules into membranes of different geometry was given by Israelachvili, Mitchell and Ninham in 1975.[1] The wide acceptance of their model lies in the elegant way in which they bridged the gap between the entropic, energetic reasoning of the physicists and the geometrical reasoning of biologists. The most known output of their reasoning is the packing criterion, also known as the packing parameter. This is a geometrical factor which is intrinsic to a surfactant molecule and depends on the volume of the hydrophobic chain v_c, the surface area of the hydrophilic head a and the length of the hydrophobic chain l_c.

$$p = \frac{v_c}{a \cdot l_c} \qquad \textit{Equation 1}$$

Depending on the value of the packing parameter, a certain equilibrium morphology can be expected for a solution of surfactant molecules at the right concentration and temperature. A schematic overview of the structures formed when the packing parameter lies within a certain range of values is shown in Figure 1.

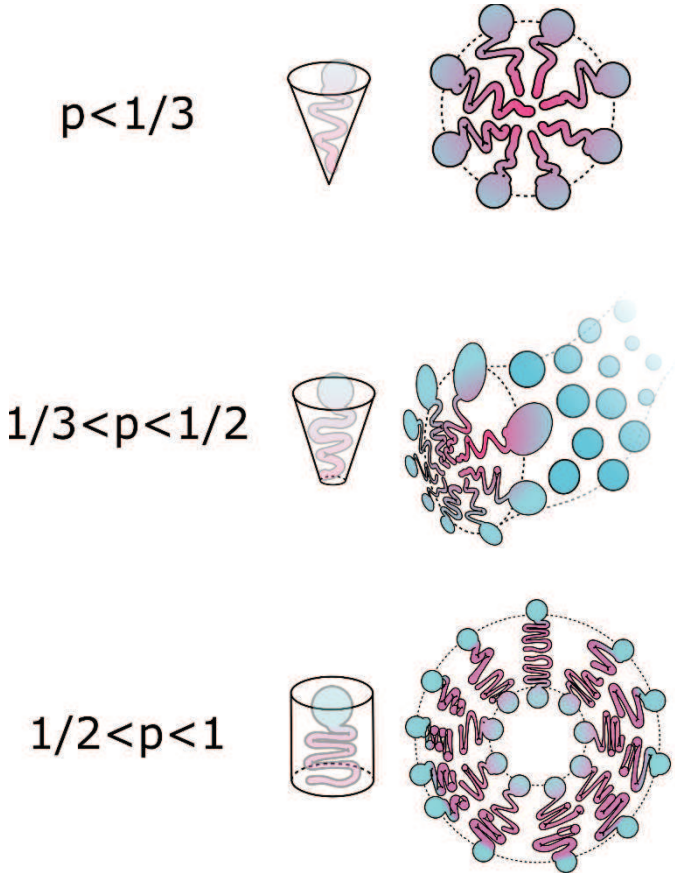

Figure 1 Overview of the different morphologies with their corresponding packing parameters. On the top are spherical micelles, in the center are elongated ones and on the bottom are bilayer morphologies (polymersomes or vesicles).

This is the basis of the theory of surfactant micelle morphology and although this concept could be loosely applied to block copolymer kinetically frozen micelles, this is an improper approach. This is because such micelles can be trapped far from equilibrium, therefore the estimation of a copolymer intrinsic packing parameter, depending only on the length of the blocks, is not necessarily related to the conformation that is found at the moment of micellization. It is a known fact that the morphology of kinetically frozen micelles is highly dependent on the process of formation.[2] To further justify this aspect, an overview of the main formation processes for diblock copolymer kinetically frozen micelles will be given in the following paragraphs.

As mentioned in the second chapter, the major contributions for the formation of kinetically frozen micelles were given by Eisenberg et al. The concept of using highly asymmetrical block copolymers to form micelles with large cores and small coronas was object of a theoretical study of de Gennes from 1978.[3] This was further developed by Halperin in 1990[4,5] who introduced the term “crew cut” micelles, inspired by popular hairstyle of the early 20th century, to distinguish micelles with a large core and short corona from the “hairy micelles” having a small core and large corona.

The work of Eisenberg on PS based copolymers, which started in the mid-90s, can be considered as the beginning of the development of usable experimental techniques for the formation and application of kinetically frozen micelles. The initial technique, presented in 1994, consisted in dissolving highly asymmetric PS-PAA copolymers in a good solvent, DMF, and by slowly adding a corona selective solvent which is miscible with DMF. This process gradually decreases the solvent quality for the copolymer until cloud point is reached. This moment is believed to be the one in which organic solvent swollen micelles of high aggregation number are formed. This can be imagined as the moment in which the solvent quality has decreased so much, by the addition of water, that some PS-PEO rich regions of DMF start forming separate domains in the solution. This stage can be therefore seen as a DMF in water emulsion stabilized by the copolymers, or as a solution of solvent swollen micelles in water. After this stage the DMF, PS-PAA and water solutions are further diluted in water and dialyzed for timescales of the order of a week to remove all the DMF in solution. A scheme of this technique is shown in Figure 2.

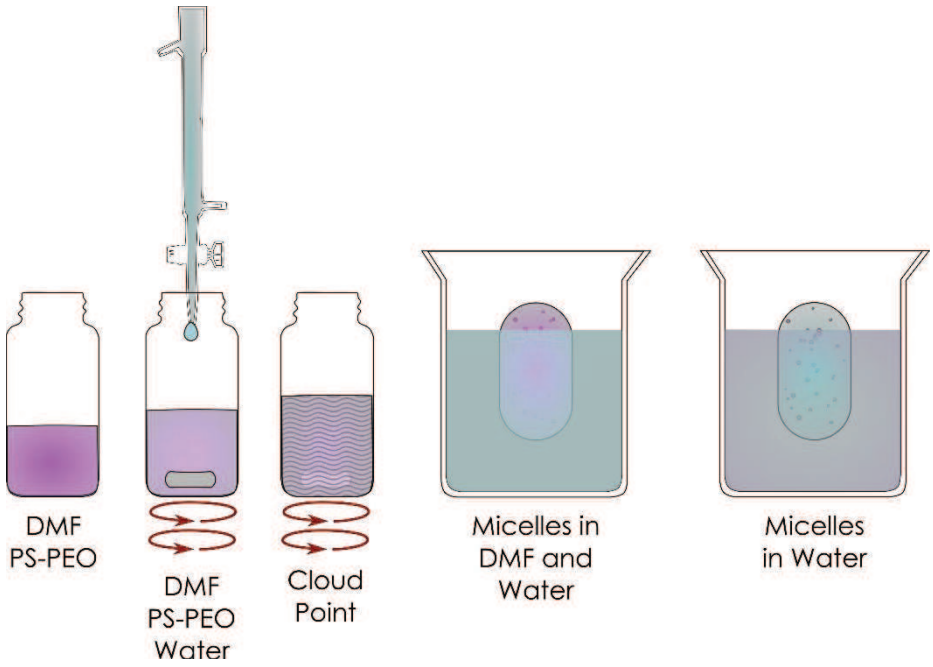

Figure 2 Micelle formation method proposed by Eisenberg et al. The copolymer is initially dissolved in an organic solvent compatible with both blocks. The dropwise addition of a block selective solvent causes the formation of the micelles. By dialysis the organic solvent is removed from the micelle solution resulting in kinetically frozen copolymer micelles in water.

The potential of this technique was clear thanks to the finding that different co-solvents, water or methanol, resulted in micelles of different sizes. This difference allowed to rule out the equilibrating processes of unimer exchanges between the micelles, proving that the PS-PAA micelles were kinetically frozen to a certain size upon formation. The use of different co-solvents is therefore the first documented step towards obtaining control of micelle morphology independently of the block size of the copolymers used.

In the following two years the technique was applied to a series of PS-PAA copolymers with different block lengths resulting in the widest range of micelle morphologies observed by transmission electron microscopy at the time.[6,7] The potential of this technique for the preparation of nanoparticles for biological applications was even more clear when the same method was applied to PS-PEO, again to prepare a wide range of micelle morphologies. These were all stable and not affected by the drawbacks of dynamic micelles such as destabilization upon dilution.[8]

For both the PS-PAA and PS-PEO micelles however, the authors reported the occurrence of polymorphism. The coexistence of different morphologies in the same sample of micelles is one of the major drawbacks of kinetically frozen micelles since it can limit their applications. The authors addressed this issue by stating that due to the slow addition of the selective solvent, and consequently the slow and gradual change in solvent properties, the experimental preparation conditions can cross a phase boundary between two different morphologies.

In 1996, Zhang et al. showed how morphology changes in crew cut micelles were possible with the addition of ions in the water phase while maintaining fixed the copolymer in the organic solvent.[7] This was done for both PS-PAA micelles using $CaCl_2$ or HCl and for PS-PEO micelles using NaCl. In their results they show how increasing amount of ions led to the morphology transition from spheres to rods, vesicles and what they called large compound vesicles (LCVs). This last new morphology has since been referred to as budding vesicle and appears as a microsized aggregate of vesicles, reminding a foam.

This was the first report of the amazing morphology control that can be achieved on kinetically frozen micelles through formulation efforts. In just a few years it was possible to go from simple stable spherical particles, to the ability to form stable morphologies that had previously not even been observed.

The next major step forward in this field was done in 2008 by Zhu et al. when they developed the emulsion evaporation method.[9] This consisted, as mentioned in the first chapter, in substituting the water miscible organic solvent (i.e. DMF) with a water insoluble one (i.e. chloroform). In this way the organic solvent containing the copolymer can form an emulsion with water. Each emulsion droplet acts as a shrinking volume which confines the copolymer in gradually smaller volumes. This confinement within the chloroform droplets and its complete evaporation will lead to the formation of micelles. A scheme of the method is shown in Figure 3.

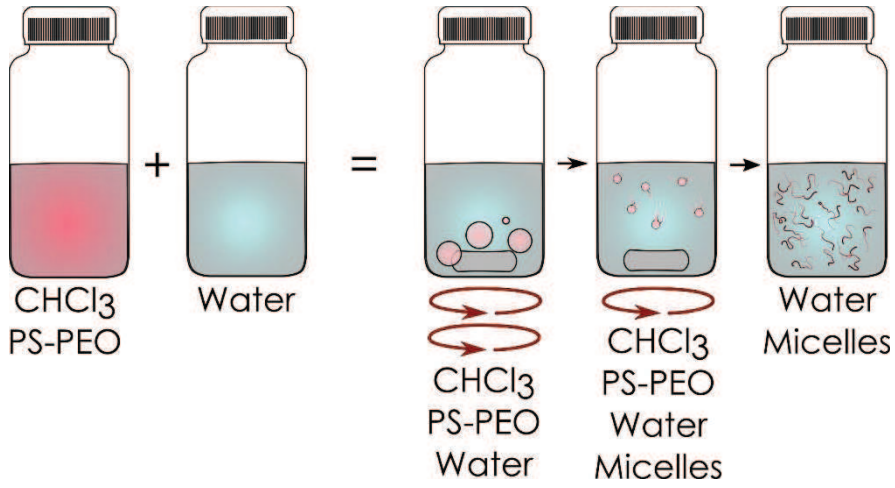

Figure 3 Method of micelle formation proposed by Zhu et al. The copolymer is dissolved in chloroform and this solution is added to water. An emulsion between the two solvents is stabilized by mechanical mixing. The emulsion is mixed until the chloroform has evaporated and a solution of micelles in water is left.

This method can be applied to a wide range of block copolymer compositions, but most importantly it allowed the possibility to incorporate hydrophobic polymers and nanoparticles in the core of the micelles directly from their formation. Another non negligible advantage of the emulsion evaporation method is the elimination of the dialysis step, making the whole micelle formation process faster lasting only approximately one or two days depending on the copolymer used.

In the initial stage of the development of this technique Zhu et al. showed its potential by forming different morphologies using different block copolymers and different blends of homo polymers and di-block copolymers. In the following year they showed how the addition of a water soluble co-surfactant (i.e. SDS) would make it possible to tune the morphology of the final assemblies.[10]

The transition between morphologies in this case was following the opposite direction than the addition of ions in the miscible solvents technique. Polymers which would spontaneously form budding vesicles would form vesicles, strings of vesicles, elongated micelles and spherical micelles with an increasing amount of SDS.

This technique shows the same kind of freedom in micelle formation that was shown by Zhang et al. however, formulation wise and keeping in mind the final applications of these objects, it can be arguable whether it represents a real improvement. As a general approach, it is regarded as preferable to reduce the amounts of ingredients in a system. From the researcher's point of view this simplifies the system by facilitating the interpretation of the results. From the point of view of the development of applications it is also better to reduce the ingredients to reduce costs and unwanted interactions. It is important to consider that the addition of NaCl in water has a well-defined behavior on the hydration of PEO, and after micelle formation the excess of salts can be removed by dialysis or using a desalting column. The addition of SDS in the emulsion, however, will affect both the copolymer-

solvent interactions and the solvent-solvent interactions, ultimately leading to the formation of mixed micelles which could have mixed and complex interactions, for example with the proteins in an in-vivo environment.[11]

A more recent approach towards the control of PS-PEO micelles through the emulsion evaporation method was proposed by Su et al. in 2014.[12] In their paper they have shown how the addition of co-surfactant (i.e. PAA) or the use of co-solvent with different boiling points can lead to similar morphological transitions. Their results show definitely an effect of the solvent used on the morphology of the micelles: the more volatile dichloromethane results in the formation of elongated micelles, while the slower evaporating 1,2-dichloroethane results in the formation of vesicles. While surely the solvent evaporation rate has an impact on the morphology of the micelles, in their results discussion, they consider the behavior of both solvents to be identical with the exception of their evaporation rate. This is a naïve approach since the two solvents, as stated in their own paper, have a different solubility with water, and as we have shown in the previous chapter, the water in chloroform diffusion in the presence of block copolymers is a non-negligible factor in the formation of micelles through the emulsion evaporation method.

We propose a new method which we believe is a step forward with respect to both the methods developed by Eisenberg and Zhu. This is based on the findings described in the previous chapter, and it is specifically based on capturing the different stages of the water in chloroform emulsions which is stabilized by the PS-PEO. By doing this we are able to tune the morphology of the assembled micelles. When developing this new method, we wanted to eliminate the necessity of a mechanically stabilized emulsion since this leads to results of scarce reproducibility and high degree of polymorphism. By constructing this technique around the spontaneous emulsification behavior studied in the previous chapter, we wanted to develop a technique which made it possible to freeze the system in different stages of the water in chloroform emulsion. Finally, eliminating the mechanical stirring we removed the shear stress imparted to the sample during mixing. This shear stress is sufficiently strong to break the micelles during their formation so eliminating it would, for example, make it possible to form very long micelles.

3.2 Results and Discussion

Chloroform has a higher density than water (1.489 g/mL at 25 °C), but, at 25 °C and, without the addition of any surfactants, the surface tension of chloroform with air is 26.67 $mN \cdot m^{-1}$ which is smaller than that of water with air: 71.99 $mN \cdot m^{-1}$.[13,14] This makes it possible to deposit chloroform droplets

onto a water surface, provided that the added mass is small enough to be balanced by the energy gained through the formation of the chloroform-air interface. This continues to be possible when using a chloroform solution containing amphiphilic PS-PEO allowing us to develop a setup based on this feature. In this work we used two PS-PEO copolymers with two different block ratios: PS_{16k}-$PEO_{7.5k}$ (32% w_{EO}) and $PS_{9.5k}$-PEO_{18k} (65% w_{EO}). Considering the packing parameter of these two copolymers, they are expected to form different micelle morphologies.[1] In the literature the emulsion evaporation method was used to form elongated micelles with PS_{16k}-$PEO_{7.5k}$[15] and spherical micelles with the $PS_{9.5k}$-PEO_{18k}.[9] However, in the previous chapter we have shown how these two copolymers can form a wide range of morphologies and in this chapter we show how to control this behavior. A schematic representation of the micelle formation setup is shown in Figure 4.

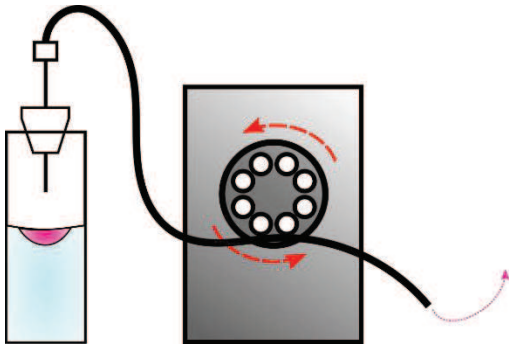

Figure 4 Schematic of the micelle formation setup. On the left is the cuvette filled with water and with a droplet of chloroform deposited at the water air interface. The cuvette is connected to a peristaltic pump which is extracting vapor from the sealed cuvette.

We connected the cuvette containing water and chloroform to a peristaltic pump in order to control the evaporation rate of the organic solvent. We used three speeds on the pump which correspond to three arbitrary evaporation rates that we will denote as x1, x4 and x8.

As soon as the chloroform is deposited onto the water, a water in chloroform emulsion is formed, as shown in chapter 2, and the interface between the two solvents starts receding. This is mainly due to the evaporation of the organic solvent. The reduction of solvent mass facilitates the spreading of the droplet. Moreover, the accumulation of amphiphilic copolymers at the chloroform-water interface will decrease the surface tension which could also provide a driving force for a spreading effect of the chloroform droplet. After a certain amount of time, depending on the flow rate applied with the peristaltic pump and the copolymer used, the chloroform-water interface becomes unstable and the formation of filaments or droplets can be observed from the previously smooth interface. In Figure 5 is shown the evolution of the chloroform-water interface upon destabilization for both copolymers. On the left is the more hydrophilic $PS_{9.5k}$-PEO_{18k} and on the right the more hydrophobic PS_{16k}-$PEO_{7.5k}$.

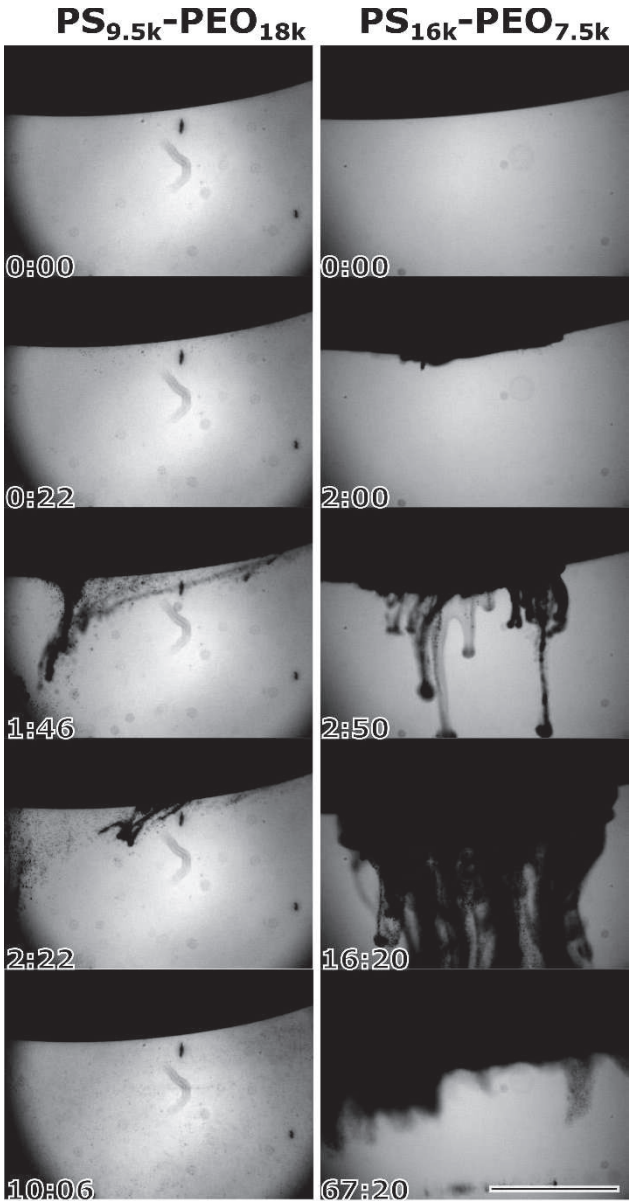

Figure 5 Evolution of the chloroform droplet from instability at minimum (1x) flow rate. On the left $PS_{9.5k}$-PEO_{18k} is shown. Upon visible surface instability, small droplets of chloroform in water are formed. This is followed by a more pronounced stream of chloroform droplets diffusing towards the water phase. As a result a chloroform in water micro-emulsion is formed within ten minutes from the onset of surface instability. Complete evaporation of the volatile dispersed phase will result in a water solution of spherical micelles. On the right the PS_{16k}-$PEO_{7.5k}$ is shown. Upon surface instability, this copolymer caused the formation of elongated finger-like instabilities. The growth of these structures continued for approximately one hour. After this time, the solution appeared to be locally turbid. This was due to localized networks of elongated micelles. Scale bar 1 mm, time stamps in min:sec.

In the presence of the more hydrophilic copolymer ($PS_{9.5k}$-PEO_{18k}, Figure 5 left column) small droplets of chloroform were formed at the interface between the two solvents and diffused into the water phase. This was followed by a more pronounced stream of droplets. All these droplets were formed within a period of 10-15 minutes from the visible onset of instability. The small droplets formed the dispersed phase of a chloroform in water micro-emulsion which completely evaporated within the following hour. After this process the water phase of the cuvette became turbid. This water solution was characterized by SEM and revealed the presence of spherical micelles as shown in Figure 6 a.

The more hydrophobic copolymer (PS_{16k}-$PEO_{7.5k}$, Figure 5 right column) undergoes a more critical destabilization. This begins with the formation of long bundles of fingers which grow downwards from the chloroform/water interface. The fingers continue their growth for approximately one hour. After this time the solution appears locally turbid due to the presence of these long filament bundles that extend vertically along the whole vial. The elongated micelles formed in this process are shown in Figure 6 d. While the observations presented in Figure 5 were done at the slowest evaporation rate, in Figure 6 (b, c, e and f) are reported the morphologies obtained by increasing the evaporation rate.

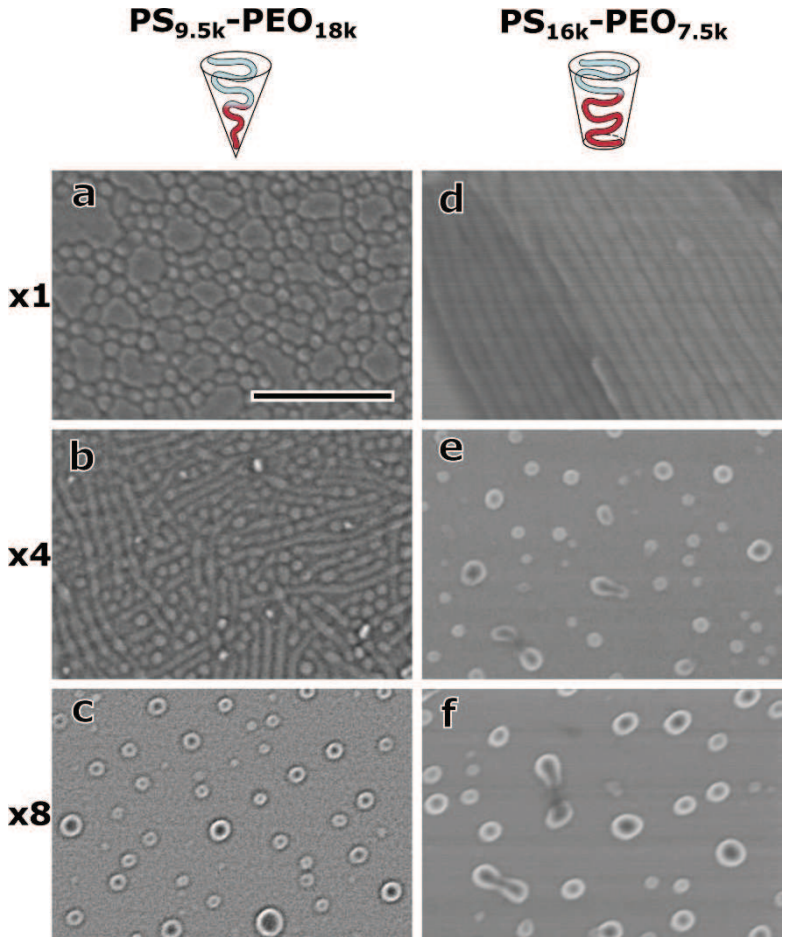

Figure 6 Different morphologies obtained for the different evaporation rates and visualized using Scanning Electron Microscopy. On the left $PS_{9.5k}$-PEO_{18k} and on the right PS_{16k}-$PEO_{7.5k}$. Ultimately both copolymers lead to similar vesicular morphologies. a) spherical micelles, b) elongated and spherical micelles, c) vesicles, d) elongated micelles, e) and f) vesicles. Scale bar 500 nm.

The more hydrophilic $PS_{9.5k}$-PEO_{18k} formed spherical micelles at the lowest evaporation rate. This is in agreement with the results of the emulsion evaporation reported in the literature and with the results obtained for planar interfaces and suspended droplets in the previous chapter. Increasing the flow rate caused the formation of elongated micelles and finally vesicles. The formation of elongated micelles from $PS_{9.5k}$-PEO_{18k} was also observed in the previous chapter from chloroform droplets which were adsorbed on the glass substrate. The more hydrophobic PS_{16k}-$PEO_{7.5k}$ at the lowest flow rate

formed elongated micelles, this again is in agreement with the results obtained from the evaporation of suspended droplets. Increasing the evaporation rate caused a transition to a vesicular morphology which is also in agreement with what we have shown in the previous chapter when observing the adsorbed droplets. The characteristic sizes of the micelles were estimated from SEM images and are listed in Table 1.

Table 1 Overview of the morphologies and sizes obtained using both copolymers as a function of the pump flow rate. The average diameters of the structures are reported.

	x1	*x4*	*x8*
$PS_{9.5k}$-PEO_{18k}	Spherical	Elongated / spherical	Vesicle
	45 ± 5 nm	33 ± 3 / 42 ± 4 nm	58 ± 18 nm
PS_{16k}-$PEO_{7.5k}$	Elongated	Vesicle	Vesicle
	55 ± 5 nm	56 ± 16 nm	72 ± 18 nm

We observed a trend of decreasing morphological curvature with increasing evaporation rate. This is similar to the results obtained by Su et al.[12] A schematic representation of the results obtained from our experiments are shown in Figure 7.

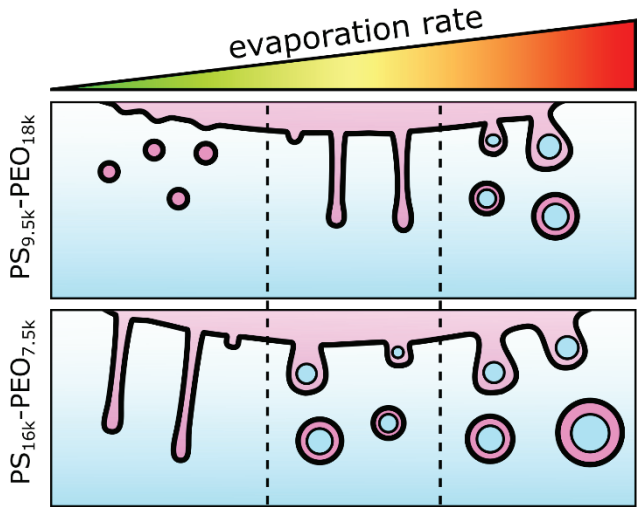

Figure 7 Schematic overview of the results obtained. An increase in evaporation rate led to a decrease in curvature of the micelles formed.

We also observed the presence of objects at the water air interface affecting light transmission in the samples of PS_{16k}-$PEO_{7.5k}$ which formed elongated micelles (last row of the right column of Figure 5) and in all the samples which formed vesicles (Figure 8). Since the chloroform had been fully evaporated, these must have been either polymer aggregates or micelles.

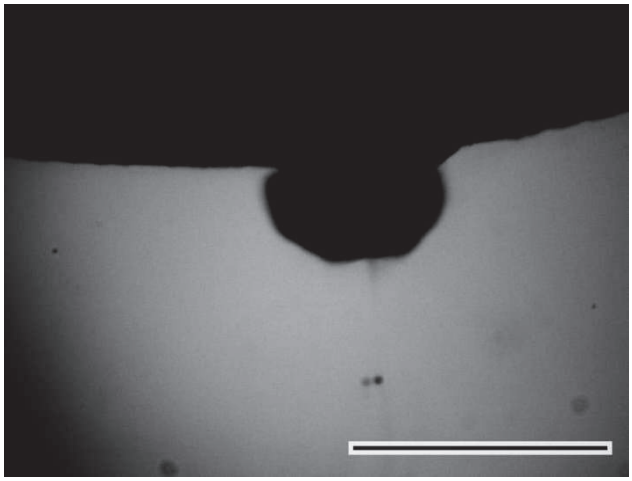

Figure 8 Copolymer aggregate formed at the air-water interface when the evaporation rate exceeded the rate of spontaneous emulsification/micellization. Scale bar 1 mm.

We investigated these structures by SEM and found that what is formed at low evaporation rate (last row, right column of Figure 5) is simply a network of elongated micelles (Figure 9). These micelles were identical to those shown in Figure 6 d.

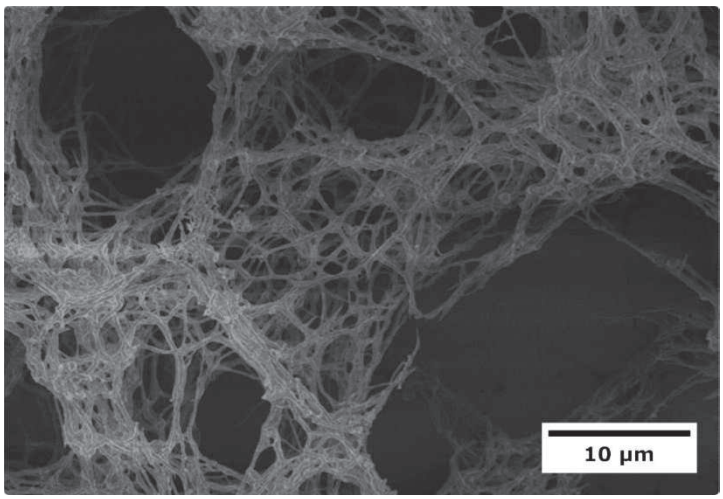

Figure 9 Network of elongated micelles made using PS_{16k}-$PEO_{7.5k}$ at a 1x flow rate. After formation a fraction of the micelles remains entangled at the air-water interface.

On the other hand, what was formed at the high evaporation rate was a dome-like polymer aggregate. Upon further inspection of these aggregates by scanning electron microscopy (Figure 10) we could observe that they had a rough surface made of spheres. This morphology is reminiscent of the budding vesicles formed from adsorbed chloroform droplets containing PS_{16k}-$PEO_{7.5k}$ shown in the previous chapter. This suggests that these structures are formed when the solvent is removed too fast with respect to the dynamics of surface instability by which vesicles are expelled from the main droplet.

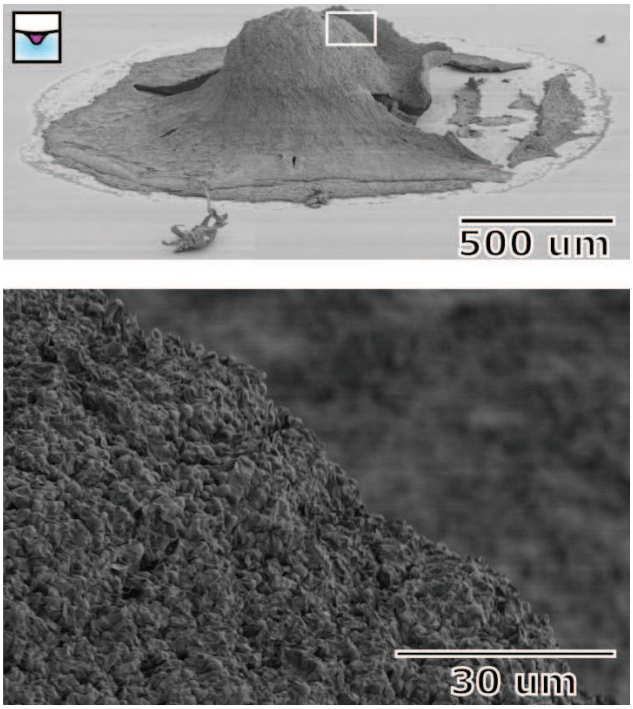

Figure 10 Scanning Electron Microscopy image of the budding vesicle aggregate which is formed at high (x4 for PS16k-PEO7.5k or x8 for both copolymers) evaporation rate. The image on top gives an overview of the aggregate. Below is shown a detail of the surface populated with spherical aggregates. On the top left a scheme of the aggregate formed as a pending droplet on the interface between water and air.

These residual macroscopic aggregates show the importance of the balance between the copolymer's bulk diffusion, their rearrangement at the solvent-solvent interfaces and the rate of solvent evaporation. While chloroform is present it acts as a plasticizer on the polystyrene blocks which are then able to diffuse within the bulk and to change their conformation at the solvent interface. In the absence or near-absence of chloroform the copolymers will have limited mobility to accommodate the interfacial instability. In our experiments, we could clearly distinguish between the situations when macroscopic aggregates were formed, and situations in which the whole copolymer mass was converted into micellar structures.

Following the hypothesis presented in the previous chapter, the spontaneous curvature of a copolymer coated interface depends in a complex way on the surface density and conformation of the amphiphilic molecules. This is due to the peculiar solubility of PEO which favors dissolution along the interface between water and a second solvent.

The problem of the orientation of amphiphilic molecules at an interface between two media has been studied for liquid-solid interfaces[17–20] and for liquid-air interfaces.[21] However, due to the experimental difficulties of measuring the orientation of molecules at a liquid-liquid interface, there haven't been many studies on the matter. Moreover, the few which were performed were done using small surfactant molecules.[22] Nonetheless, it is possible to hypothesize that PEO block copolymers

assume different conformations, depending on the surface density, at a liquid-liquid interface. The different conformations, corresponding to different surface densities, will induce different strains on the curvature of the solvent-solvent interface. A schematic representation of this behavior is shown in Figure 11.

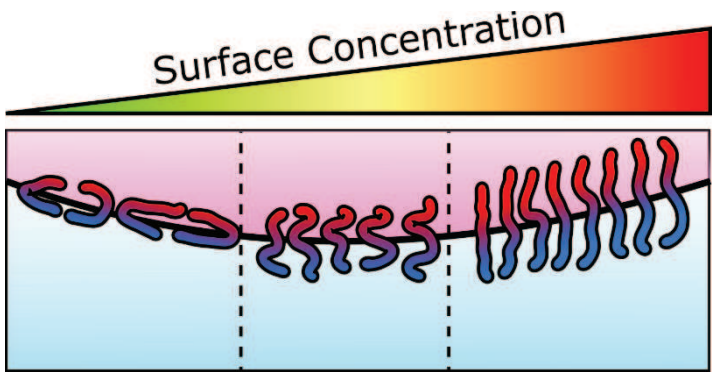

Figure 11 Schematic representation of the adsorption states of amphiphilic molecules at an interface with relation to the surface concentration.

This behavior would in turn affect the spreading parameter of the copolymers. [23] This is the difference between the work of adhesion and the work of cohesion of a substance at an interface. This quantity provides an idea of the wetting properties of a substance on a given surface.[23] This factor has been linked to the morphology of micelles formed at the water-air interface.[24] For a given block copolymer and surface, this factor is affected by the length of the blocks. Different surface conformations of the copolymers however would affect this factor by changing the "effective length" of the blocks at the interface. We therefore hypothesize that, due to the chloroform evaporation, the spreading parameter of a given copolymer at the chloroform-water interface is gradually changing due to the increase in surface concentration, and subsequent change in the adsorption state of the PEO block. This behavior is what causes the transition from an emulsion to a liquid foam and finally to a sponge phase within the chloroform. The morphology of the micelles is decided by the adsorption state of the copolymer at the onset of surface instability. We can therefore formulate a hypothesis in relation to the speed of evaporation of the chloroform. When the solvent evaporation is slow enough, the adsorption state of the copolymer assumes the dense brush configuration and therefore the micelles formed represent more closely the traditional packing parameter of the copolymer. When the solvent evaporation is too fast, the copolymers never reach high surface densities or the brush configuration and therefore have a different spreading parameter and form a different micelle morphology which does not necessarily represent the packing parameter of the copolymer estimated from the length of the blocks. This hypothesis is coherent with the fact that elongated micelles of $PS_{9.5k}$-PEO_{18k} are formed during fast evaporation where the copolymer has an effectively "shorter" PEO chain due to the closed

to parallel adsorption state at the water-chloroform interface. This would make the copolymer induce similar surface curvature as the PS_{16k}-$PEO_{7.5k}$ does in the dense brush conformation.

In both these cases the formation of the micelles occurs after the formation of a sponge phase within the chloroform. The difference is that in the first case the dense brush configuration is achieved and the interface spontaneous curvature which is caused by the copolymer block length ratio becomes the dominant factor. In the second case, instead, the sponge morphology is compressed and inverted into cylindrical structures in water. Finally, when the evaporation rate is very fast, surface instability is met before the sponge phase is formed. This corresponds to a situation in which the copolymers are still parallel along the interface and thin bilayer vesicles are formed by the outwards pressure of the water droplets who find themselves confined in a copolymer dense chloroform solution. In Figure 12 is shown an overview of the formation mechanisms for the $PS_{9.5k}$-PEO_{18k}. This polymer is shown since it covered all the three possible morphologies.

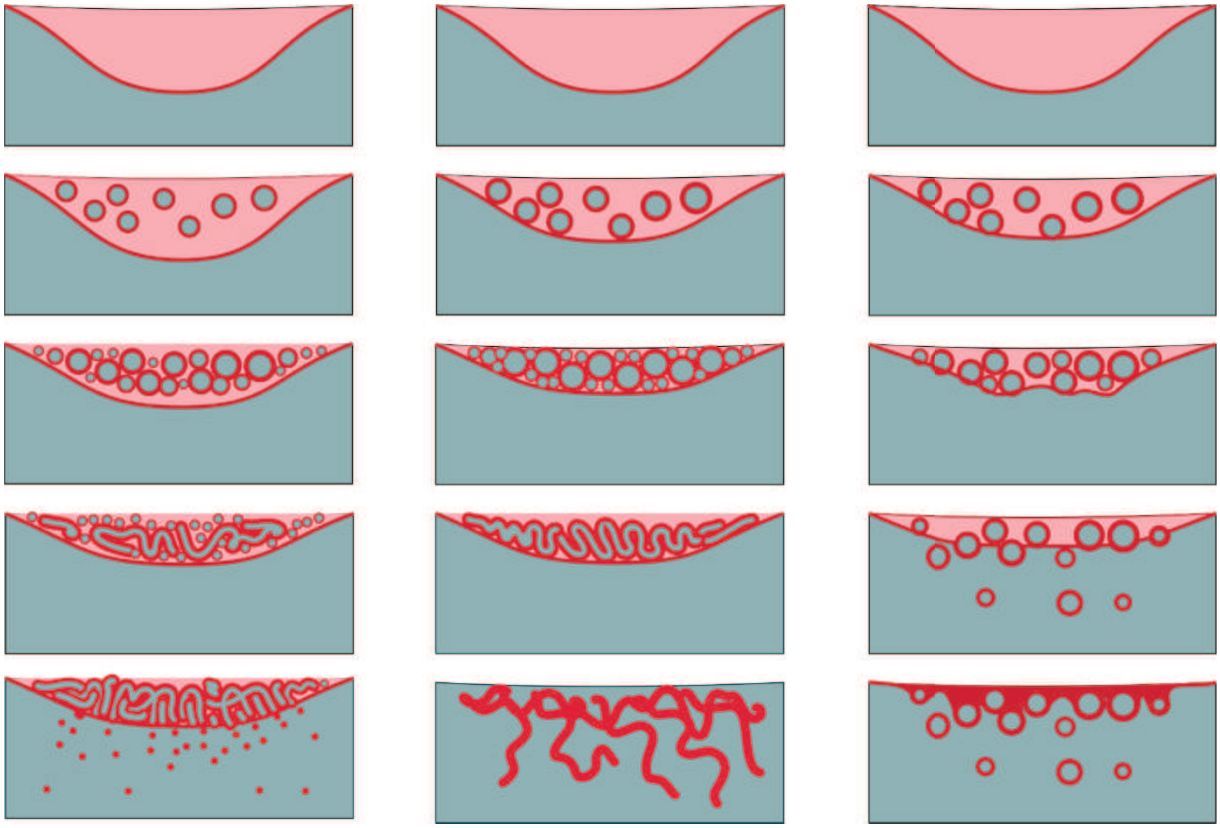

Figure 12 Overview of the different formation mechanisms of the $PS_{9.5k}$-PEO_{18k} micelles. From left to right is increasing the evaporation rate and from top to bottom are shown the characteristic timeframes in succession. In the initial moment a chloroform solution containing copolymer is placed on top of a water volume and the copolymer is adhering at the interface

between the two solvents. This causes the formation of a water in chloroform emulsion. If the solvent evaporation is fast enough, these water droplets are expelled from the chloroform phase and enter the water as bilayer vesicles. If the evaporation rate is slower the amount of water droplets increases while the chloroform volume decreases by evaporation. This triggers the transition from an emulsion to a sponge phase. If the evaporation rate is sufficiently slow the copolymers rearrange at the interface forming a dense brush which causes the formation of spherical micelles due to the spontaneous curvature induced at the interface. If the evaporation rate is faster, the sponge phase is compressed triggering an emulsion inversion which results in cylindrical micelles of PS-PEO in water.

To summarize our hypothesis it is useful to consider the evolution of the water in chloroform. In the initial state the water forms a dispersed emulsion within the chloroform. This proceeds to become a liquid foam in which the emulsion droplets are confined within the chloroform phase. Finally the liquid foam undergoes a transition into a sponge phase. When the solvent removal rate is faster than the transition into a sponge phase the system is trapped in the emulsion or the liquid foam state. Under these conditions happens the formation of vesicles and budding vesicles. Slower solvent removal rate allows the formation of a sponge phase. In this state two scenarios are possible: on one hand there is the faster solvent removal which inhibits the rearrangement of the copolymers and results in the inversion of the sponge phase forming cylindrical micelles. On the other hand is the slower solvent removal which allows the copolymers to rearrange at the interface and form micelles which correspond closely to their packing parameter.

3.3 Conclusions

In conclusion we have developed a technique which makes it possible to form micelles of controlled morphology in a fast process which requires only a few hours. This technique allows to change the morphology of the micelles by tuning the evaporation rate of the organic solvent. We have found that increasing the evaporation rate of the solvent allows to form micelles of increasingly low membrane curvature: from spheres to cylinders and to bilayers.

These results show for the first time the possibility to control the morphology of kinetically frozen micelles simply changing physical parameters while maintaining the formulation of the system constant. On a more fundamental level, this allowed us to shed light on the reasons for the polymorphism which affects the micelles formed by emulsion evaporation. When these emulsions are formed by mechanical mixing, the polydispersity of the droplets and the mixing itself will induce different water in chloroform emulsions affecting the micelle morphology. On a more practical level, this technique made it possible to form micelles of different morphology independently from the copolymer used. Until now, without the addition of co-surfactants, the formation of elongated micelles was restricted only to a very specific block length ratio of the copolymers. This technique opens up new possibilities in the formation of elongated micelles of very specific core/corona block length ratio. This is particularly interesting, as it will be described in chapter 4, for the mechanical properties of micelles, and in chapter 5, for the aspect of biological applications. This is because the

sizes of both blocks would affect the mechanical properties of the micelles, while the corona size would affect the ability of the micelles to circulate *in vivo*.

Another purely practical advantage of this technique is the fact that, by eliminating the mechanical stirring, it prevents the fracture of elongated micelles during their formation. This made it possible to form very long PS_{16k}-$PEO_{7.5k}$ which approached the mm length scale. By gently vortexing a vial in which these micelles were formed, it was possible to form macroscopic bundles of elongated micelles (Figure 13). The possibility to form such a nanostructured fiber is interesting from the point of view of materials science and it could be interesting to study further.

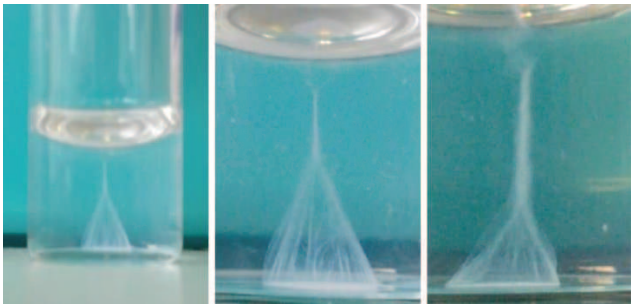

Figure 13 Bundles of elongated micelles of PS_{16k}-$PEO_{7.5k}$ forming a microscopic thread.

3.4 Experimental Section

Materials

The copolymers PS_{16k}-$PEO_{7.5k}$ and $PS_{9.5k}$-PEO_{18k} were purchased from Polymer Source. Anhydrous Chloroform ≥ 99%, 0.5 – 1% ethanol as stabilizer was purchased from Sigma Aldrich. MilliQ water was used for all experiments. All materials were used without further purification.

Micelle Formation

PS-PEO is dissolved in chloroform to prepare stock solutions of 10 mg/mL. One mL of milliQ water is added to a 3.5 mL 1x1 cm quartz cuvette. 10 µL of copolymer stock solution are added at the water-air interface using a glass syringe. The cuvette is sealed with a PTFE cap. The PTFE cap had been perforated and fitted with a syringe needle connected to a peristaltic pump REGLO Digital MS-2/8 (ISMATEC). The tubing used with the peristaltic pump has an inner diameter of 1.52 mm. The cuvette is placed in a thermostated holder at 25 °C.

Horizontal Microscopy

A horizontal microscope setup was used to observe the evolution of the chloroform/water interface. A 10x objective with a long working distance (15mm) was used in transmission and connected to an Infinity2 camera (Lumenera) to capture the images.

Scanning Electron microscopy

5x5 mm silicon chips were treated with plasma and coated with 5 µL of 0.1 mg/mL micelle solution. These were imaged using a SU8000 UHR Cold-Emission FE-SEM Scanning Electron Microscope (Hitachi, Japan). The samples were imaged at 1kV acceleration voltage. The micelle samples were imaged without the addition of a conductive coating. The larger aggregates were sputtered with gold using a Bal-Tec SCF 050 Sputter Coater. A coating of approximately 10 nm was applied using a current of 40 mA and a sputtering time of 30 seconds at a working distance of 50 mm.

3.5 References:

[1] J. N. Israelachvili, D. J. Mitchell, B. W. Ninham, J. Chem. Soc. Faraday Trans. 2 1976, 72, 1525.

[2] R. C. Hayward, D. J. Pochan, Macromolecules 2010, 43, 3577–3584.

[3] P. G. de Gennes, Solid State Physics, Academic Press, New York, 1978.

[4] A. Halperin, Macromolecules 1990, 23, 2724–2731.

[5] A. Halperin, M. Tirrell, T. P. Lodge, Adv. Polym. Sci. 1992, 100, 31–71.

[6] L. Zhang, A. Eisenberg, Science 1995, 268, 1728–1731.

[7] L. Zhang, A. Eisenberg, J. Am. Chem. Soc. 1996, 118, 3168–3181.

[8] K. Yu, A. Eisenberg, Macromolecules 1996, 29, 6359–6361.

[9] J. Zhu, R. C. Hayward, J. Am. Chem. Soc. 2008, 130, 7496–7502.

[10] J. Zhu, N. Ferrer, R. C. Hayward, Soft Matter 2009, 5, 2471.

[11] A. Nordskog, T. Futterer, H. Von Berlepsch, C. Boutcher, A. Heinemann, H. Schlaad, Phys. Chem. Chem. Phys. 2004, 6, 3123–3129.

[12] M. Su, Z. Su, Macromolecules 2014, 47, 1428–1432.

[13] N. R. Pallas, Y. Harrison, Colloids and Surfaces 1990, 43, 169–194.

[14] A. W. Adams, A. P. Gast, Physical Chemistry of Surfaces, 1997.

[15] P. J. Glazer, L. Bergen, L. Jennings, A. J. Houtepen, E. Mendes, P. E. Boukany, Small 2014, 10, 1729–1734.

[16] R. Granek, R. C. Ball, M. E. Cates, J. Phys. II 1993, 3, 829–849.

[17] T. F. Tadros, An Introduction to Surfactants, De Gruyter, 2014.

[18] N. A. Klimenko, COLLOID J. USSR 1978, 40, 1105.

[19] N. A. Klimenko, COLLOID J. USSR 1979, 41, 781.

[20] N. A. Klimenko, A. A. Tryasorukova, A. A. Permilovskaya, COLLOID J. USSR 1974, 36, 624–626.

[21] B. Rippner Blomqvist, T. Wärnheim, P. M. Claesson, Langmuir 2005, 21, 6373–6384.

[22] M. C. Messmer, J. C. Conboy, G. L. Richmond, J. Am. Chem. Soc. 1995, 117, 8039–8040.

3.5 References:

[23] E. Lugscheider, K. Bobzin, Surf. coatings Technol. 2003, 165, 51–57.

[24] G. Li Destri, A. A. Malfatti Gasperini, O. Konovalov, Langmuir 2015, 31, 8856–8864.

4 Mechanical properties of Micelles

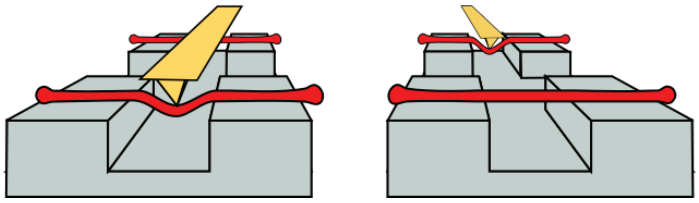

The mechanical properties of nanowires have often been shown to differ from those of bulk materials. When the diameter of nanowires is decreased below critical values, effects of surface tension and (supra)molecular organization become dominant on the material properties. In this chapter we used a direct three-point bending measurement to determine the mechanical properties of self-assembled poly(styrene)-b-poly(ethylene oxide), core-shell "hanging" elongated micelles. This technique eliminates any interaction between the elongated micelles and the substrate, this is critical for supramolecular elongated micelles whose structure and properties depend strongly on their local environment. Proceeding this way we were able to evaluate the subtle contribution of corona crystallization to the mechanical modulus of copolymer elongated micelles of various core sizes. By coupling direct atomic force microscopy (AFM) measurements to differential scanning calorimetry (DSC) data we show that the presence of a crystalline corona strongly increases the modulus of the copolymer elongated micelles.

4.1 Introduction

The mechanical characterization of nanowires has gained a lot of traction in recent years due to the plethora of applications that span from nano-electronics, nano-textiles, sustained drug delivery, tissue scaffolding and nanosensors.[1–5] In order to develop tailored applications for nanowires it is necessary to know their mechanical properties and how those relate to the macroscopic behavior of more complex, possibly composite, materials.

When it comes to the mechanical characterization of nanomaterials the Atomic Force Microscope (AFM) is the most versatile technique available. This is a relatively new technique, developed in 1986 as a variant of the Scanning Tunneling Microscope. It consists in a sample stage which can be moved in three directions x, y and z with respect to a tip which has a curvature radius of few nanometers. The tip is fixed at the end of a flexible cantilever. In order to produce an image, the sample is moved and scanned line by line by the tip. The interaction between tip and sample generates a bending in the cantilever. This bending is measured by monitoring the displacement of a laser beam which is reflected from the back of the cantilever onto a four quadrant photodiode. A scheme of an AFM is shown in Figure .

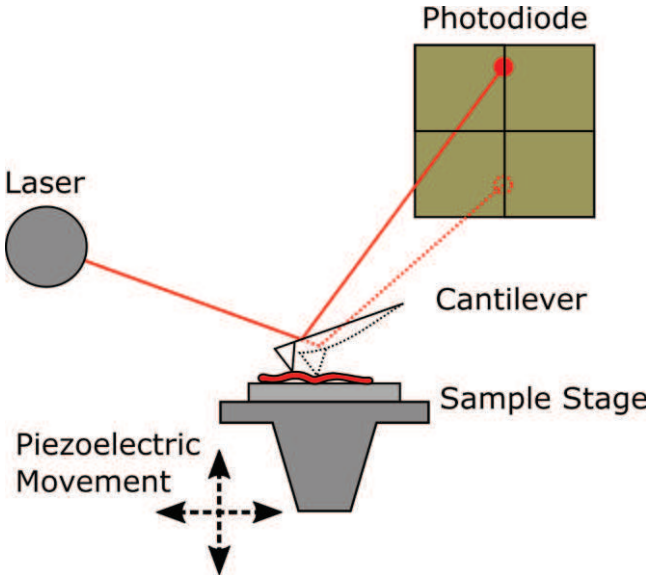

Figure 1 Schematic of the AFM, changes in topography of a sample can cause a deflection in the cantilever. This is reflected as a displacement of the laser beam on the four quadrant photodiode and translated into physical height differences in the sample.

The displacements of the laser spot on the photodiode are translated into a height profile of the sample in exam. However, by knowing the mechanical properties of the cantilever in use, it is possible to convert the displacement of the laser beam into force applied by the cantilever. This makes it possible to combine topography scans with the ability to perform force measurements such as nano-indentation. More recent AFM developments have made it possible to couple, in real time, the

acquisition of topographical information together with a series of material properties such as the elastic modulus or the work of adhesion.[6,7] While the possibilities of characterization are very broad, the main drawback of AFM lies in the requirement of adsorbing a sample on a solid substrate. In some situations this will not cause any alteration of the sample's properties, however this is not the case for self-assembled nanowires and nanoparticles which obtain their shape mainly due to surface tension and solvent-polymer interactions. The introduction of an interface can drive conformational changes within the micellar structures which hinder the possibility to link the properties measured to those of the original nanoparticles. Nonetheless, AFM has been successfully used to characterize samples which are less susceptible to structural changes upon adsorption.[8,9]

In this introduction we briefly present the different methods used to characterize the mechanical properties of nanowires using AFM. In Figure 2 are schematically shown three main approaches. All three approaches require the deposition of nanowires from a solution onto a substrate.

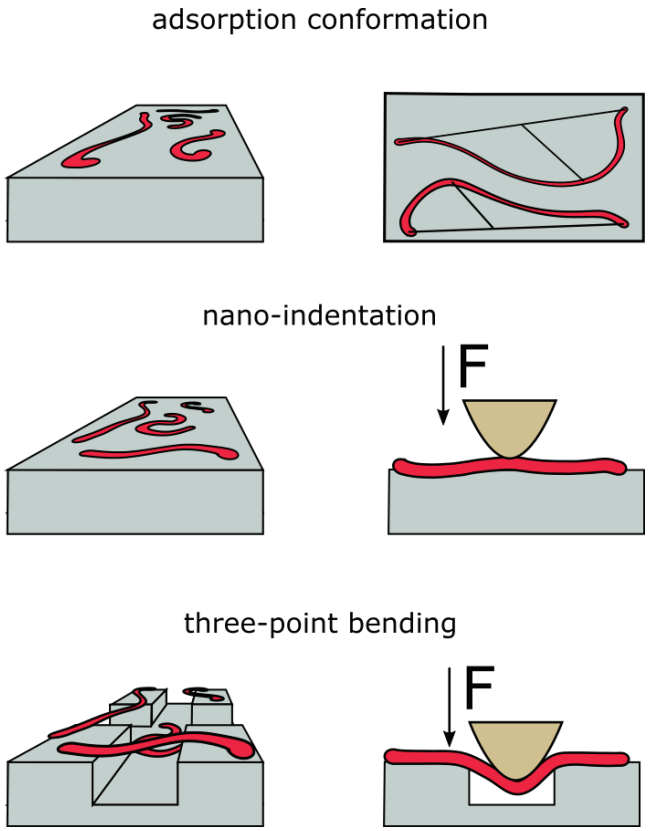

Figure 2 Schematic of the methods used to determine the mechanical properties of micelles. The first method is used to determine the persistence length of nanowires from their thermal deviation from a straight line. The second method consists in direct local measurements of the mechanical properties of the material by nano-indentation. The third method is a three-point bending test which removes the influence of the substrate and probes the properties of the nanowire on a larger scale than nano-indentation

In the first case topography scans are acquired and the nanowire end-to-end distance and contour length are traced, either by hand or using an automated image analysis software. In presence of

bending, the end-to-end distance will be smaller than the contour length of the nanowire. When the nanowire contour length is much smaller than its persistence length the deviations from a straight conformation are used to determine the persistence length.[10–15] This method doesn't require any calibration of the experimental setup. While it is a very straightforward method, it relies on the assumption that the equilibrium conformation of the nanowire is a straight line. This excludes the presence of defects and of residual stresses along the backbone of the nanowires.

The second, more direct, approach utilizes AFM force curves to determine directly the properties from a single nanowire. A force curve is performed by moving the tip towards the sample, in the z direction, until a certain cantilever deflection is measured. After this, the tip is retracted from the sample. During both sections of the force curve, the approach and retract, the cantilever deflection as a function of position is recorded. The output is the set of two curves representing approach and retract as shown in Figure 3.

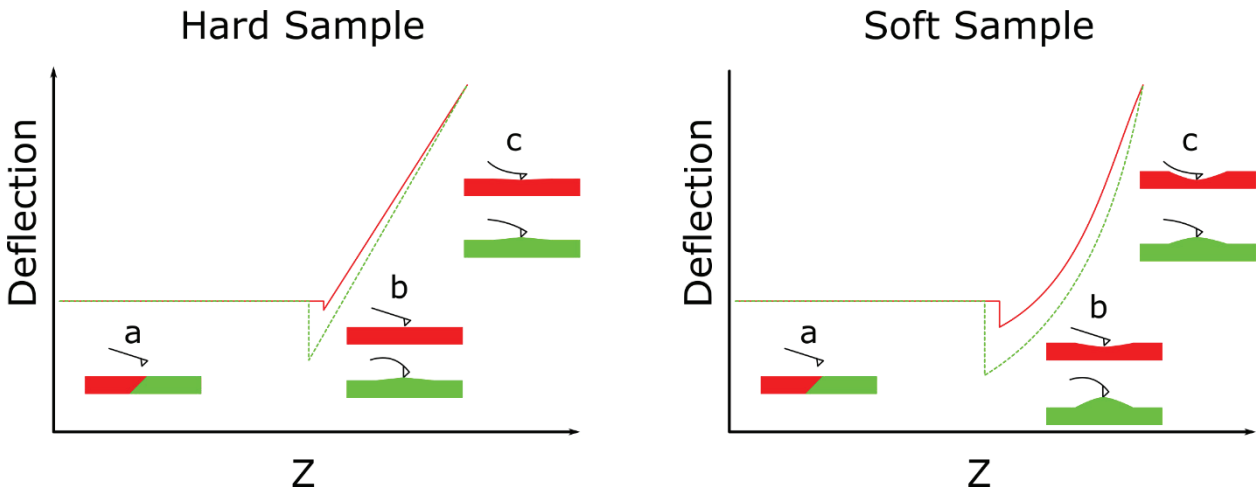

Figure 3 Schematic representation of two sets of force curves. In red and green are respectively the approach and retract curves. The three main sections of a force curve are labelled as a, b and c and are represented in the small figures. These are respectively the section of no contact, the contact point and the deflection. On the left is represented a force curve on a hard sample and on the right one on a soft sample.

As previously mentioned, it is necessary to obtain cantilever specific calibration parameters in order to convert the deflection vs position curves into force vs indentation depth curves. This requires two steps: the determination of the cantilever spring constant and deflection sensitivity. The most accurate method to obtain the spring constant is the thermal noise method which produces an error of approximately 5% on the obtained values.[16–18] The calibration of the deflection sensitivity is done by measuring the slope of a force curve performed on an infinitely hard substrate. This step further increases the measurement error by 2%.[16] Once the calibration is performed it is possible to obtain meaningful information from the force vs indentation depth curves utilizing a mathematical model. The most notable one is the Hertz model which describes the non-adhesive contact between two

elastic bodies. More complex models derived from this include the effects of sample-tip adhesion. These are the JKR and DMT models which are respectively used depending on if the area of adhesion lies only inside or also outside the tip sample contact area.[19–21] The Hertz model is shown for reference in Equation 1.

$$F = \frac{4}{3} E^* \sqrt{R} d^{3/2} \qquad \textit{Equation 1}$$

Here *F* is the force applied by the tip, *E** the reduced elastic modulus, *R* the tip radius and *d* is the indentation depth. The reduced elastic modulus is function of the Poisson modulus of the tip and sample and of the elastic modulus of tip and sample (Equation 2).

$$\frac{1}{E^*} = \frac{1 - \upsilon_m^2}{E_m} + \frac{1 - \upsilon_i^2}{E_i} \qquad \textit{Equation 2}$$

Where the indices *i* and *m* stand for indenter and material respectively. Ideally the indenter has an infinite modulus of elasticity and low Poisson ratio resulting in a null second term. All of these models are developed with the assumption that the radius of curvature of the tip is infinitely smaller than that of the sample. While this does not necessarily comply with nanowires and nanoparticles, using appropriate corrections it has been shown how these models can still be used at the nano-scale.[9,22,23]

The third approach is the most complex in terms of sample preparation. It requires the fabrication of a substrate which allows the suspension of the nanowires in exam. This makes it possible to perform nano-scale three point bending tests. This method has several advantages over the previous two approaches. The first important one being the exclusion of influence from an underlying substrate. Another less evident advantage is that while nano-indentation measurements probe the local mechanical properties of a nanowire, bending measurements cause a larger scale deformation of the nanowire along its backbone and the results are therefore influenced by a larger portion of the sample.[24] The elastic modulus of a suspended beam is determined using the classical Euler Bernoulli beam theory:

$$E = \frac{L^3}{192I} \cdot \frac{F}{d}$$ *Equation 3*

Here *E* is the elastic modulus of the sample, *L* is the length of the suspended fraction of the beam, *F* is the force applied, *d* is the indentation depth and *I* is the second moment of inertia of the beam and it is equal to $\pi D^4/64$. This model describes the situation in which a beam is clamped at both ends, models describing non clamped situations have a different numerical coefficient.

In contrast with the Hertz model, the results of a three point bending test do not depend on the AFM tip radius of curvature, but only on the diameter of the structure in exam. Moreover, the assumption for the validity of such a model is that the force is applied on the central point of the suspended nanowire. While this assumption might be problematic for nanowires with a diameter of only a few nanometers, it is generally a less restricting requirement than that of the Hertz model. The main bottleneck with this method lies in the complexity of sample preparation which can be very daunting. The most common approach for polymer nanowires and nanowires is to simply deposit a droplet of nanowire solution onto a porous substrate and to look for suitable suspended particles.[1,25] While this may seem straightforward, AFM is a relatively slow microscopy technique and samples which present high adhesion and small topography variation, such as polymer nanowires, often require particularly slow scan speeds in order to obtain accurate topography scans. Coupling the limitations of AFM with the randomness of drop casting hinders the possibility to obtain statistically valid data sets on the sample in exam. Comparing the limitations and advantages of these three approaches the three point bending test, when suitable, delivers the most accurate characterization of the mechanical properties of a nanowire.[24]

Thanks to the development of these techniques, many different polymer nanowires have been characterized and one general pattern has arisen: that is the sudden increase in mechanical properties when the diameter of the nanowires goes below a certain threshold. Two main explanations have been proposed for this behavior. On one hand there is the influence of an increasing surface to volume ratio supported by Cuenot et al.[25–27] and on the other hand there is the onset of supramolecular confinement proposed by Arinstein et al.[28–30] The deformation of a straight beam requires the formation of new surface area. This is what lies behind the former hypothesis. When a beam has a very high surface to volume ratio, a deformation requires the formation of extra surface. This causes the deformation to cost more energy which is what effectively acts as a strengthening on the nanowire. The latter hypothesis explains the increase in elastic modulus as due to the confinement of supramolecular structures. Even in amorphous polymer nanowires there are regions in which the macromolecules have correlated orientation resulting in domains of supramolecular structures. When the transversal size of the nanowire is comparable with the size of these supramolecular structures, a

confinement effect on the orientation-correlated domains causes an increase in mechanical properties.

In this chapter we determined the mechanical properties of elongated PS-PEO micelles through three point bending tests. The ease of fabrication and functionalization of these elongated micelles, together with their very high aspect ratio, make them suitable for several nanowire applications. In order to simplify the experimental setup and to increase reproducibility of the measurements, we developed a technique, based on molecular combing, to generate highly ordered arrays of suspended micelles.[31–33] This rational sample deposition technique removes the random aspect of drop casting and simplifies the data acquisition process. Since the elongated micelles are directionally ordered, it is possible to predict the location of the suspended portions. This makes it possible to adjust the force applied with the AFM during scanning and to avoid fracturing the suspended micelles during the initial topography scan. Micelles of different diameter were prepared using different blends of PS-PEO and PS and their modulus was measured. Finally, Differential Scanning Calorimetry (DSC) measurements on the dry elongated micelles made it possible to explain the results obtained.

4.2 Results and Discussion

The PS-PEO elongated micelles were prepared following the solvent evaporation directed self-assembly in the presence of two solvents.[34,35] This technique allows the formation of elongated micelles with lengths of up to hundreds of micrometers (Figure 4) which makes them viable for composite materials or tissue scaffolds of macroscopic scale. Moreover, since the copolymers are non-soluble in water processes such as unimer exchange, scission and fusion, the well-known dynamic processes which characterize block copolymer micelles are hindered. These elongated micelles are therefore kinetically frozen in specific configurations.[36–38]

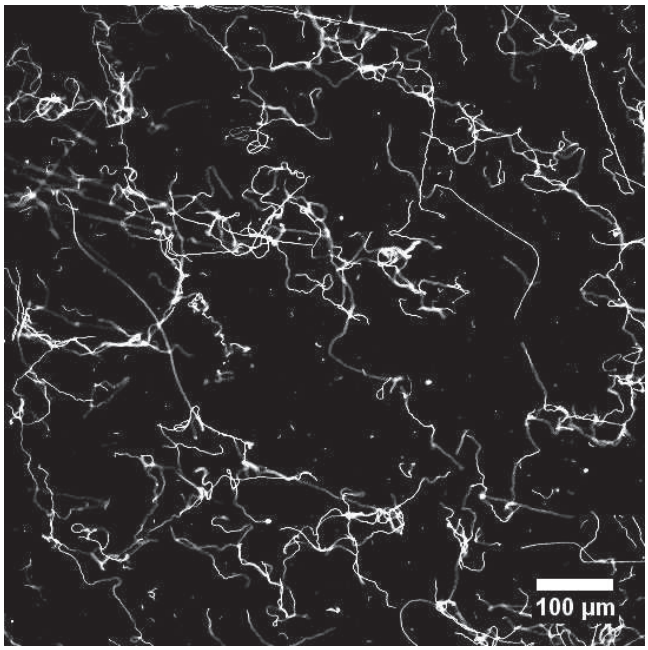

Figure 4 Fluorescence microscopy image of the ultra-long PS-PEO elongated micelles in aqueous solution. A fluorescent dye was incorporated in the core of the elongated micelles.

Elongated micelles of increasing diameter were prepared using blends of PS-PEO copolymer and PS homopolymer. The weight fraction of polystyrene is calculated with respect to the mass of PS-PEO in the solution. Increasing weight fractions of added homopolymer resulted in increased diameters as shown in

Table 1. The values were obtained by drying samples of elongated micelles and imaging them by Transmission Electron Microscopy (TEM). The diameter was measured from the TEM images of different elongated micelles. Since the elongated micelles were in their dry state during the bending experiments this measurement correctly reflects the diameter of the elongated micelles probed. An

example of the TEM images used is shown in Figure 5 Transmission Electron Microscopy images of the plain block copolymer micelles. On the right is a close-up image showing a “head” of a micelle.

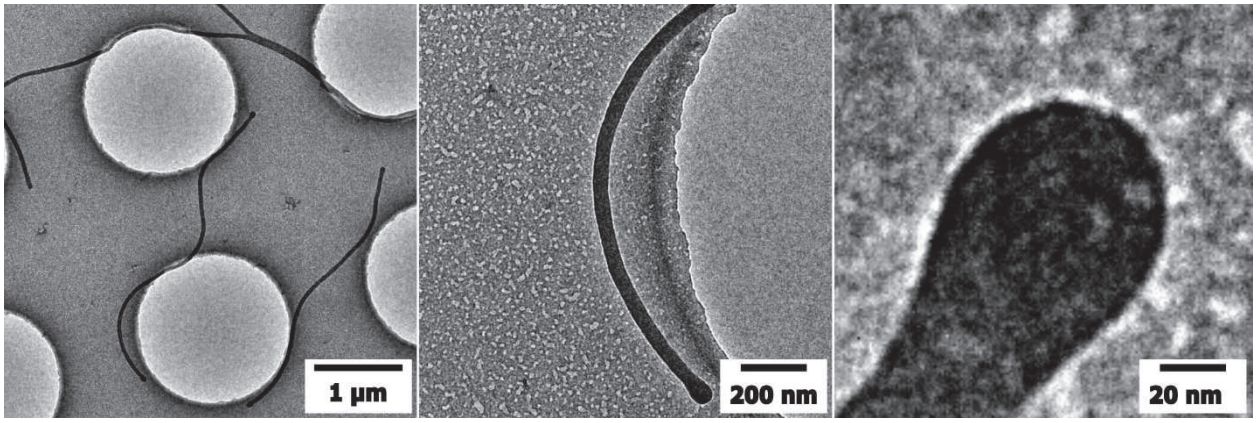

Figure 5 Transmission Electron Microscopy images of the plain block copolymer micelles. On the right is a close-up image showing a “head” of a micelle.

Table 1 Diameter and apparent elastic modulus of the PS16k-PEO7.5k elongated micelles for each fraction of added homo polystyrene. Quantities measured from TEM micrographs.

PS8k [wt%]	*Diameter [nm]*	E_{app} *[GPa]*
0	39 ± 2	20.6 ± 4.0
5	43 ± 2	6.6 ± 1.5
20	51 ± 4	4.3 ± 1.7
40	63 ± 4	4.8 ± 1.3

As mentioned in the Introduction, the preparation of partially suspended elongated micelles for three point bending tests has been achieved mostly by drop-casting a solution of elongated micelles onto a microporous substrate.[1,25] We approached the problem in a more rational way using the technique of Glazer et al.[33] Highly ordered arrays of elongated micelles are achieved by adding a droplet of elongated micelle solution onto micro-patterned poly(dimethylsiloxane) (PDMS) stamps with regularly spaced micro-pillars and dragging this droplet along one direction with the help of a paper tissue. The elongated micelles are pinned onto the PDMS pillars thanks to the drying and dragging effect and the formation of dewetting defects and are aligned across several pillars in the flow direction of the solution. A schematic overview of the sample preparation is shown in Figure 6.

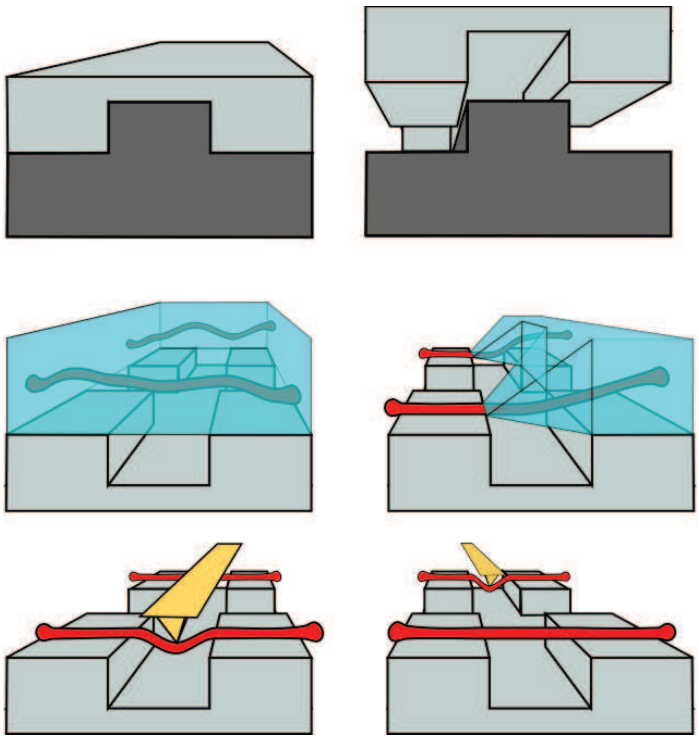

Figure 6 Schematic overview of the sample preparation. In the top row the PDMS stamps are removed from thesilicon molds. In the middle row the micelle in water solution is deposited onto the pillars. The micelles are then adsorbed on the pillars by the formation of dewetting defects. Once the sample is dry AFM measurements are possible on the partially suspended elongated micelles.

To verify the order achieved with such a technique we performed Scanning Electron Microscopy on the PDMS samples. A SEM image of a sample of suspended elongated micelles is shown in Figure 7.

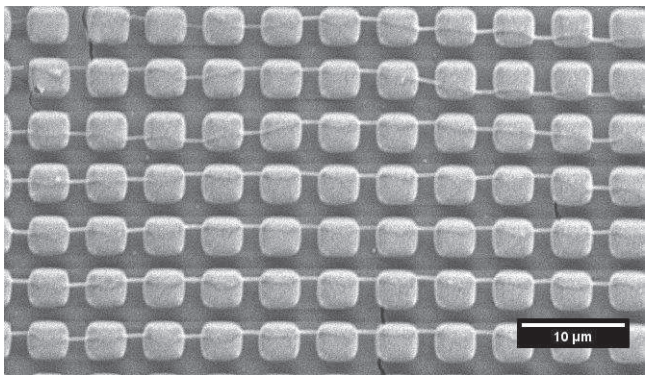

Figure 7 SEM micrograph of the aligned PS-PEO elongated micelles on PDMS pillars. This image shows the high degree of ordering of the nanowires on the pillars.

Once the samples were successfully prepared, it was possible to use them to determine the mechanical properties of the micelles by AFM. Although the elongated micelles have a core-shell structure, the Young's modulus of the PEO shell, considering the molecular weight used, is orders of

magnitude smaller than that of the PS core.[39] This allows us in a first approximation to neglect the contribution of the shell and to consider the elongated micelles as a uniform PS rod. Without any surface tension or supramolecular contributions the expected modulus should therefore be in the range of that of bulk polystyrene: ~ 3.5 GPa.

After obtaining a topography scan and localizing the suspended elongated micelles, the AFM tip is used to apply a force on the central point of the suspended elongated micelle (schematic illustration in Figure 8). Knowing the mechanical properties of the cantilever being used, the force vs displacement curve is obtained from which the properties of the elongated micelle can be determined.

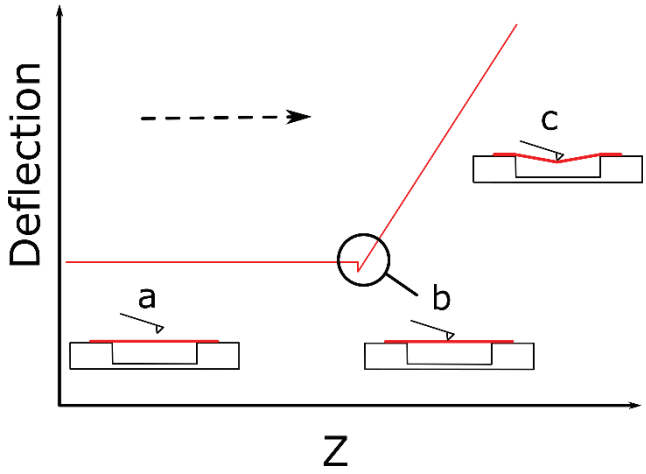

Figure 8 Schematic overview of a bending test force curve. The red curve indicates the deflection as a function of the Z position of the cantilever. The dashed black arrow indicates the travel direction of the cantilever. In section a there is no contact between the elongated micelle and the tip and therefore no deflection is registered. In point b contact is made between the tip and the sample. Finally in section c the linear slope which corresponds to the bending of the elongated micelle is measured as a deflection.

Using the classical Euler-Bernoulli beam theory and assuming a clamped configuration in which the elongated micelles are not sliding along the pillars, for small beam displacements the force-displacement curve will be linear and described by Equation 4:

$$F = \frac{192 E_{app} I}{L^3} d \qquad \text{Equation 4}$$

Where: *F* is the force applied by the AFM tip, *d* the beam deflection in the *z* direction, *L* the length of the suspended beam, E_{app} is the apparent Young's modulus that is given not only by bulk material properties, but also by surface tension and confinement effects, and *I* is the second moment of inertia of the elongated micelle. Approximating the elongated micelle as a uniform cylinder $I = \pi D^4/64$. The slope of the indentation curve, corresponding to the stiffness of the beam, is used to derive the apparent Young's modulus. The values for the apparent Young's modulus are shown in Table 1. An example of the force curved used to obtain this data is shown in Figure 9. The spring constant of the

different elongated micelles corresponds to the slope of the curves. Since the spring constant is not a material property, but it depends on the geometry of the sample in exam, the trend of these slopes is not obvious.

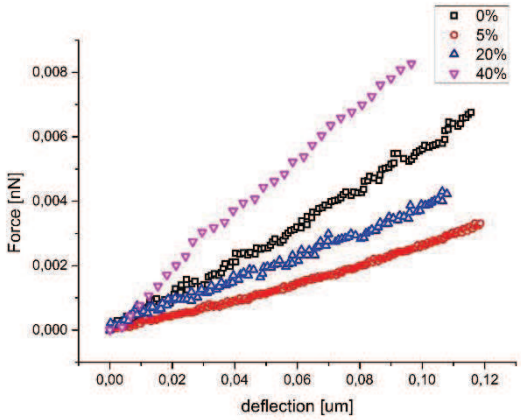

Figure 9 Force vs deflection for each different suspended elongated micelle. Each curve shows an elongated micelle with a different homopolymer concentration.

The values obtained show a significant difference between the pure block copolymer elongated micelles and those formed adding extra polystyrene. The high surface to volume ratio of these elongated micelles needs to be taken into account when determining their mechanical properties. To do this we use the model provided by Cuenot et al.[26] which considers the influence of the increasing surface area during bending deformation. Using the following equation (Equation 5) we can take into account the contribution to the modulus which is given by the surface energy of the elongated micelle:

$$E = E_{app} - \frac{8}{5}\gamma(1-\nu)\frac{L^2}{D^3} \qquad \textit{Equation 5}$$

Where the surface energy is approximated to γ = 40 mJ/m^2 and ν = 0.4 is used for the Poisson ratio. Both these values are in agreement with experimental values obtained for both PS and PEO.[41] *L* and *D* are the length and diameter of the elongated micelle respectively. The values of the apparent elastic modulus of the micelles can be corrected from the contribution given by the increase in surface area during bending. The results obtained are shown in Figure 10 together with the diameter of the elongated micelles as a function of added homopolymer.

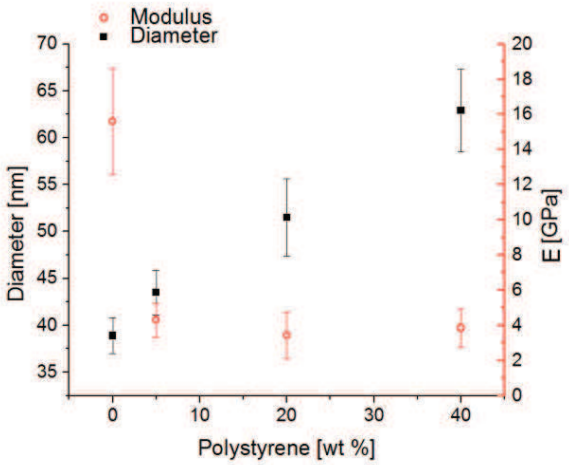

Figure 10 Diameter (in black squares) and Young's modulus (in red open circles) of the elongated micelles as a function of added homo-polymer. The errors on the diameter measurements are given by the standard deviation of the measurements. The errors on the moduli are given by the propagation of the ones on the diameters.

These values show a clear difference between the block copolymer elongated micelles and those that have been swollen using the homopolymer. The former ones have a Young's modulus which is 4 - 5 fold higher than bulk polystyrene while the latter ones are very close to bulk values of PS. This effect can be ascribed to the crystallinity of the PEO corona which was assessed performing differential scanning calorimetry on the different elongated micelles. The DSC results, rescaled relative to the block copolymer mass in the sample, are shown in Figure 11.

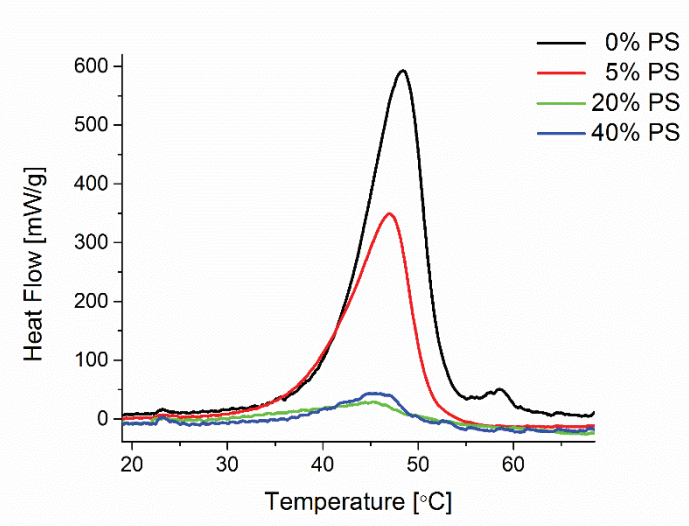

Figure 11 Differential Scanning Calorimetry of the elongated micelles for each homopolymer fraction. The data shown corresponds to the second heating scan at a rate of 10.00 °C/min. The data is expressed in mW/g where the mass is given by the block copolymer mass in the sample. The peak at 45-50 °C corresponds to the fusion of PEO crystallites. The addition of homopolymer hinders the formation of such crystallites reducing the peak intensity.

A clear difference is visible in the crystallization peak of the PEO block which is found at 45-50°C. The area under the peaks is directly related to the amount of crystallites which are melting once the temperature of fusion of PEO is reached. Already in the sample with 5% added polystyrene there is a

45% decrease of the area under the peak, in the 20% and 40% samples the peak is reduced by more than 90%. Once the elongated micelles are swollen with homopolymer in their core, the corona grafting density will decrease. This decrease in chain density can induce a transition of the corona conformation from brush to a mushroom regime.[42] This will cause a decrease in the density of crystallites in the corona of the elongated micelles. Moreover, a different PEO configuration in the various elongated micelles would also suggest that the evaluation of surface energy contributions cannot be done using a constant value. Given the difference in the crystallite density of the PEO it is safe to assume that the surface energy of the corona of pure block copolymer elongated micelles will be higher than that of the homopolymer swollen ones. If we would consider the modulus of the elongated micelles to be that of bulk polystyrene we could, using Equation 5, estimate the maximum value for the surface energy of the crystalline PEO corona to be 260 mJ/m^2. While it is safe to assume this value as the upper limit for the surface energy of the PS-PEO elongated micelles, this quantity is an overestimate. This is due to the fact that in this model the contribution of the stiff PEO crystalline corona was not taken into account in the evaluation of the apparent modulus.

4.3 Conclusions

In conclusion we developed a rational and versatile procedure for the determination of the Young's modulus of self-assembled poly(styrene)-poly(ethylene oxide) core-shell elongated micelles by three point bending tests. Moreover, the method presented here can be universally applied to polymer fibers, copolymer elongated micelles and DNA[31,32] and eliminates the substrate-sample influence on the results, a crucial step when dealing with supramolecular systems. We find that in pure PS-PEO copolymer elongated micelles, due to the supramolecular organization of the corona and core chains, the obtained modulus exceeds that of bulk polystyrene. This is due to a contribution given by the crystalline PEO corona which directly acts on the apparent modulus while also affecting the surface energy of the elongated micelle. The addition of polystyrene in the core of the elongated micelles contributes to an increase in diameter and at the same time to a decrease in crystallinity of the corona chains. This results in effectively more flexible elongated micelles whose properties approach those of bulk polystyrene.

4.4 Experimental Section

Materials

Both polymers poly(styrene)-b-poly(ethylene oxide), PS_{16k}-$PEO_{7.5k}$, and polystyrene PS8k, were purchased from PolymerSource (Canada). Chloroform anhydrous 99.9% stabilized with ethanol and the Fluorescent Dye 1,1'-dioctadecyl-3,3,3'3'-tetramethylindocarbocyanine perchlorate (DiI) were purchased from Sigma Aldrich.

Elongated micelle preparation

Stock solutions of 10 mg/mL polymer in chloroform were prepared with 0, 5, 20 and 40% of polystyrene to poly(styrene)-b-poly(ethylene oxide) weight fractions. The elongated micelles were prepared by adding 10 µL of stock solution onto 1 mL of milliQ water using the technique described in chapter 3. The vials used had a volume of 4 mL. The caps of the vials were closed and the chloroform evaporated at room temperature. The evaporation of the chloroform droplets causes a local increase in copolymer concentration which results in the formation of the elongated micelles as explained in chapter 3.

Fluorescence Microscopy

For the experiments with fluorescence microscopy 0.2 wt% of DiI (ex: 549 nm, em: 565) was added to the copolymer in the chloroform stock solution. A Nikon Eclipse TE2000E inverted microscope was used to image the elongated micelles while in water solution.

PDMS stamps preparation

The PDMS arrays of micropillars were produced by soft lithography. A master silicon mold with etched square prisms was produced by means of Deep Reactive Ion Etching. The surface of the silicon mold was treated with the vapors of a silanizing agent (Tridecafluoro-1,1,2,2-tetrahydrooctyl)trichlorosilane (ABCR, AB111444). A two component Silgard® 184 (Dow Corning) silicone elastomer kit was poured in a petri dish containing the mold. After degassing the cast polymer is cured at 60 degrees overnight.

Elongated micelle deposition

The elongated micelles were deposited on the pillars by placing a 100 µL elongated micelle solution over the patterned surface of the stamp and dragging it in one direction by capillary force using a precision wipe. The pillars act as wetting defects while the water slides over the air cushion formed in the gap between them. The hydrophilic shell of the elongated micelles is pinned on the pillars during this process and they are aligned in the direction of the droplet flow.

Scanning Electron Microscopy

SEM was performed using a FEI/Philips XL30 SFEG microscope. PDMS stamps with suspended elongated micelles were sputtered with gold (gold layer thickness: 4 nm, deposition rate 1.3nm/min) and imaged.

Transmission Electron Microscopy

A droplet of elongated micelle solution was deposited and dried on Quantifoil 1.2/1.3, Cu 200 mesh grids. The grids were imaged using a Jeol JEM transmission electron microscope at an accelerator voltage of 120 keV on a JEOL EM-11210SQCH Specimen Quick-change holder. The diameter of the elongated micelles was measured from the micrographs using ImageJ.

Atomic Force Microscopy

The atomic force microscopy measurements were performed using an NT-MDT NTEGRA microscope and NSG03 probes. Topography scans were performed in semicontact mode. The spring constant of the cantilevers was determined by thermal noise method. Force curves were performed on the central point of suspended elongated micelles.

Force Curve Acquisition and Conversion

The force curves were performed on the central point of the suspended micelles obtained from the topography scans. The raw force curves were obtained as cantilever deflection as a function Z position of the cantilever and an example is shown in Figure 12.

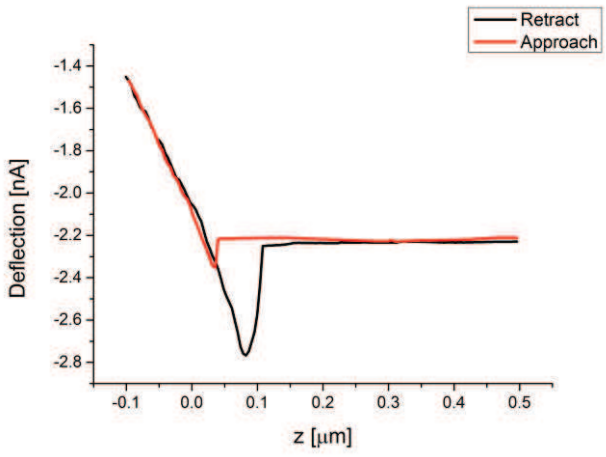

Figure 12 Example of a force curve on a suspended micelle.

The non-destructivity of the measurements was ensured by repeating the force curves several times on the same suspended micelles and verifying that the same results would be obtained through consecutive measurements. This can be seen from the overlay of eight consecutive force curves overlaid in Figure 13. Moreover, the micelles could still be imaged in topography scans after the force curve acquisition.

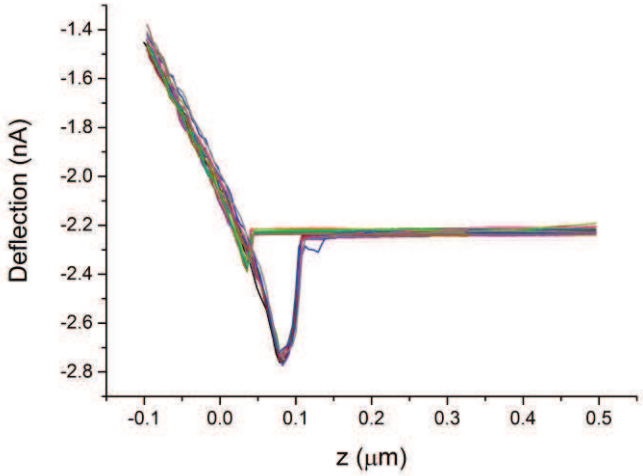

Figure 13 Overlay of eight force curves consecutively performed on a single suspended micelle. The same slope was obtained from all the measurements.

The force curves were converted into Force vs indentation depth by knowing the spring constant of the cantilever used and the deflection sensitivity of the cantilever. The latter was evaluated by performing a force curve on a bare silicon substrate and obtaining the slope of the curve. For reference, an overlay of a force curve on bare silicon, and one on a suspended micelle are shown in Figure 14.

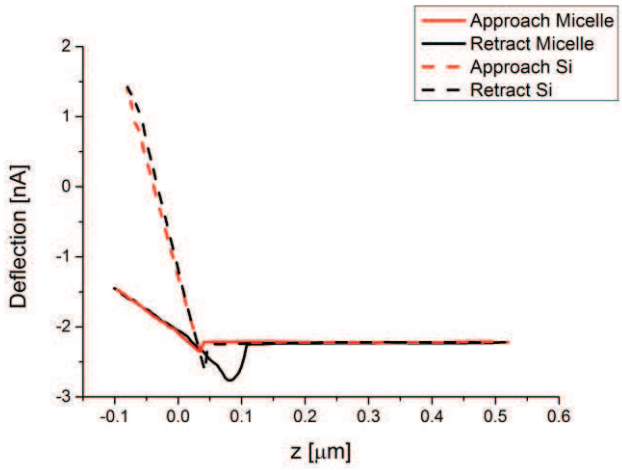

Figure 14 Overlay of the same force curve shown in Figure 12 together with a force curve performed on a bare silicon substrate. The contact point of both approach curves was matched.

From these it was possible to obtain the force curves expressed as Force per indentation depth. This was done only for the approach curves which were the ones necessary to estimate the spring constant of the suspended micelles. Moreover, only the portion following the contact between the tip and the micelle was shown. An overlay of the converted curves is shown in Figure 15.

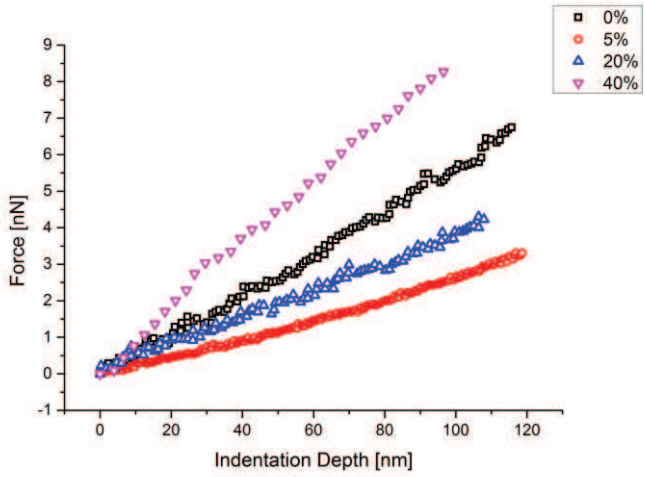

Figure 15 Force vs deflection for each different suspended elongated micelle. Each curve shows an elongated micelle with a different homopolymer concentration.

The slope of these curves corresponds to the spring constant *(k_m)* of the micelles which can be used to evaluate their elastic modulus using the following form of equation 6:

$$E_{app} = \frac{192\,I}{L^3}\frac{F}{d} = \frac{192\,I}{L^3}k_m \qquad \textit{Equation 6}$$

This model is applicable since the spring constant of the cantilevers used was an order of magnitude larger than that of the micelles.

The major contribution to the error on the moduli is given by the uncertainty on the diameter measurement which appears in the area modulus of inertia.

Differential Scanning Calorimetry

The samples were dried using a FreeZone 4.5 Liter lyophilizer. Samples were prepared in stainless steel holders and analyzed using a DSC 8500 Perkin-Elmer. A heating rate of 10 degrees per minute was used. The data shown corresponds to the second heating round.

4.5 References

[1] S. Shanmugham, J. Jeong, A. Alkhateeb, D. E. Aston, *Langmuir* **2005**, *21*, 10214–10218.

[2] F. Gu, L. Zhang, X. Yin, L. Tong, *Nano Lett.* **2008**, *8*, 2757–2761.

[3] H. Liu, J. Kameoka, D. Czaplewski, H. G. Craighead, *Nano Lett.* **2004**, *4*, 671–675.

[4] K. Ramanathan, M. A. Bangar, M. Yun, W. Chen, A. Mulchandani, N. V. Myung, *Nano Lett.* **2004**, *4*, 1237–1239.

[5] Y. Cao, A. E. Kovalev, R. Xiao, J. Kim, T. S. Mayer, T. E. Mallouk, *Nano Lett.* **2008**, *8*, 4653–4658.

[6] B. Pittenger, N. Erina, C. Su, *Appl. Note Veeco Instruments Inc* **2010**.

[7] I. Malovichko, S. Leesment, J. Alexander, S. Belikov, C. Wall, I. Yermolenko, S. Magonov, **n.d.**, 7–12.

[8] D. Guo, J. Li, G. Xie, Y. Wang, J. Luo, **2014**.

[9] E. P. S. Tan, C. T. Lim, *Appl. Phys. Lett.* **2005**, *87*, 1–3.

[10] C. Rivetti, M. Guthold, C. Bustamante, *J. Mol. Biol.* **1996**, *264*, 919–932.

[11] P. a Wiggins, T. van der Heijden, F. Moreno-Herrero, A. Spakowitz, R. Phillips, J. Widom, C. Dekker, P. C. Nelson, *Nat. Nanotechnol.* **2006**, *1*, 137–141.

[12] K. Rechendorff, G. Witz, J. Adamcik, G. Dietler, *J. Chem. Phys.* **2009**, *131*, 16–20.

[13] J. Bednar, P. Furrer, V. Katritch, A. Z. Stasiak, J. Dubochet, A. Stasiak, *J. Mol. Biol.* **1995**, *254*, 579–594.

[14] C. Frontali, E. Dore, A. Ferrauto, E. Gratton, A. Bettini, M. R. Pozzan, E. Valdevit, *Biopolymers* **1979**, *18*, 1353–1373.

[15] J. F. Smith, T. P. J. Knowles, C. M. Dobson, C. E. Macphee, M. E. Welland, *Proc. Natl. Acad. Sci. U. S. A.* **2006**, *103*, 15806–15811.

[16] S. M. Cook, K. M. Lang, K. M. Chynoweth, M. Wigton, R. W. Simmonds, T. E. Schäffer, *Nanotechnology* **2006**, *17*, 2135–2145.

[17] C. T. Gibson, D. Alastair Smith, C. J. Roberts, *Nanotechnology* **2005**, *16*, 234–238.

[18] R. Lévy, M. Maaloum, *Nanotechnology* **2001**, *13*, 33–37.

[19] H. Hertz, *J. fur die reine und Angew. Math.* **1881**, *92*, 156–171.

[20] K. L. Johnson, K. Kendall, A. D. Roberts, in *Proc. R. Soc. London A Math. Phys. Eng. Sci.*, **1971**, pp. 301–313.

[21] B. V. Derjaguin, V. M. Muller, Y. P. Toporov, *Prog. Surf. Sci.* **1994**, *45*, 131–143.

[22] Y. Q. Chen, X. J. Zheng, S. X. Mao, W. Li, *J. Appl. Phys.* **2010**, *107*, DOI 10.1063/1.3402937.

[23] Y. Ji, B. Li, S. Ge, J. C. Sokolov, M. H. Rafailovich, *Langmuir* **2006**, *22*, 1321–1328.

[24] Y. J. Kim, K. Son, I. C. Choi, I. S. Choi, W. Il Park, J. Il Jang, *Adv. Funct. Mater.* **2011**, *21*, 279–286.

[25] S. Cuenot, C. Frétigny, S. Demoustier-Champagne, B. Nysten, *J. Appl. Phys.* **2003**, *93*, 5650–5655.

[26] S. Cuenot, C. Frétigny, S. Demoustier-Champagne, B. Nysten, *Phys. Rev. B* **2004**, *69*, 1–5.

[27] S. Cuenot, S. Demoustier-Champagne, B. Nysten, *Phys. Rev. Lett.* **2000**, *85*, 1690–1693.

[28] A. Arinstein, M. Burman, O. Gendelman, E. Zussman, *Nat. Nanotechnol.* **2007**, *2*, 59–62.

[29] A. Arinstein, E. Zussman, *J. Polym. Sci. Part B Polym. Phys.* **2011**, *49*, 691–707.

[30] M. Burman, A. Arinstein, E. Zussman, *EPL (Europhysics Lett.* **2011**, *96*, 16006.

[31] J. Guan, B. Yu, L. J. Lee, *Adv. Mater.* **2007**, *19*, 1212–1217.

[32] J. Guan, P. E. Boukany, O. Hemminger, N.-R. Chiou, W. Zha, M. Cavanaugh, L. J. Lee, *Adv. Mater.* **2010**, *22*, 3997–4001.

[33] P. J. Glazer, L. Bergen, L. Jennings, A. J. Houtepen, E. Mendes, P. E. Boukany, *Small* **2014**, *10*, 1729–1734.

[34] R. Granek, R. C. Ball, M. E. Cates, *J. Phys. II* **1993**, *3*, 829–849.

[35] J. Zhu, R. C. Hayward, *J. Am. Chem. Soc.* **2008**, *130*, 7496–7502.

[36] S. Jain, F. S. Bates, *Macromolecules* **2004**, *37*, 1511–1523.

[37] Y. M. Wang, C. M. Kausch, M. S. Chun, R. P. Quirk, W. L. Mattice, *Macromolecules* **1995**, *28*, 904–911.

[38] T. Nicolai, O. Colombani, C. Chassenieux, *Soft Matter* **2010**, *6*, 3111–3118.

[39] A. Jee, H. Lee, Y. Lee, M. Lee, *Chem. Phys.* **2013**, *422*, 246–250.

[40] S. Timoshenko, J. M. Gere, *Theory of Elasticity Stability*, McGraw, **1961**.

[41] D. K. Owens, R. C. Wendt, *J. Appl. Polym. Sci.* **1969**, *13*, 1741–1747.

[42] P. Kingshott, H. Thissen, H. J. Griesser, *Biomaterials* **2002**, *23*, 2043–2056.

5 *In vitro* & *In vivo* evaluation of spherical and elongated PS-PEO micelles*

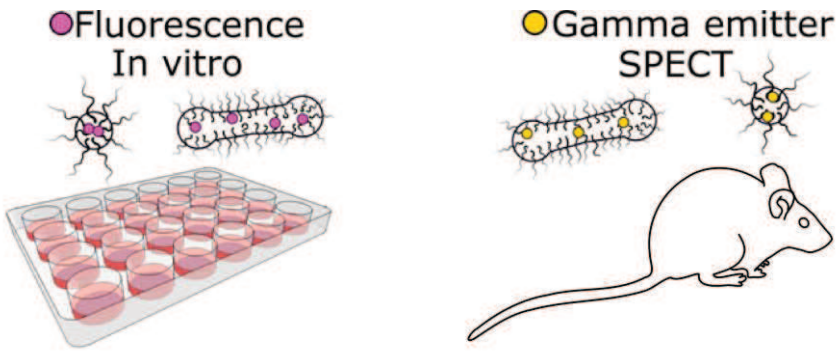

Understanding how nanoparticle properties such as size, shape and surface functionality influence their biodistribution and circulation time, is essential for the development of therapies base on the Enhanced Permeability and Retention. In this chapter an assessment of the influence of morphology on *in vivo* biodistribution was tackled using polystyrene-b-poly(ethylene oxide) micelles of spherical (mean diameter of 170 and 106 nm) and elongated (mean diameter/length of 92/600 nm) morphologies. The glassy nature of polystyrene guarantees the morphological stability of the carriers *in vivo*. Using HeLa cells the cytotoxicity of the particles was evaluated and the cellular uptake was studied *in vitro* by incorporating the fluorescent dye DiI. Finally, by encapsulating ^{111}In in the core of the carriers, an assessment of the longitudinal *in vivo* biodistribution of the particles in healthy mice was performed with low-dose SPECT scans at 0, 24 and 48 hours post injection. Quantified SPECT scans illustrated prolonged blood circulation, longer than 24 hours, for all micelles studied. Dynamics of micelle accumulation in the liver and other organs of the Reticuloendothelial System showed a size-dependent nature and late stage liver clearance was observed for the elongated morphology. Our results can contribute to the design of new diagnostic and therapeutic nanoparticles and to the optimization of existing EPR-based therapies.

* Chapter based on: *In vivo* Biodistribution of Stable Spherical and Filamentous Micelles Probed by High-sensitivity SPECT

Laurence Jennings, Oleksandra Ivashchenko, Irene J. C. Marsman, Adrianus C. Laan, Antonia G. Denkova, Gilles Waton, Frederik J. Beekman, François Schosseler, Eduardo Mendes

Under Review in Advanced Healthcare Materials

5.1 Introduction

It is often the case for drug molecules to have poor water solubility. This renders the ability to design highly potent drugs useless unless it is coupled with the ability to deliver them to the specific site which requires treatment. The general strategy to enhance the solubility and delivery of hydrophobic drugs is to encapsulate them into a nano or microcarrier. The most common approaches towards encapsulation of drugs include both liquid (i.e. nano-emulsions) or solid (e.g. nanoparticles, micelles, liposomes, dendrimers…) vehicles. The development of nanocarriers is a complex task which requires a broad knowledge spanning from the chemical synthesis and physicochemical characterization to create the nanoparticles and tune their properties, and finishing with a thorough knowledge of the biological processes which affect the behavior of the nanoparticles *in vivo*.

While the previous chapters covered the purely physicochemical aspect of formation and characterization of the micelles, this chapter will be focused on how these properties will affect their performance in-vitro and in-vivo.

The obstacles for targeted therapy using nanoparticles are given by the same mechanisms and barriers which prevent foreign objects, such as microbes and viruses, from entering and harming a living host. Throughout evolution, we developed a complex immune system which works in perfect balance with our tissues and organs, each of which contains physical and chemical barriers allowing to maintain the required equilibrium of the physiological processes.

The main organs and tissues which actively take part in the clearance of foreign particles are the blood, kidneys, liver and spleen. Since the most common administration pathway for nano and microparticles is by intravenous injection, all of these tissues and organs will contribute to the biodistribution of the particles. The injected solution travels with the blood towards the heart, through the right ventricle and subsequently through the lungs. Here in the lungs a first passive filtering mechanism is performed by the fine capillary network with diameters ranging from 3 to 6 µm. If the particles are able to pass through this network, they are transported with the blood to the left ventricle. From there they are transported with the oxygen rich blood towards the kidneys, liver, spleen, gut and the central nervous system. Each of these organs provides one or more, active or passive, filtering mechanisms to capture, promote clearance or directly expel foreign objects.

Throughout the permanence of nanocarriers in circulation there will be an interaction with the proteins present in the blood. The most abundant protein in plasma is human albumin, a 67 kDa protein. Albumin is known to have non-specific interactions with hydrophobic particles.[1,2] By physical

adsorption on nanoparticles, albumin can slightly increase the circulation time of nanoparticles, and by effectively enlarging the nanoparticle it will reduce renal clearance.[3,4]

Another family of proteins which interact with hydrophobic nanocarriers are the lipoproteins and apolipoproteins which are responsible for the transport of lipids in the bloodstream. These are particularly important because of their interaction with liposomes. Lipoproteins are known to exchange phospholipids with the liposomes causing their destabilization and release of encapsulated substances.[5–7]

Finally there is the complement system, composed by a number of small proteins and part of the innate immune system, which takes his name from the fact that it complements the ability of antibodies and phagocytes in clearing foreign object from circulation. The complement system can be activated directly by pathogens or indirectly by pathogen bound antibodies. This leads to a cascade of reactions occurring on the surface of pathogens which results in the formation of active components. The opsonins and dysopsonins proteins of the complement system are responsible for the accelerated clearance of nanoparticles from circulation by liver and spleen respectively.[2,8] These bind to the surface of nanoparticles activating the complement cascade making the nanoparticles susceptible to macrophage recognition and phagocytosis.[9,10] Opsonization depends on surface properties and hydrophobicity of the carriers and PEO coating is still the golden standard to reduce opsonization.[11,12] Block copolymer micelles containing a PEO block have the advantage of having an intrinsic PEO shell avoiding the need for PEGylation.

The next filtration stage occurs within the kidneys. These are divided into two sections, the outer cortex and the inner Medulla. A capillary network in the cortex, the glomerulus, has the function of filtering the blood thanks to a highly fenestrated endothelium.[13] This is followed by the glomerular basement membrane which contributes to the filtration of negatively charged components in the blood.[13] These two filtration mechanisms are accompanied by the presence of mesangial cells which possess phagocytic properties and prevent the accumulation of debris within the kidneys.[14] The kidneys can allow the passage of very small nanoparticles such as quantum dots (~5 nm). Most block copolymer micelles will be too large to be filtered by the kidneys.[15]

The liver performs his filtration through a series of permeable discontinuous capillaries known as sinusoids. These have a diameter of a few microns (5-10) and a pore size of 100 - 150 nm. Here are the Kupfer cells which compose the 80-90% of the total number of macrophages in the body and belong to the Reticuloendothelial System (RES). Particle size plays an important role on Kupfer cell phagocytosis. Larger particles require more energy for the deformation of the macrophage cytoskeleton. Together with the size, the radius of curvature of the particles has an effect on the

particles.[16–18] The liver is one of the organs of the RES which should be mostly affected by the shape effects of nanoparticles. This was shown by *in vitro* tests which have shown that high aspect ratios particles can reduce phagocytosis.[19–21]

Finally the spleen is another organ which has several sieving mechanisms. The blood flow is divided into two pathways: one is a closed vasculature system and the other is an open one. In the open vasculature, the blood is directed towards the parenchyma which is divided into red and white pulp where phagocytes and lymphocytes are respectively found. High stiffness and sizes above 200 nm are known to contribute to splenic sequestration of nanocarriers.[22–24] The spleen of mice is different from the spleen of humans or rats since it lacks the sinusoids in the closed vasculature system network. Due to this difference, particular caution is necessary when trying to translate spleen uptake of nanoparticles between mice and humans since it is known that different areas of the spleen contribute to particle retention.[23]

All these filtration mechanisms already provide the guidelines for the production of correctly sized and shaped nanoparticles. However, since the final objective of this project is the development of EPR therapies, it is necessary to also take into account other parameters when designing nanoparticles for targeted radionuclide therapy. With respect to healthy tissues, solid tumors have an excessive growth rate which causes an oxygen depletion in their core. As a consequence, the tumor releases cytokines and signaling molecules that induce the formation of new blood vessels.[25,26] These are highly defective blood vessels characterized by gaps of 600 to 800 nm[27] between the endothelial cells, promoting the EPR effect.[28,29] A plethora of nanoparticles have been formulated to study their ability to passively target tumors through this effect. These have been object of studies on their *in vivo* biodistribution,[30] cell penetration[31] and tumor penetration.[32]

From what was discussed earlier, it is clear that the behavior of nanoparticles *in vivo* is strongly affected by their size, surface chemistry and mechanical properties. The large nano- (diameter > 200 nm) and micro-particles are generally cleared from the blood circulation within the first hour after administration. At the same time, particles below 6 nm are also rapidly cleared by the kidneys. The combination of an average size ($10 < d < 150$ nm) and neutral surface charge allows the particles to reach the longest *in vivo* circulation times by not being recognized as foreign bodies.[33] Prolonged circulation time is an aspect of fundamental importance when exploiting the EPR effect since it increases the chances of carrier extravasation. The majority of the studies performed in the field of EPR effect were done using spherical particles. This is partially due to the simplicity of preparation and standardized characterization of spherical particles as opposed to elongated ones. Therefore, the influence of morphology on the behavior *in vivo* is rather unexplored.

In recent years, however, theoretical studies and experimental work have suggested the advantages of using oblate and high aspect ratio particles for biological applications. Decuzzi et al. have shown through simulation that there exists an optimal aspect ratio for particles that maximizes adhesive strength to membranes.[34] Mitragotri et al. have shown that the morphology of polystyrene microparticles influences phagocytosis mechanisms and that elongated polystyrene nanoparticles target lungs and brain endothelium more efficiently than their spherical counterparts.[21,35] Geng et al.[36] have shown in a pioneering work that elongated poly(ethylene glycol)-block-poly(ε−caprolactone) filomicelles significantly outperform spherical ones in terms of circulation time and tumor cell apoptosis when loaded with Taxol. However, the PEO-PCL filomicelles display an elongated to spherical transition due to the hydrolytic degradation of the core forming block. This results in a system which is not ideal to understand the fundamental differences between the biokinetics of spherical and elongated morphology *in vivo*.[37]

Herein we used the polystyrene-b-poly(ethylene oxide) micelles as a model system to perform an *in vitro* and non-invasive *in vivo* study of the effect of micelle morphology on their biokinetics. As shown in the previous chapters, these micelles are frozen in a conformation which is far from equilibrium. This is possible thanks to the high hydrophobicity of the PS block which results in the micelles having no unimer exchange and therefore no equilibrating processes.[38–42] Moreover, it has been shown that PS-PEO micelles, thanks to their strong hydrophobicity, can be used as long circulating carriers.[43] Another advantage of the PS-PEO micelles lies in their formation method through emulsion evaporation. Thanks to this it is possible to encapsulate hydrophobic molecules and apolar complexes in the core of the micelles upon formation. In this chapter, first a fluorescent dye was incorporated and fluorescently labelled micelles were used for *in vitro* cellular uptake experiments. After this, ^{111}In was encapsulated and radiolabeled micelles were used for *in vivo* biokinetics studies by Single Photon Emission Computed Tomography (SPECT) in healthy mice.

Thanks to the recent developments of high resolution preclinical Single Photon Emission Computed Tomography (SPECT) this technique has gained a major importance as a valuable research tool for the study and development of nanocarriers. Radioisotopes emitting γ radiation (high energy photons) are suitable for imaging purposes thanks to their ability to penetrate tissue with minimum interaction. The functioning mechanism of a SPECT equipment is based on the detection of gamma rays onto a photodetector and, through computational algorithms, the source of the photon is estimated. This allows a two dimensional reconstruction of the localization of the gamma emitters. Through the acquisition of reconstructions from different angles it is possible to obtain a three dimensional model of the areas where the gamma emitters are localized. By combining the functional imaging of SPECT

with the anatomical imaging of x-ray computed tomography (CT) it is possible to have an overview of the biodistribution of a particular radiolabeled compound.

5.2 Results and Discussion

Three types of micelles were prepared and characterized to be evaluated in-vitro and in-vivo, the two types of spherical ones, sPSS (spherical Polystyrene small) and sPSL (spherical Polystyrene large), were prepared by tuning the evaporation rate of the organic solvent. Changes in micelle morphology caused by similar conditions have been previously reported in the literature.[44] The larger micelles, sPSL, were obtained through a fast evaporation rate (approximately 4 hours for 100 µL of chloroform in water), while the smaller ones, sPSS, were obtained by a slower more sustained evaporation rate (approximately 24 hours for 100 µL of chloroform in water). The formation of elongated micelles, ePSS (elongated Polystyrene small), was only possible with a slow evaporation rate of the solvent. This is due to the different mechanism behind the formation of the spherical and elongated micelles as described in Chapter 3 of this thesis. The three types of micelles with their forming copolymer and their size characterization performed by dynamic light scattering (DLS), atomic force microscopy (AFM) and scanning electron microscopy (SEM), are reported in Table 1.

Table 1 List of the micelles used. The diameters of the two spherical micelles are hydrodynamic diameters obtained by DLS while the diameter and length of the elongated micelles were obtained by SEM measurements.

Micelle type	*Copolymer*	*Diameter [nm]*			*Length [nm]*
		DLS	AFM	SEM	SEM
sPSS	$PS_{9.5k}$-PEO_{18k}	106 ± 8	120 ± 21	/	/
sPSL	$PS_{9.5k}$-PEO_{18k}	170 ± 7	190 ± 32	/	/
ePSS	$PS_{9.5k}$-PEO_{5k}	/	92 ± 12	31 ± 3	600 ± 310

AFM was used to verify the results obtained by DLS. Topography scans for all three samples are shown in Figure 1.

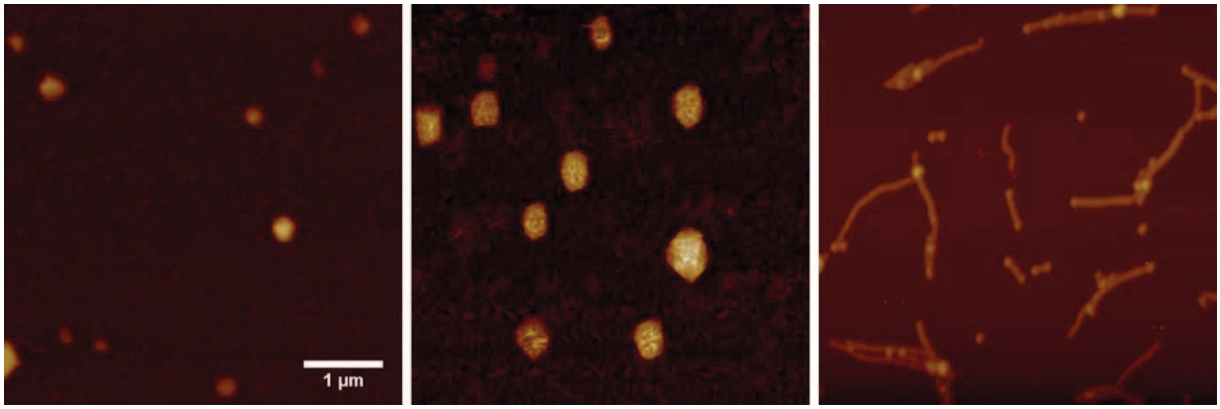

Figure 1 Atomic Force Microscopy semi-contact topography scan of the three micelles. From left to right are the sPSS, sPSL and ePSS micelles. The diameter of the micelles is obtained from the full width at half maximum of the topography scans.

The elongated micelles, ePSS, were too large to be characterized using light scattering so microscopy techniques had to be used. Fluorescence microscopy has been previously used to determine the length distribution of elongated micelles,[36] however, the resolution limit of optical microscopy prevents distinction between anything which is below the diffraction limit of visible light (approximately 200 nm). If the length distribution of elongated micelles is determined by fluorescence microscopy it would appear shifted towards higher values by neglecting the contribution of the smaller micelles. In order to avoid this, SEM was used to determine the length of the micelles.

As shown in the previous chapters, as formed, the elongated micelles have a very broad length distribution that reaches hundreds of microns. In order to make them suitable for in vivo applications, the micelles were shortened using a high power homogenizer. The strong shear stress applied during mixing fractured the micelles and resulted in a more narrow length distribution with an average length of 0.6 µm (Figure 2).

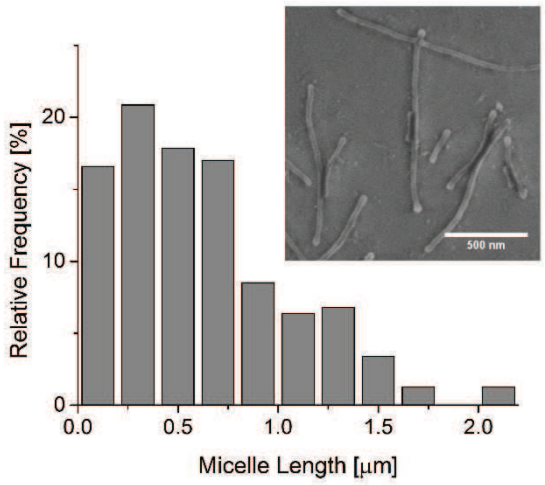

Figure 2 Length distribution of the micelles after homogenization. The longest micelles are fractured into many shorter ones. The lengths were measured from SEM micrographs like the one shown in the inset.

The diameter of the ePSS micelles was also obtained by SEM and AFM and is respectively: d_{SEM} = 31 ± 3 and d_{AFM} = 92 ± 11 nm.

The hydrodynamic diameters obtained by DLS for the spherical micelles, take into account the hydrated poly(ethylene-oxide) corona of the micelles. In contrast, the diameter measured by SEM for the elongated micelles does not take into account the presence of the PEO corona. This is due to the contrast being generated only by the more electronically dense polystyrene core. For this reason, it is not possible to directly compare the values obtained by DLS or by SEM. In order to bridge this difference AFM has been used to study the size of the micelles. The size obtained for the spherical micelles by AFM is consistent with the values obtained by DLS. The value obtained by AFM for the ePSS exceeds that obtained by SEM due to the contribution of the corona. We can conclude that although a direct comparison between the scattering techniques and the microscopy techniques will not be possible, AFM is an appropriate technique when comparing the cross sectional dimensions of block copolymer micelles of different morphologies.

Having characterized the morphology and size of the micelles, their behavior in-vitro was evaluated. The cytotoxicity of the micelles on human cervical (HeLa) cells was determined using the water soluble tetrazolium assay (WST-1) for four micelle concentrations, between ~0.005 mg/mL and ~5 mg/mL, and three incubation times: 24, 48 and 72 hours. The results are shown in Figure 3. At the concentrations used in this work, there is no visible effect of micelle morphology on their cytotoxicity.

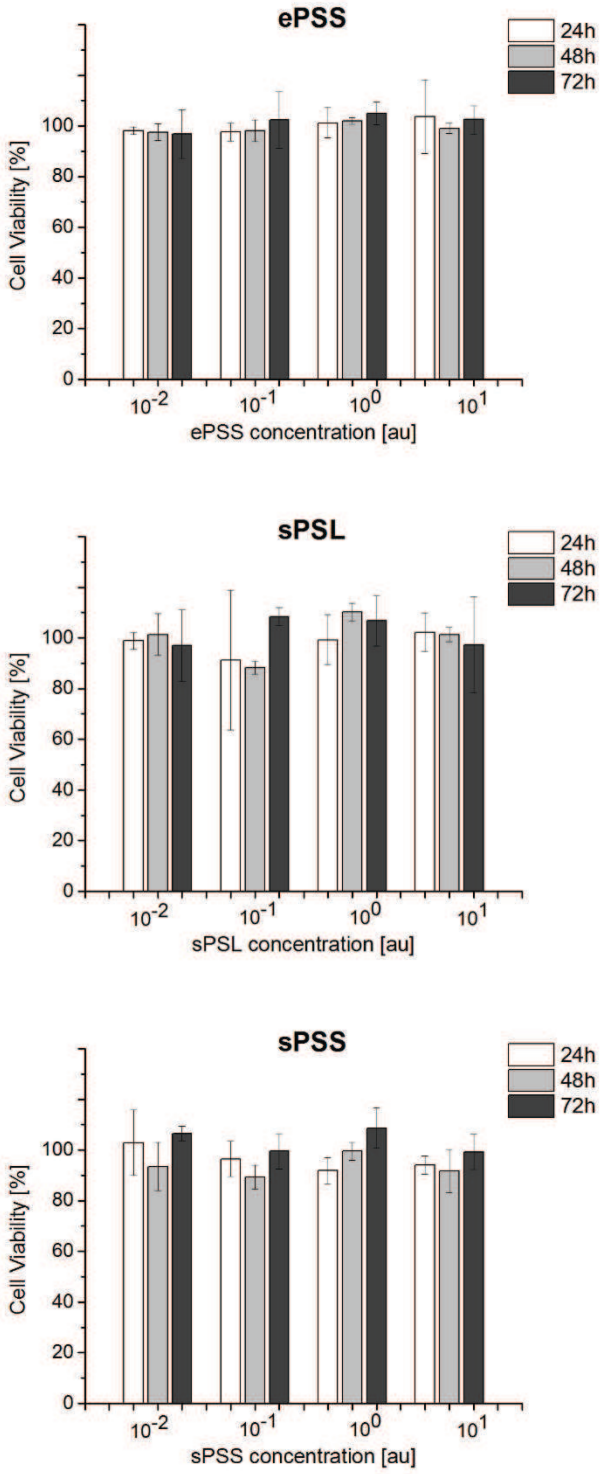

Figure 3 Cell viability for the three micelle morphologies. Four concentrations, from 0.005 mg/mL to 5 mg/mL were tested for three incubation times: 24, 48 and 72 hours. No cytotoxic effects are visible when using the micelles in these doses.

Morphology-dependent cytotoxicity has been previously shown for carbon based, gold and hydroxyapatite nanoparticles.[45–47] Although the cytotoxicity of spherical PS-PEO micelles with various block copolymer molecular weights has already been assessed,[43] this is not the case for elongated PS-PEO micelles. The plain micelles displayed no cytotoxic effects in-vitro up to 5 mg/mL which was

more than double the concentration used for in-vivo studies. This shows how the PS-PEO micelles can be used as a tool to explore possible morphology related improvements to existing therapies.

To further characterize the behavior of the micelles in-vitro, the rate of internalization in HeLa cells of fluorescently labelled micelles was determined using confocal fluorescence microscopy. Micelles were loaded with the fluorescent dye DiI to track their internalization in HeLa cells. The average fluorescence per cell was determined from confocal micrographs and is related to the total amount of fluorescent dye internalized by the cells. The results are shown in Figure 4.

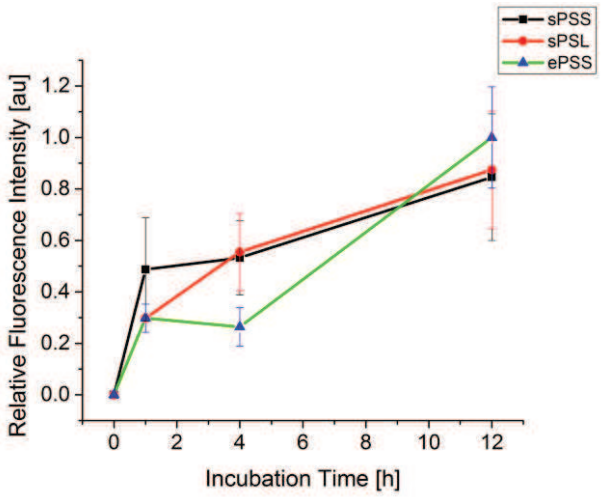

Figure 4 Internalization of spherical and elongated fluorescently labeled micelles in HeLa cells. The fluorescence was measured from CLSM images and averaged per cell. The results are normalized relatively to the maximum fluorescence measured.

A confocal microscopy image of the three cells showing the internalized micelles after 12 hours of incubation time is shown in Figure 5. The micelles appear distributed uniformly within the cytoplasm, however in the case of the ePSS the micelles appear to be accumulating more preferentially surrounding the nucleus.

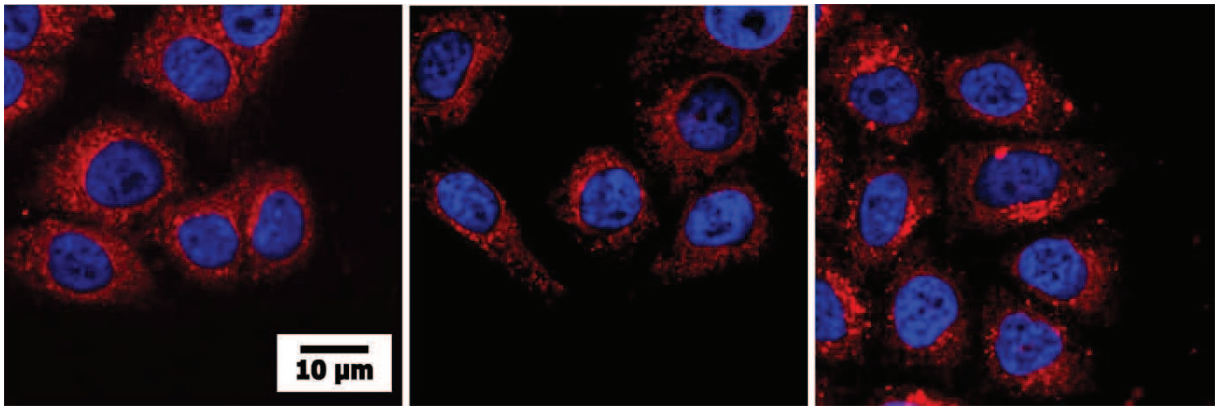

Figure 5 HeLa cells showing the internalized micelles after 12 hours of incubation time. In blue are the nuclei stained with DAPI and in red are the micelles stained with DiI. On the left are the sPSS, in the center the sPSL and on the right are the ePSS. While all micelles appear distributed throughout the cytoplasm, the elongated micelles show more accumulation around the nucleus.

The results show that within the first hour of incubation the smaller spherical micelles, DiI-sPSS, are most rapidly internalized in the cells. After four hours of incubation both spherical micelles (sPSS and sPSL) show the same internalization value while the elongated micelles, DiI-ePSS, are lagging behind. This can be due to the relatively large length distribution of the DiI-ePSS. The micelles on the shorter side of the length distribution will behave similarly to large spherical micelles. However the fraction of longer elongated micelles will be adhering to the cells and internalized through slower pathways.[19] After 12 hours of incubation time, finally, the total amount of fluorescence in the cells is approximately the same for all three micelle types. The apparently faster rate of internalization of the DiI-ePSS in the later stages of internalization is due to the fact that the longer micelles also encapsulate larger amounts of DiI dye per micelle.[36] In order to confirm these results, a full study using flow-cytometry is required.

In order to transition from an in-vitro setting, towards an accurate in-vivo SPECT characterization of the micelles, it was necessary to radiolabel them. The method used to encapsulate the radioisotope ^{111}In in the core of the micelles is based on the method developed by Laan et al. where the isotope is complexed with the lipophilic chelator tropolone. This is a water soluble weakly negatively charged molecule which forms lipophilic complexes with the positively charged ^{111}In (oxidation state of 3+) in water solution at pH 7.4. These lipophilic complexes migrate to the chloroform phase during the evaporation of the emulsion that is required for the formation of the micelles. As the chloroform evaporates, the complex will be entrapped in the hydrophobic core of the micelles.

The encapsulation efficiency depends on the partition of indium-tropolone complexes between the aqueous and organic phases of the emulsion. The unencapsulated ^{111}In is separated from the radiolabeled micelles using size exclusion chromatography. The elution profiles are shown in Figure 6.

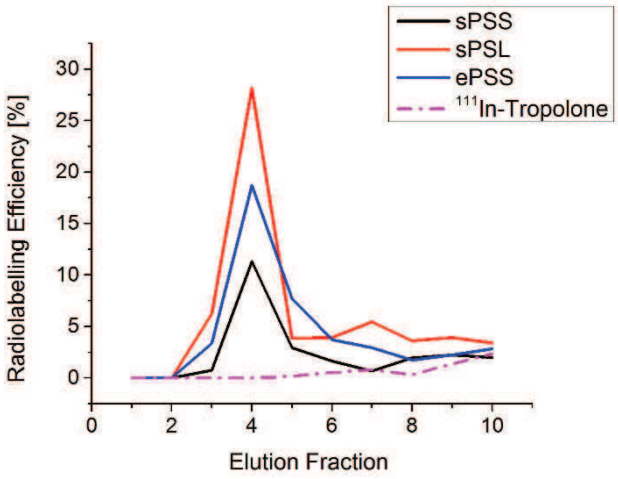

Figure 6 Elution profile of the 111In labelled micelles. Free 111In-tropolone is used as a control. In the first five fractions the micelles are eluted while free 111In-tropolone is retained in the column.

Free ^{111}In-tropolone is shown as a control. By selecting the elution fractions 3 to 5, all free ^{111}In is excluded from the micelle solution. The total radiolabeling efficiencies are shown in Table 2. No changes in size were found when characterizing the plain micelles and the radiolabeled ones.

Table 2 Radiolabeling efficiency of the different micelles.

Micelle type	*Encapsulation efficiency*
^{111}In-sPSS	13%
^{111}In-sPSL	30%
^{111}In-ePSS	22%

This technique represents a very promising one step labelling method that can be applied to different copolymers and different morphologies resulting in a simple pathway towards gamma emitting micellar nanocarriers.

Having radiolabeled micelles it was possible to perform in-vivo studies on the biodistribution of the different micelles in healthy mice. Figure 7A shows the top view maximum intensity projections of follow-up total body SPECT/CT scans for three mice, depicting the longitudinal changes in the biodistribution of ^{111}In-sPSS (top), ^{111}In-sPSL (middle) and ^{111}In-ePSS (bottom) micelles. At the same time, quantified uptake of the compound in multiple organs of interest (Figure 7B) provides an absolute quantitative measure of the micelle distribution in the tissue.

The zero hours post injection (p.i.) images (Figure 7A) illustrate high blood circulation (17.6 ± 3.6 %ID/mL ^{111}In-sPSS, 17.4 ± 6 %ID/mL ^{111}In-sPSL, 15.0 ± 3.6 %ID/mL ^{111}In-ePSS, based on heart uptake values) and rapid spleen uptake (12.2 ± 4.3 %ID/mL ^{111}In-sPSS, 11.0 ± 1.3 %ID/mL ^{111}In-sPSL, 24.7 ± 0.4 %ID/mL ^{111}In-ePSS) for all compounds studied. At the same time, the presence of a renal shell image at 0 hours p.i. scans should indicate fast renal clearance of the compounds. Nevertheless, the near absence of bladder activity accumulation by the end of 0 hours p.i. scans (i.e. 30 minutes p. i.) and the remaining renal cortex shell image on the later stage scans (24 and 48 hours p.i) suggest the trapping of the micelles in the renal cortex tissue. This is consistent with the values of kidney uptake on quantification plots (Figure 7B) that remains on an almost constant level during the three days of follow-up studies. SPECT images at 24 hours p.i. show high level of activity elimination from the main vessels and the heart (6.1 ± 2.2 %ID/mL ^{111}In-sPSS, 4.2 ± 0.6 %ID/mL ^{111}In-sPSL, 4.6 ± 1.3 % ID/mL ^{111}In-ePSS) of the animals, that is later followed by total clearance of the compounds from the blood (to the level of background signal) prior 48 hours p.i. imaging. At the same time, the liver and spleen uptake become more prominent with time. For the ^{111}In-sPSL there is an increase of 3.3 times in the spleen uptake, from 0 to 24 hours p.i., while for the ^{111}In-ePSS the increase is 2.6 times. Liver accumulation of the ^{111}In-sPSS micelles remains almost constant during three days of imaging, while a small increase in spleen accumulation (12.2 ± 4.4, 14.3 ± 1.8 and 17.3 ± 0.9 %ID/mL at 0, 24 and 48 hours p.i) is observed.

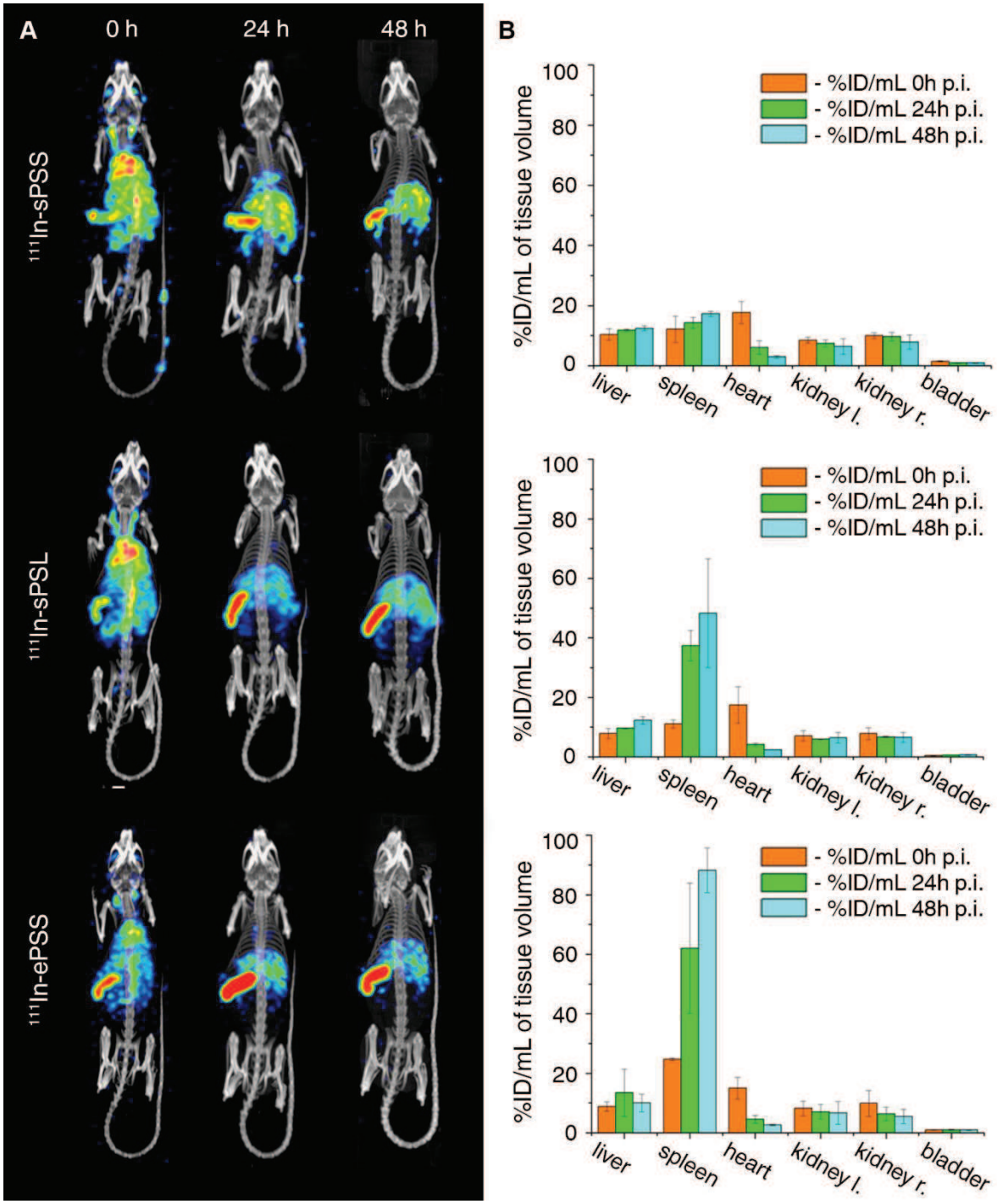

Figure 7 A - Maximum intensity projections of follow-up total body SPECT/CT scans of three mice at 0, 24 and 48 hours post injection of 111In-sPSS (top), 111In-sPSL (middle) or 111In-ePSS (bottom) compound respectively. B - quantified uptake of the compounds in multiple organs of interest, calculated from corresponding SPECT/CT scans.

Fused SPECT/CT slices of 48 hours p.i. scans with focus on the abdominal area of the animal (Figure 8) show detailed late stage biodistribution of ^{111}In-sPSS (top), ^{111}In-sPSL (middle) and ^{111}In-ePSS (bottom) micelles.

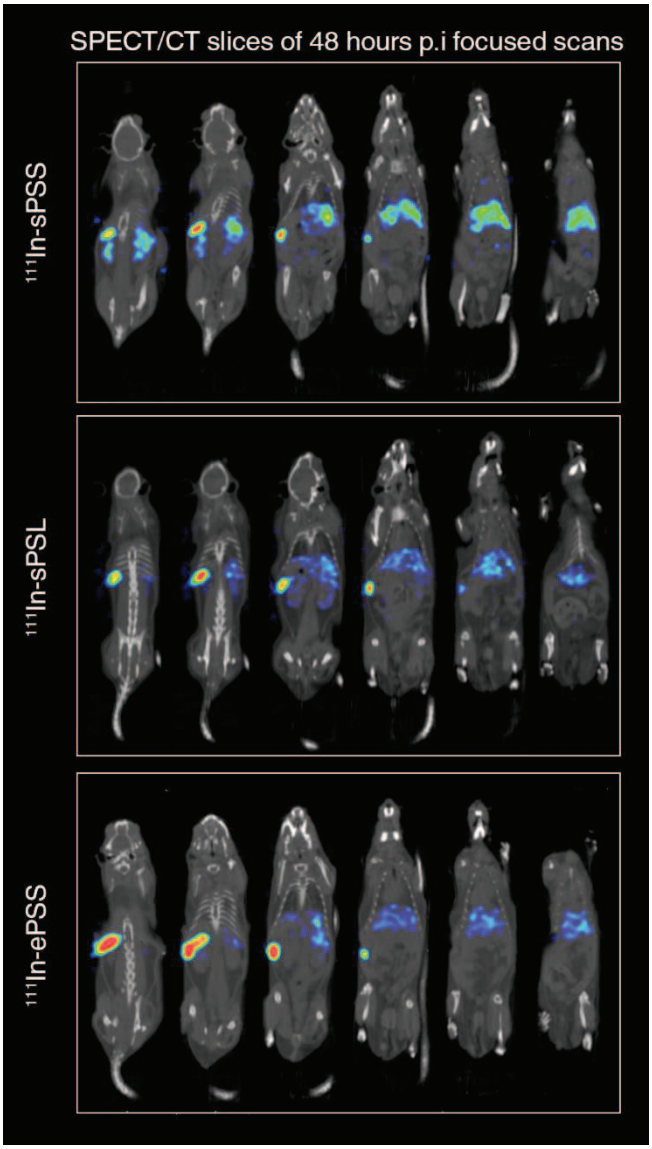

Figure 8 Fused SPECT/CT slices of focused abdominal area scans (right) at 48 hours post injection of 111In-sPSS (top), 111In-sPSL (middle) or 111In-ePSS (bottom) compound respectively.

Closer examination of activity distribution on the coronal slices (Figure 9, Figure 10 and Figure 11) reveals relatively high level of uptake and homogeneous distribution of ^{111}In within the liver for spherical (sPSS, sPSL) and partial clearance of the compound for elongated (ePSS) micelles. The major site of accumulation for all compounds studied was the spleen. At the same time, a remaining signal from the renal cortex shell was present on all images.

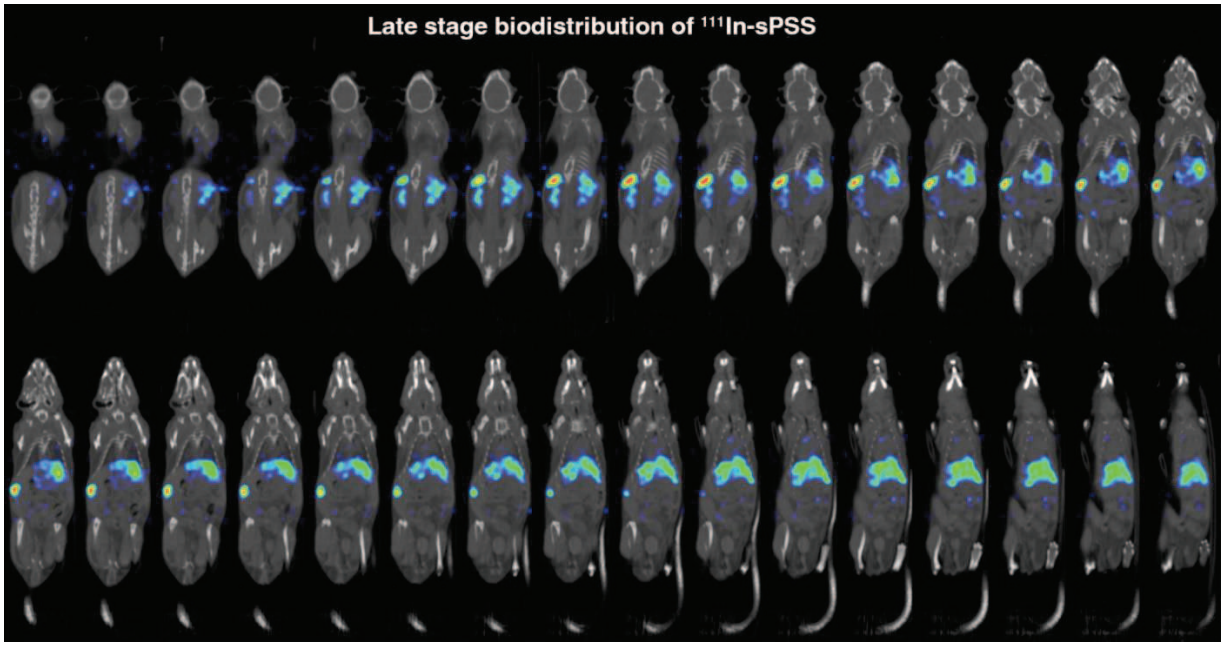

Figure 9 Fused SPECT/CT slices of late stage biodistribution of 111In-sPSS, obtained from 48 h p.i. SPECT scan with focusing on abdominal area of the animal.

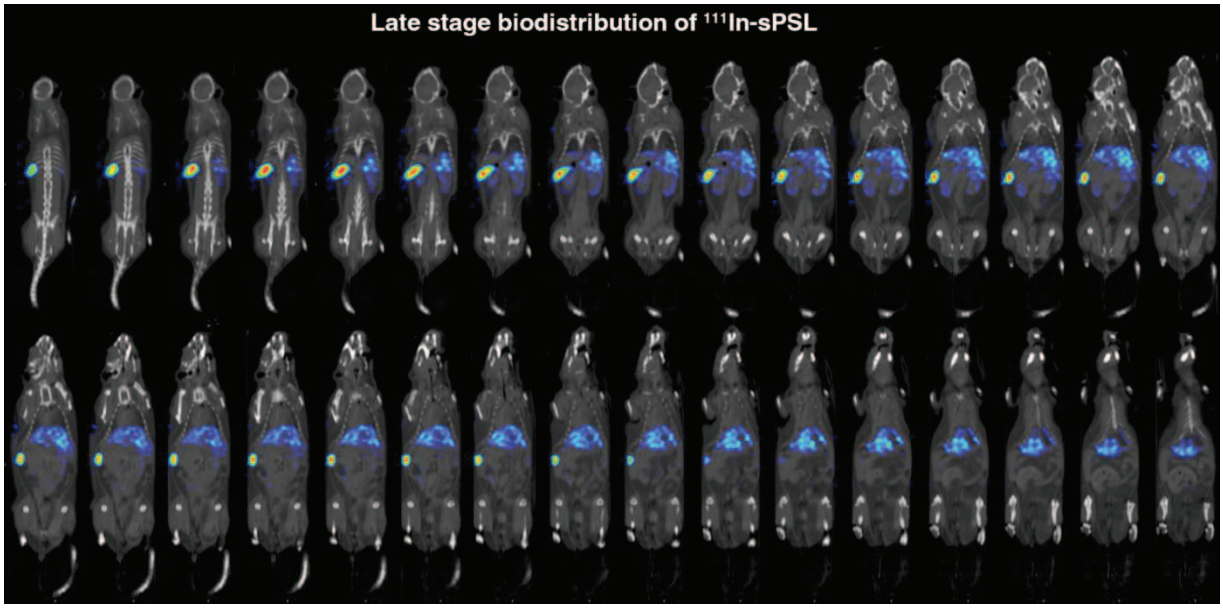

Figure 10 Fused SPECT/CT slices of late stage biodistribution of 111In-sPSL, obtained from 48 h p.i. SPECT scan with focusing on abdominal area of the animal.

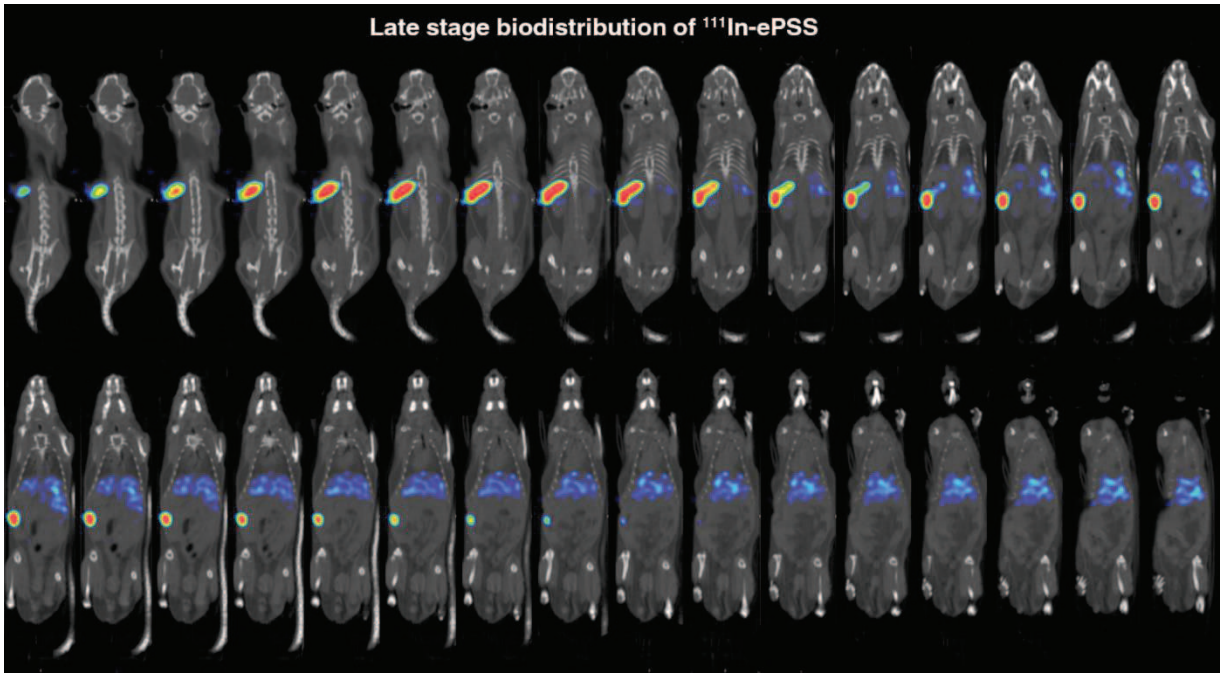

Figure 11. Fused SPECT/CT slices of late stage biodistribution of 111In-ePSS, obtained from 48 h p.i. SPECT scan with focusing on abdominal area of the animal.

Comparison between organ accumulation of ^{111}In-sPSS, ^{111}In-sPSL and ^{111}In-ePSS micelles for all time points are shown in Table 3.

Table 3 Comparison of accumulation rates of 111In-labelled sPSS, sPSL and ePSS micelles in the kidney, liver and spleen of the animals at 0, 24 and 48 h p.i.

Organ	*Compound*	*Uptake in the organs of interest [%ID/mL]*		
		0 h	24 h	48 h
Heart	^{111}In-sPSS	17.7 ± 3.7a)	6.1 ± 2.2	3.0 ± 0.4
	^{111}In-sPSL	17.4 ± 6.1	4.2 ± 0.6	2.4 ± 0.1
	^{111}In-ePSS	15.0 ± 3.6	4.6 ± 1.3	2.7 ± 0.2
Liver	^{111}In-sPSS	10.4 ± 1.9	11.8 ± 0.4	12.5 ± 0.8
	^{111}In-sPSL	7.9 ± 1.7	9.6 ± 0.2	12.3 ± 1.3
	^{111}In-ePSS	8.8 ± 1.5	13.5 ± 8.0	10.1 ± 3.0
Spleen	^{111}In-sPSS	12.2 ± 4.4	14.3 ± 1.8	17.3 ± 0.9
	^{111}In-sPSL	11.1 ± 1.4	37.5 ± 5.1	48.3 ± 18.2
	^{111}In-ePSS	24.7 ± 0.4	62.0 ± 21.9	88.2 ± 7.5

a)Standard deviation of the uptake within one study group of the animals

Our results demonstrated that the carrier with the fastest initial clearance is ^{111}In-ePSS, the carrier with the longest circulation time is ^{111}In-sPSS which showed the highest %ID/mL heart uptake value (Figure 7B) in the 24 hours p.i. scan. This value represents an average activity concentration in the blood passing through the heart. ^{111}In-sPSL and ^{111}In-ePSS showed slightly lower heart uptake values at 24 hours p.i. (Figure 7B, Table 3), but all three morphologies show no statistical difference in blood activity concentration at 48 hours p.i.. Furthermore, significant late stage increase in spleen uptake of ^{111}In-sPSL and ^{111}In-ePSS (Figure 7B) suggests a circulation time of the compounds that is longer than 24 hours. These results correlates with previously reported[43] long circulation times for PS-PEO micelles and suggest a good potential for EPR effect related applications. However, based on our results we can state that the high aspect ratio and flow alignment of elongated micelles cannot provide an order of magnitude increase in circulation time as was previously suggested in Geng et al. for the PEO-PCL filomicelles.[36,48] The different behavior of the PS-PEO micelles and the PEO-PCL ones can be caused by the different stiffness of the two core forming blocks.

The difference in longitudinal *in vivo* biodistribution of the three micelle types can be explained with their size and morphology. The general trend observed is that the PS-PEO nanocarriers accumulate in the spleen, liver and renal cortex. The nanocarriers with larger characteristic dimensions accumulate preferentially in the spleen, while the smallest are divided equally between spleen and liver. Nanoparticles which are larger than 100 nm have been shown to preferentially accumulate in the spleen rather than the liver which is consistent with our results with the spherical micelles.[49] Moreover, stiffer carriers have also been reported to accumulate preferentially in the spleen rather than the liver.[50] As a result of the combination of their sizes and stiffness, given by the polystyrene core, the elongated micelles show a remarkably specific spleen uptake. Since the spleen is the primary organ of the immune system this result could lead to interesting applications for vaccine delivery.[51] It must be noted that these experiments were carried out on mouse models which have a non-sinusoidal spleen while rat or human spleens have a sinusoidal structure. The sinusoidal sleeves provide an extra layer of filtration for carriers which have high rigidity, sizes larger than 200 nm and elongated shapes.[22,23] Regarding the liver, Kupffer cells, responsible for the accumulation of nanoparticles, have a rough surface which promotes phagocytosis of particles with a diameter between 1 and 3 μm.[19,21] The carrier which mostly represents this range are the elongated micelles ePSS along their long axis. However, our results show that the small spherical particles are being preferentially uptaken in the liver. Elongated micelles have been shown to align under flow and hinder phagocytosis. This could explain the reduced liver uptake, however, the circulation time of several days reported for flexible elongated PEO-PCL micelles is still an order of magnitude larger than the circulation time of stiff elongated PS-PEO micelles.[36,48] Whether the reduced circulation time is due

to the core stiffness of elongated micelles by promoting spleen uptake, which indirectly contributes to a reduction of the accumulation in the liver, remains to be investigated.

5.3 Conclusions

Spherical and elongated micelles of polystyrene-b-poly(ethylene oxide) were prepared using a co-solvent evaporation method which allows the encapsulation of hydrophobic dyes and complexed radioisotopes. This theranostic device shows great versatility for research purposes since markers, as long as they are hydrophobic, can potentially be encapsulated without costly formulation efforts. As a benchmark for these carriers a fluorescent dye was incorporated to study their internalization *in vitro*. No cytotoxic effects for the different micelle morphologies were found for concentrations up to 5 mg/mL. Subsequently, the micelles were loaded with ^{111}Indium-tropolone complexes to evaluate their biodistribution *in vivo* in healthy animals. The micelles distribute between liver and spleen for all the three samples tested. The smallest spherical micelles accumulate in the liver and spleen with no preference. The larger spherical ones are more preferentially accumulating in the spleen, suggesting the crossing of a cutoff threshold. Finally, the elongated ones show a remarkable accumulation in the spleen due to their size and stiffness. This particular behavior of the elongated micelles can provide possible applications for vaccine delivery.

5.4 Experimental Section

Materials

Poly(styrene-b-ethylene oxide) block copolymers $PS_{9.5k}$-PEO_{18k} (M_n/M_w = 1.09) and $PS_{9.5k}$-PEO_{5k} (M_n/M_w = 1.04) were purchased from Polymer Source Inc. (Polymer Source Inc., Canada). Anhydrous Chloroform ≥ 99%, 0.5 – 1% ethanol as stabilizer, fluorescent dye 1,1'- Dioctadecyl-3,3,3',3'-tetramethylindocarbocyanine perchlorate (DiI), Sephadex® G-25 and Fetal Bovine Serum (FBS), were purchased from Sigma Aldrich (Sigma-aldrich Chemie B.V., The Netherlands). Sterile Phosphate Buffered Saline (PBS), 0.25% Trypsin-Ethylenediaminetetraacetic acid (EDTA) and Penicillin-Streptomycin were purchased from Gibco (Fischer Scientific, The Netherlands). BioWhittaker Dulbecco's Modifed Eagle Medium (DMEM) and Ham's F10 were purchased from Lonza (Lonza Benelux B.V., The Netherlands). Vectashield- 4',6-diamidino-2-phenylindole (DAPI) was purchased from Vector Laboratories (Brunschwig Chemie, The Netherlands). Glass stirring bars, one cm long, were purchased from VWR (VWR International, France). Silicon substrates, 5x5 mm polished, were purchased from Siltronix (Siltronix B.V., France). The radioactive ^{111}In-chloride was provided by IDB Holland (IDB Holland B.V., The Netherlands). All the reagents were used as received unless stated otherwise.

Micelle formation

A stock solution was prepared by dissolving 10 mg/mL block copolymer in chloroform. A 100 µL aliquot of the stock solution was added to 2.3 mL of PBS. After this, an emulsion between the two immiscible solvents was formed by stirring using a glass coated magnetic stirring bar. The emulsion was stirred until complete evaporation of the chloroform.

Three different micelle types were prepared: two of spherical and one of elongated morphology. The spherical ones were formed using $PS_{9.5k}$-PEO_{18k}. By controlling the evaporation rate of the chloroform phase in the emulsion spherical micelles of two different diameters were obtained. The large spherical micelles, sPSL, were formed by leaving the vial open during the evaporation stage. The small spherical micelles, sPSS, were formed by maintaining the vial closed during the whole evaporation stage. Elongated micelles, ePSS, were formed using $PS_{9.5k}$-PEO_{5k} and by keeping the vial closed during the evaporation stage. The vials used were not air tight so, slow, evaporation was possible even in the closed vials.

Fluorescently labeled micelles were prepared by including fluorescent dye DiI directly to the stock solution in 0.02 wt% to copolymer weight.

Spherical micelle characterization

The intensity weighted particle size distribution and average hydrodynamic diameter of the spherical micelles were obtained by DLS. Each micelle sample was diluted to a concentration of 0.1 mg/mL and measured using an ALV/DLS/SLS-5020F experimental setup (ALV Laser Vertriebsgesellshaft GmbH, Germany) with a He-Ne laser (14 mW, λ_0 = 632.8 nm), a compact ALV/CGS-8 Goniometer system, and an ALV-7002 autocorrelator at scattering angles from 20º to 120°. The CONTIN method was used for the analysis of the normalized autocorrelation functions of the scattered intensity.

AFM was used to obtain topographic scans of the spherical micelles. Ten µL of micelle solution were spin coated onto 5x5 silicon substrates and these were imaged using an NTegra microscope (NT-MDT Co., Russia) in semi contact mode with an NSG03 cantilever (k = 1.7 N/m).

Elongated micelle characterization

The diameter and length of the elongated micelles was determined by SEM. Droplets of 10 µL of micelle solution were diluted to 0.1 mg/mL and spincoated onto 5x5 mm silicon substrates. These were imaged using a SU8000 UHR Cold-Emission FE-SEM Scanning Electron Microscope (Hitachi, Japan). The samples were imaged at 1 kV acceleration voltage and without applying any conductive coating to the sample.

The diameter of the elongated micelles was also measured by AFM, using the same procedure and equipment as for the spherical micelles.

The length distribution of the elongated micelles was reduced using an Ultra Turrax IKA T10 basic homogenizer (IKA, Germany). Each sample of 2.3 mL was homogenized at 30k RPM for 30 seconds in total.

Micelle radiolabeling

A solution of 2.3 mL PBS (pH 7.4) and 1 mM tropolone was prepared. The required amount of ^{111}In was added to this aqueous solution and stirred using a glass coated magnetic stirring bar for 5 minutes, allowing the formation of tropolone ^{111}In complexes. After this, a 100 µL aliquot of polymer stock solution was added and an emulsion with water was formed by stirring the two immiscible solvents with a glass magnetic stirring bar. The emulsion was mixed until evaporation of chloroform.

Purification of the radiolabeled micelles from unencapsulated and uncomplexed tropolone and ^{111}In was performed by size exclusion chromatography using Sephadex® G-25 gel. Elution fractions were

collected and the activity of each fraction was counted in a 2480 Wizard2 Automatic Gamma Counter (PerkinElmer Nederland BV, The Netherlands).

***In vitro* model**

The evaluation of the carriers' *in vitro* was carried out using HeLa cancer cells. These were cultured in full DMEM medium containing 10% FBS and 100 units/mL penicillin-streptomycin. The cells were kept at 37°C in humidified atmosphere (5% CO2 in air). The cells were harvested by trypsinization with trypsin-EDTA.

Cytotoxicity

The cytotoxicity of the PS-PEO micelles was determined using the WST-1 ver. 16 (Roche Life Science, Switzerland) colorimetric assay. WST-1 contains the 2-(4-Iodophenyl)-3-(4-nitrophenyl)-5-(2,4-disulfophenyl)-2H-tetrazolium salts which are cleaved to formazan by cellular enzymes. Increase in the number of viable cells results in an increase of enzymatic activity, which translates to an increased amount of formazan dye. The amount of formazan dye was measured against blank samples in 96 well plates using a Powerwave XS multiwell spectrophotometer (Biotek, United States). The absorbance of the formazan product was measured at 440 nm. For each micelle sample four different concentrations, from 0.005 mg/mL to 5 mg/mL, were incubated for 24, 48 and 72 hours.

Fluorescence uptake

Cells were seeded in 6-well plates, each containing one borosilicate glass slide 20 x 20 mm, at a density of 5 x 105 cells/well in 1.5 mL of medium. These were incubated at 37°C and 5% CO2 for 24 hours. After this, 300 µL of micelle solution was added to each well to obtain a final concentration of 1.3 mg of micelles per well. The samples were left for different incubation times, after which the coverslips were rinsed with PBS to remove all non-uptaken micelles and sealed on a glass slide using transparent Roti® liquid barrier marker. Five µL of Vectashield-DAPI were added between the coverslip and the glass slide to stain the nuclei and preserve fluorescence in the sample. Confocal images of the samples were made using a LSM 710 confocal microscope with a Fluar 40x/1.30 Oil M27 objective (Carl Zeiss Microscopy GmbH, Germany). The DAPI signal was excited using a 405 nm diode (emission 460 nm), while the DiI using a 543 nm He-Ne laser (emission 563 nm). From confocal micrographs of the cells, the average DiI signal per cell was measured. Control samples with no added micelles were used for background correction.

Animal handling

Animal experiments were performed with C57Bl/6 mice according to protocols approved by the Animal Ethical Committee of the UMC Utrecht and in accordance with Dutch Law on Animal experimentation. SPECT/CT imaging was used as a noninvasive method to access circulation dynamics and tissue deposition of ^{111}In-labelled micelles.

Three study groups of two animals each were assigned for imaging with ^{111}In-sPSL, ^{111}In-sPSS or ^{111}In-ePSS micelles respectively. All animals were anesthetized with isoflurane (2% in air) and injected with activity via the tail vein. The average injected activities per study group were 1.45 MBq (1.5 mg) ^{111}In-sPSL, 0.26 MBq (1.8 mg) ^{111}In-sPSS and 0.42 MBq (1.5 mg) ^{111}In-ePSS respectively. After this, total body SPECT/CT scans of 30 minutes were acquired at 0 (just after the injection), 24 and 48 hours p.i.. To obtain more detailed information on the late-stage biodistribution of the compound in the spleen and the liver of the animals, additional 30 minutes acquisitions focused on the abdominal area were performed immediately after the end of the 48 hours p.i. total body SPECT/CT scans.

SPECT/CT imaging and data analyzing

All animals were imaged in a U-SPECT+/CT scanner (MILabs B.V., The Netherlands). This system is equipped with three stationary scintillator detectors that are arranged in triangular setup and an integrated X-ray micro-CT system.[52]

The SPECT scans were acquired in a list-mode data format with an extra-ultra-high-sensitivity mouse pinhole collimator (XUHS-2.0 mouse collimator).[53] After this, SPECT image reconstructions were carried out with a pixel-based order-subset expectation maximization (POSEM)[54] algorithm that included resolution recovery and compensation for distance-dependent pinhole sensitivity.[55] For the SPECT images in this paper, we used 4 subsets and 12 iterations image reconstruction with an isotropic 0.4-mm-voxel grid. Triple-energy-window based Compton scatter correction was performed according to King et al.[56] A 20% ^{111}In photopeak window was centered at 171 keV. Two background windows were placed on both sides of the photopeak window with a width of 4% of the photopeak, i.e. 6.8 keV each. Hereafter, non-uniform attenuation correction and absolute quantification of SPECT images was performed according to Wu et al.[57]

Corresponding CT scans were acquired with a tube setting of 55 kV and 615 µA. In total, 2 frames of 182 projections over 360° were acquired in step and shoot rotation mode. The acquired projection data was reconstructed using SkyScan NRecon software to generate a 3-D CT image on 0.1693 x 0.1693 x 0.1695 mm voxel grid.

To calculate the uptake of radiolabeled micelles in the organ of interest, the registered to CT and quantified SPECT images were analyzed using PMOD 3.6 biomedical image analyzing software (PMOD,

Switzerland). A three-dimensional region-of-interest (ROI) was manually drawn to encompass the radioactivity uptake in the organ whose boundary was delineated in the three-dimensional CT images. Separate ROIs were drawn for the radioactivity uptakes in the heart, liver, spleen, left and right kidneys, and the bladder. The % injected dose (%ID) per mL of tissue volume (%ID/mL) value was calculated for every imaging time point using Equation (1).

$$\%\,\mathbf{ID/mL\ of\ tissue} = \frac{\mathbf{Total\ activity\ in\ the\ ROI\ (MBq)}}{\mathbf{Volume\ of\ the\ ROI\ (mL)\ x\ Total\ injected\ dose\ (MBq)}}\mathbf{x100}\% \qquad (1)$$

For visual representation in the manuscript the reconstructed volumes of SPECT scans were post-filtered with a 1.2 mm full width at half maximum three-dimensional Gaussian filter.

Animal handling, image reconstruction and SPECT data evaluation, was performed as part of a hands-on formation on SPECT supervised by O. Ivaschenko, another fellow of the Trace ‘n Treat consortium who is working in MILabs.

5.5 References

[1] T. Blunk, M. Lück, A. Calvör, D. F. Hochstrasser, J.-C. Sanchez, B. W. Müller, R. H. Müller, Eur. J. Pharm. Biopharm. 1996, 42, 262–268.

[2] G. Gaucher, K. Asahina, J. Wang, J.-C. Leroux, Biomacromolecules 2009, 10, 408–416.

[3] K. Ogawara, K. Furumoto, S. Nagayama, K. Minato, K. Higaki, T. Kai, T. Kimura, J. Control. release 2004, 100, 451–455.

[4] F. Kratz, J. Control. Release 2008, 132, 171–183.

[5] K. M. Wasan, D. R. Brocks, S. D. Lee, K. Sachs-Barrable, S. J. Thornton, Nat. Rev. Drug Discov. 2008, 7, 84–99.

[6] W. V Rodrigueza, M. C. Phillips, K. J. Williams, Adv. Drug Deliv. Rev. 1998, 32, 31–43.

[7] T. M. Allen, Biochim. Biophys. Acta (BBA)-Biomembranes 1981, 640, 385–397.

[8] M. Lundqvist, J. Stigler, G. Elia, I. Lynch, T. Cedervall, K. A. Dawson, Proc. Natl. Acad. Sci. 2008, 105, 14265–14270.

[9] M. J. Walport, N. Engl. J. Med. 2001, 344, 1058–1066.

[10] P. F. Zipfel, C. Skerka, Nat. Rev. Immunol. 2009, 9, 729–740.

[11] K. Knop, R. Hoogenboom, D. Fischer, U. S. Schubert, Angew. Chemie Int. Ed. 2010, 49, 6288–6308.

[12] J. M. Harris, R. B. Chess, Nat. Rev. Drug Discov. 2003, 2, 214–221.

[13] B. Haraldsson, J. Nyström, W. M. Deen, Physiol. Rev. 2008, 88, 451–487.

[14] A. F. Michael, Aust. N. Z. J. Med. 1981, 11, 83–87.

[15] H. S. Choi, W. Liu, F. Liu, K. Nasr, P. Misra, G. Moungi, J. V Frangioni, Nat. Nanotechnol. 2010, 5, 42–47.

[16] H. Harashima, K. Sakata, K. Funato, H. Kiwada, Pharm. Res. 1994, 11, 402–406.

[17] W. Jiang, B. Y. S. Kim, J. T. Rutka, W. C. W. Chan, Nat. Nanotechnol. 2008, 3, 145–150.

[18] J. A. Champion, A. Walker, S. Mitragotri, Pharm. Res. 2008, 25, 1815–1821.

[19] N. Doshi, S. Mitragotri, PLoS One 2010, 5, 1–6.

[20] J. A. Champion, S. Mitragotri, Pharm. Res. 2009, 26, 244–249.

[21] J. A. Champion, S. Mitragotri, Proc. Natl. Acad. Sci. U. S. A. 2006, 103, 4930–4934.

[22] Z. Liu, C. Davis, W. Cai, L. He, X. Chen, H. Dai, Proc. Natl. Acad. Sci. U. S. A. 2008, 105, 1410–1415.

[23] M. Demoy, J. P. Andreux, C. Weingarten, B. Gouritin, V. Guilloux, P. Couvreur, Pharm. Res. 1999, 16, 37–41.

[24] M. Cho, W.-S. Cho, M. Choi, S. J. Kim, B. S. Han, S. H. Kim, H. O. Kim, Y. Y. Sheen, J. Jeong, Toxicol. Lett. 2009, 189, 177–183.

[25] T. Mustonen, K. Alitalo, J. Cell Biol. 1995, 129, 895–898.

[26] H. F. Dvorak, J. A. Nagy, D. Feng, L. F. Brown, A. M. Dvorak, Curr. Top. Microbiol. Immunol. 1999, 237, 97–132.

[27] T. M. Allen, P. R. Cullis, Science 2004, 303, 1818–1822.

[28] H. Maeda, Adv. Enzyme Regul. 2001, 41, 189–207.

[29] H. Maeda, J. Wu, T. Sawa, Y. Matsumura, K. Hori, J. Control. Release 2000, 65, 271–284.

[30] X. Sun, R. Rossin, J. L. Turner, M. L. Becker, M. J. Joralemon, M. J. Welch, K. L. Wooley, Biomacromolecules 2005, 6, 2541–2554.

[31] W. Zauner, N. A. Farrow, A. M. R. Haines, J. Control. Release 2001, 71, 39–51.

[32] A. S. Mikhail, S. Eetezadi, S. N. Ekdawi, J. Stewart, C. Allen, Int. J. Pharm. 2014, 464, 168–177.

[33] R. R. Arvizo, O. R. Miranda, D. F. Moyano, C. a. Walden, K. Giri, R. Bhattacharya, J. D. Robertson, V. M. Rotello, J. M. Reid, P. Mukherjee, PLoS One 2011, 6, 3–8.

[34] P. Decuzzi, M. Ferrari, Biomaterials 2006, 27, 5307–5314.

[35] P. Kolhar, A. C. Anselmo, V. Gupta, K. Pant, B. Prabhakarpandian, E. Ruoslahti, S. Mitragotri, Proc. Natl. Acad. Sci. U. S. A. 2013, 110, 10753–8.

[36] Y. Geng, P. Dalhaimer, S. Cai, R. Tsai, M. Tewari, T. Minko, D. E. Discher, Nat. Nanotechnol. 2007, 2, 249–255.

[37] Y. Geng, D. E. Discher, J. Am. Chem. Soc. 2005, 127, 12780–12781.

[38] Y. M. Wang, C. M. Kausch, M. S. Chun, R. P. Quirk, W. L. Mattice, Macromolecules 1995, 28, 904–911.

[39] S. Jain, F. S. Bates, Macromolecules 2004, 37, 1511–1523.

[40] C. Allen, D. Maysinger, A. Eisenberg, Colloids Surfaces B Biointerfaces 1999, 16, 3–27.

[41] J. Zhu, R. C. Hayward, J. Am. Chem. Soc. 2008, 130, 7496–7502.

[42] K. Yu, A. Eisenberg, Macromolecules 1996, 29, 6359–6361.

[43] S. M. D'Addio, W. Saad, S. M. Ansell, J. J. Squiers, D. H. Adamson, M. Herrera-Alonso, A. R. Wohl, T. R. Hoye, C. W. MacOsko, L. D. Mayer, et al., J. Control. Release 2012, 162, 208–217.

[44] M. Su, Z. Su, Macromolecules 2014, 47, 1428–1432.

[45] G. Jia, H. Wang, L. Yan, X. Wang, R. Pei, T. Yan, Y. Zhao, X. Guo, Environ. Sci. Technol. 2005, 39, 1378–1383.

[46] Y. Zhang, D. Xu, W. Li, J. Yu, Y. Chen, J. Nanomater. 2012, 2012, DOI 10.1155/2012/375496.

[47] X. Zhao, S. Ng, B. C. Heng, J. Guo, L. Ma, T. T. Y. Tan, K. W. Ng, S. C. J. Loo, Arch. Toxicol. 2013, 87, 1037–1052.

[48] D. a. Christian, S. Cai, O. B. Garbuzenko, T. Harada, A. L. Zajac, T. Minko, D. E. Discher, Mol. Pharm. 2009, 6, 1343–1352.

[49] X. Duan, Y. Li, Small 2013, 9, 1521–1532.

[50] N. Bertrand, J. C. Leroux, J. Control. Release 2012, 161, 152–163.

[51] Y. Yang, T. Neef, C. Mittelholzer, E. Garcia Garayoa, P. Bläuenstein, R. Schibli, U. Aebi, P. Burkhard, J. Nanobiotechnology 2013, 11, 36.

[52] F. van der Have, B. Vastenhouw, R. M. Ramakers, W. Branderhorst, J. O. Krah, C. Ji, S. G. Staelens, F. J. Beekman, J. Nucl. Med. 2009, 50, 599–605.

[53] O. Ivashchenko, F. van der Have, M. Goorden, R. M. Ramakers, F. J. Beekman, J. Nucl. Med. 2015, 56, 470–476.

[54] W. Branderhorst, B. Vastenhouw, F. J. Beekman, Phys. Med. Biol. 2010, 55, 2023–2034.

[55] F. Van Der Have, B. Vastenhouw, M. Rentmeester, F. J. Beekman, IEEE Trans. Med. Imaging 2008, 27, 960–971.

[56] M. A. King, S. J. Glick, P. H. Pretorius, R. G. Wells, H. C. Gifford, M. V Narayanan, T. Farncombe, Emiss. Tomogr. Acad. Press. San Diego 2004.

[57] C. Wu, J. R. de Jong, H. A. Gratama van Andel, F. van der Have, B. Vastenhouw, P. Laverman, O. C. Boerman, R. A. J. O. Dierckx, F. J. Beekman, Phys. Med. Biol. 2011, 56, N183–N193.

6 Conclusions and Future Outlook

This thesis is the result of three years of research within the Trace 'n Treat consortium and performed between the Institut Charles Sadron and the Delft University of Technology. The work comprised in this thesis provides an overview of the formation, characterization and testing of micelles of different morphology for biological applications. In this section the main results of each chapter will be highlighted together with suggestions for further research or for the possible applications of the results obtained.

In Chapter 2 we studied the formation of micelles through the emulsion evaporation method. This method had always been studied as a black box where different formulations were the input and the output were, for the most part, nano or microparticles characterized solely through electron microscopy images. In this work we directly studied the whole process by breaking it down into simpler sections. This was done by initially observing a planar interface between PS-PEO rich chloroform and water in the absence of solvent evaporation. Subsequently we observed the behavior of evaporating emulsions of PS-PEO rich chloroform in water. Two major findings were described in this chapter. First of all we have shown how the peculiar solubility of poly(ethylene oxide), and its weakly amphiphilic nature, drive the spontaneous formation of water in chloroform emulsions in the ternary system water/chloroform/PS-PEO. This occurred regardless of the block length ratio of the copolymer. The importance of this observation lies first of all in the fact that it provides a completely different vision of the problem of micelle formation through emulsion evaporation. Moreover, it makes it possible to explain how nanoparticles having a bilayer morphology are formed through this technique. Finally, it provided a hint towards the possibility of controlling the polymorphism of aggregates produced through this technique.

Through the observations presented in this chapter we provided a hypothesis for the formation of elongated micelles through the co-solvent evaporation method. This is based on the presence of the water in chloroform emulsion which is progressively confined by the evaporation of the chloroform phase. We propose the transition from a liquid foam phase to a sponge phase to be the key for the formation of elongated micelles. Further evaporation of the chloroform would cause a confinement on the water domains of the sponge phase and this would trigger a phase inversion resulting in the formation of cylindrical micelles with a hydrophobic core and a hydrophilic corona.

In the third chapter we used these findings to develop a method to produce micelles of controlled morphology. The technique presented in this chapter is innovative in the approach and has several

advantages with respect to the current state of the art of formation of kinetically frozen micelles by emulsion evaporation. This was achieved by depositing a solution of PS-PEO rich chloroform at a water-air interface of a cuvette partially filled with water. This made it possible to have a system where the chloroform evaporation rate can be tuned utilizing a peristaltic pump. We have found that upon deposition of the PS-PEO chloroform solution on the water-air interface, a water in chloroform emulsion is formed. This is in agreement with the observations described in the second chapter. Evaporation of the chloroform results in the destabilization of the chloroform water interface and in the formation of PS-PEO micelles in water. We have found that increasing the evaporation rate of the solvent would result in the formation of micelles of decreasing interfacial curvature (i.e. spherical – elongated – vesicular). This is achieved by tuning the balance between solvent removal and arrangement of the copolymers at the chloroform water interface. The advantage of this technique is that it decouples the block length ratio of a copolymer from the possible micelle morphologies obtained from the same copolymer. This makes it possible, for example, to have a greater range of block copolymers which can form elongated micelles. Such formulation possibility is of particular importance for bio-related applications since it allows to decouple the size of the corona block and core block from the morphology. As an example, It is possible that the core size of a micelle affects its mechanical properties, encapsulation abilities, stability and drug release properties while the corona block affects the circulation time and biocompatibility of the micelles. The morphology on the other hand has been shown to play a very important role in the biodistribution and overall targeting efficacy. Until now only very specific block length ratios would allow the formation of elongated micelles. The method presented in this chapter opens up a whole new approach for the formulation and testing of micelles of different morphology having application tailored block lengths. Moreover, thanks to the absence of a mechanical stirring, the formation of these micelles occurs in the absence of shear stress. This made it possible to form macroscopic threads of elongated micelles. The possibility to easily form macroscopic nanostructured materials is of high interest in the field of tissue engineering for example where biocompatible nanofibers are objects of interest.

In the fourth chapter we presented a technique to determine the mechanical modulus of elongated micelles through three point bending tests. To do this we prepared micelles of different diameter using blends of PS-PEO and the homopolymer PS. We have shown how increasing amounts of PS resulted in PS-PEO micelles of increasingly large diameter. Subsequently we used micropatterned silicon molds to prepare poly(dimethyl siloxane) stamps with micro-sized pillars. The pillars had micrometer sized gaps between each other. Using the technique presented by Glazer et al. we deposited the elongated micelles across the pillars. In this way arrays of partially suspended micelles were formed. We then performed three point bending tests with the aid of an Atomic Force Microscope. We found that the

elastic modulus of the micelles would decrease abruptly when homopolymer was added to the core: the thicker micelles were also the more flexible. We performed Differential Scanning Calorimetry and found that the different modulus of the micelles was due to the different contribution of the crystalline corona of the micelles. The presence of homopolymer swelling the core would decrease the density of the PEO corona resulting in a less crystalline shell.

This technique provided the ability to measure the modulus of elongated micelles with very high sensitivity while removing the influence of an underlying substrate. This made it possible to determine the subtle contribution of a crystalline corona to the modulus of micelles. These findings provide a simple pathway to tune the mechanical modulus of block copolymer micelles in their dry state.

In the fifth and final chapter we provided an *in vivo* and *in vitro* characterization of the PS-PEO micelles. The objective of the research presented in this chapter was to determine the different behavior of elongated and spherical micelles of PS-PEO. We prepared two types of spherical micelles of $PS_{9.5k}$-PEO_{18k} with different diameter, and one type of elongated micelles of $PS_{9.5k}$-PEO_{5k}. We compared the use of different size characterization techniques (i.e. dynamic light scattering, atomic force microscopy and scanning electron microscopy) for the spherical and elongated micelles. We have shown that the best technique to compare the size of the two morphologies is atomic force microscopy since this takes into account both the core and the corona of the micelles. Finally we have also shown how the length of elongated PS-PEO micelles can be shortened using a high shear homogenizer.

After having characterized the size of the nanocarriers we characterized their behavior *in vitro* and *in vivo*. No cytotoxic effects were found when testing the micelles on HeLa cells with concentrations up to 5 mg/mL. The micelles were then fluorescently labelled using the fluorescent dye DiI and their internalization in HeLa cells was studied by confocal microscopy. It was found that the elongated micelles internalize slower than the spherical ones, however their higher fluorescent dye capacity makes it possible to deliver similar amounts of dye to the cells when compared with the spherical micelles.

Finally the micelles were radiolabeled using Indium-111. The radiolabeling technique is based on the formation of apolar complexes of ^{111}In and tropolone in the water phase during the emulsion evaporation stage. The apolar complexes will partition between the two solvents and a fraction of them will be encapsulated in the micelle core upon micelle formation. The radiolabeled micelles were used to perform single photon emission tomography on healthy mice. Two aspects were studied: the circulation time and the bio distribution of the nanocarriers. We have found the longest circulating micelles to be the smaller spherical ones. However, all micelles showed circulation between 24 and 48 hours post injection. The fact that the elongated micelles didn’t circulate longer than the spherical

ones is a result which is in contradiction with the results already present in the literature. Regarding the biodistribution of the nanocarriers, we found that smaller spherical micelles would preferentially accumulate in the liver while the larger spherical ones in the spleen. The elongated micelles showed a remarkably high accumulation in the spleen which is probably due to a combination of their size and stiffness.

The results presented in this chapter provide one of the only studies available showing the effects of nanocarrier shape on their in-vivo biodistribution. Further work in this direction should involve the use of micelles of different stiffness to verify if the relatively short circulation time of the elongated PS micelles is indeed due to their stiffness. Combining the technique developed in chapter 3 with the methods described in this chapter would allow to produce and test a library of micelles of different morphologies, surface properties and stiffness. In this way an in depth study of the performance of micelles of different morphologies could be performed.

In conclusion, the innovative techniques and the methods described in this thesis provide solid foundations for the preparation of PEO based micelles of different morphologies and for their use in different applications, including biomedical ones.

7 Résumé de thèse en Français

7.1 Introduction

La production de nanoparticules est un domaine de recherche très actif grâce à la pléthore de demandes de nouveaux matériaux de taille nanométrique. Le contrôle effectif de la taille et de la morphologie des nanoparticules est d'une importance fondamentale pour leur utilisation. En particulier, les particules micellaires qui combinent un noyau hydrophobe avec une couronne hydrophile sont particulièrement prometteuses pour les applications d'administration de médicaments. Des molécules de médicament, étant généralement très hydrophobes, peuvent être efficacement encapsulées dans le noyau de ces particules micellaires. La couronne hydrophile, en même temps, confère une solubilité dans l'eau et la biocompatibilité des composés médicament-micelles. En outre, il a été montré que les nanoparticules ayant la bonne taille peuvent s'accumuler passivement dans les tumeurs solides, grâce à l'effet de perméabilité et de rétention renforcées (EPR).[1–3] Cet effet consiste dans l'extravasation de particules qui peuvent pénétrer à travers le tissu poreux de tumeurs vascularisées. Un schéma est présenté en Figure 1.

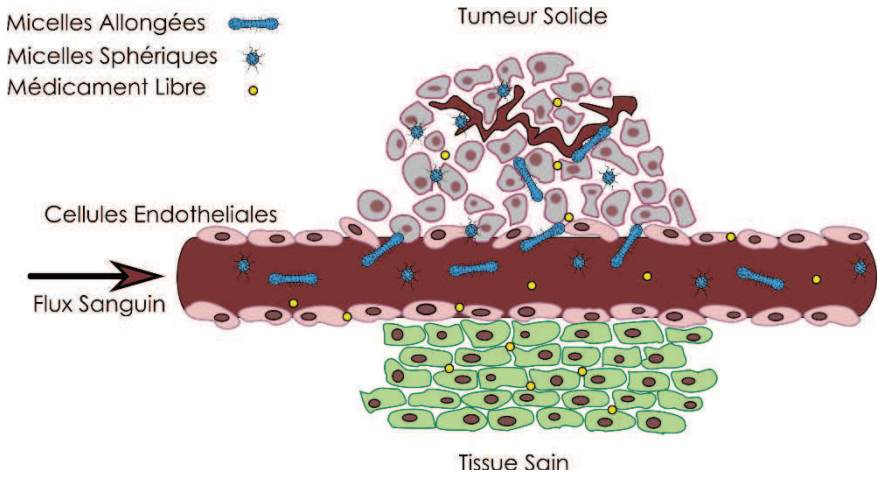

Figure 1 Représentation schématique de l'effet de perméabilité et de rétention renforcées (EPR). Les tumeurs solides vascularisées ont un tissu endothélial poreux qui permet l'extravasation de particules ayant une certaine taille et morphologie. Par contre, le médicament libre, en tant que petite molécule, peut traverser le tissu endothélial indépendamment de la présence de pores.

Une des voies les plus prometteuses vers la production simple de nanoparticules complexes est l'auto-assemblage de copolymères séquencés. En variant la qualité de solvant pour l'un des blocs du

copolymère, les chaînes isolées (unimères) tendent à s'assembler en structures supramoléculaires noyau-couronne pour minimiser l'énergie du système. Cela se produit avec de petits agents tensio-actifs solubles dans l'eau qui forment des micelles à l'équilibre thermodynamique mais aussi avec de plus grands copolymères amphiphiles. Alors que les micelles de tensioactifs sont des systèmes très dynamiques à cause de la cinétique d'échange rapide de ces petites molécules, on peut atteindre des agrégats micellaires cinétiquement figés en utilisant des copolymères dont le bloc insoluble dans le solvant utilisé a un poids moléculaire suffisamment élevé.[4,5] Les avantages d'agrégats micellaires cinétiquement figés sont multiples : la stabilité des structures ne dépend pas de la concentration en copolymère ou, dans certaines limites, de la température. Ceci permet d'éviter les fuites d'entités encapsulées dans le cœur des nanoparticules micellaires. En outre, en raison de leur nature hors équilibre, il est possible d'obtenir des morphologies très complexes.[6–8]

Dans ce mémoire, des copolymères séquencés polystyrène-b-poly(oxyde d'éthylène) (PS-POE) ont été utilisés pour préparer des véhicules micellaires de morphologies différentes adaptés pour l'imagerie nucléaire. Tout au long de ce travail qui a conduit à la préparation de ces échantillons, un accent particulier a été mis sur le développement d'une compréhension plus approfondie des processus qui conduisent à leur formation. En raison du caractère exploratoire de ce projet, des approches et développements expérimentaux originaux ont été élaborés.

7.2 La formation de micelles

La formation de micelles à base de PS-POE est généralement réalisée en utilisant un procédé d'évaporation de co-solvant.[9] Celui-ci consiste à confiner les copolymères, insolubles dans l'eau, à l'intérieur de gouttelettes de solvant organique (chloroforme) dans une matrice d'eau. La compréhension actuelle de ce phénomène est basée sur les phénomènes d'émulsification spontanée. L'évaporation des gouttelettes de chloroforme provoque une augmentation locale de la concentration en copolymère qui s'accumule à l'interface entre solvants et abaisse la tension interfaciale. Il en résulte des tensions interfaciales nulles ou négatives de manière transitoire qui favorisent une augmentation de la quantité de surface totale par un procédé d'émulsification spontanée.[10,11]

Un schéma du procédé est montre en Figure 2.

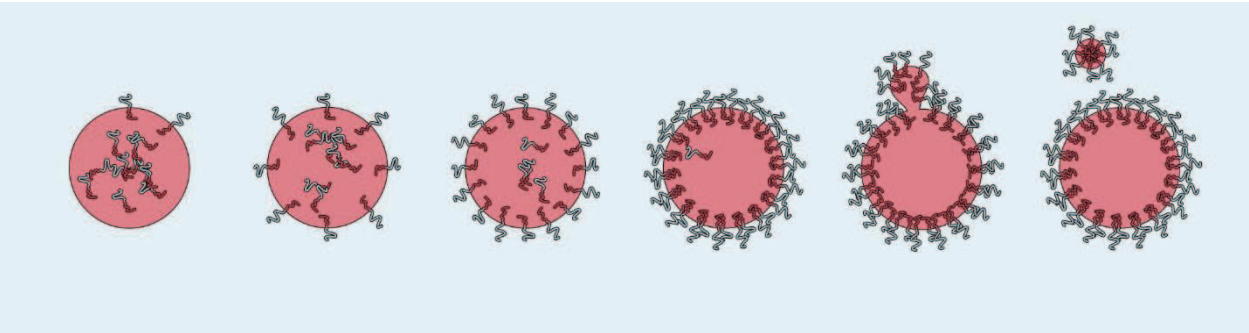

Figure 2 Schéma du procédé de formation de micelles travers l'émulsification spontanée. Les images donnent une évolution en temps de gauche à droite. Les copolymères amphiphiles s'accumulent à l'interface entre la gouttelette de chloroforme et l'eau. L'accumulation de copolymères abaisse la tension de surface entre les deux ce qui facilite les fluctuations spatiales de l'interface. La formation d'une micelle correspond à l'amplification des fluctuations à une longueur d'onde caractéristique.

Ce phénomène a été étudié jusqu'à présent comme une boîte noire dans laquelle les conditions d'émulsion initiales et les nano-objets finaux formés sont étudiés séparément en utilisant deux techniques distinctes.

Nous avons commencé par simplifier le problème en étudiant une interface planaire entre du chloroforme riche en copolymère et de l'eau, en absence d'évaporation du solvant. Par ce moyen nous avons étudié les phénomènes d'émulsification spontanée entre les deux solvants. Contrairement aux hypothèses, nous avons observé que, indépendamment du copolymère utilisé, il y a la formation d'une émulsion d'eau dans le chloroforme.

Dans la Figure 3 se trouvent des photographies et des images faites au microscope optique qui montrent des cuvettes où il y a du chloroforme riche en copolymère sous une couche d'eau. On peut voir que les deux copolymères forment une émulsion eau en chloroforme, mais que seul le plus hydrophile des deux forme aussi des micelles dans l'eau comme prévu par la théorie existante de l'émulsification spontanée.

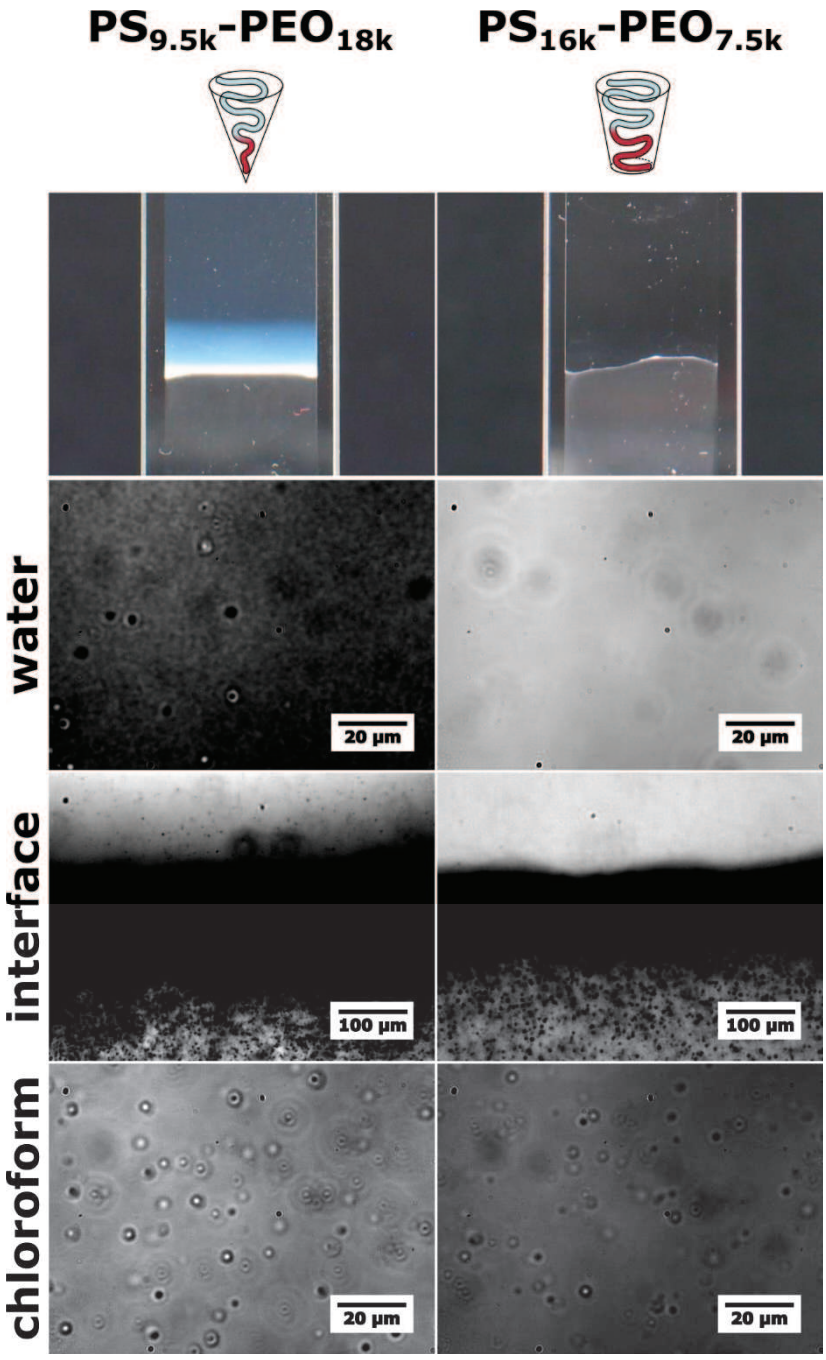

Figure 3 Vue d'ensemble des phénomènes d'émulsification spontanée entre du chloroforme riche en copolymère (en bas) et de l'eau (en haut). Les deux premières images sont des photos des cuvettes et les six autres sont des images prises au microscope. On peut voir la présence d'une émulsion d'eau en chloroforme pour les deux copolymères utilisés et une présence de micelles en eau seulement pour le copolymère plus hydrophile (phase bleutée, colonne de gauche).

Afin de mieux comprendre ce procédé très complexe et dynamique qui se déroule à des échelles de temps et de dimensions différentes, un colorant fluorescent est ajouté dans le chloroforme. Ce colorant est intégré dans le cœur des micelles lors de leur formation, ce qui permet de suivre tout le processus en temps réel : évaporation des gouttelettes de l'émulsion, déstabilisation des interfaces et finalement formation de micelles. En suivant ce phénomène en temps réel, il a été possible d'observer des événements qui sont restés inaperçus ou ont été mal interprétés.

Un exemple frappant est que la géométrie des gouttelettes peut influencer la morphologie des agrégats micellaires formés. Plus spécifiquement, pour un copolymère donné, des gouttelettes en suspension de quelques micromètres de diamètre forment préférentiellement des morphologies différentes de celles obtenues lorsque des gouttelettes plus grandes sont adsorbées et aplaties sur une surface de verre (Figure 4 et Figure 5). Ainsi les copolymères qui forment préférentiellement des micelles sphériques à partir de gouttelettes micrométriques en suspension forment des micelles allongées si les gouttelettes sont adsorbées et aplaties sur le substrat de verre. D'autres copolymères qui forment préférentiellement des micelles allongées à partir de gouttelettes en suspension, produisent des vésicules à partir de gouttelettes adsorbées.

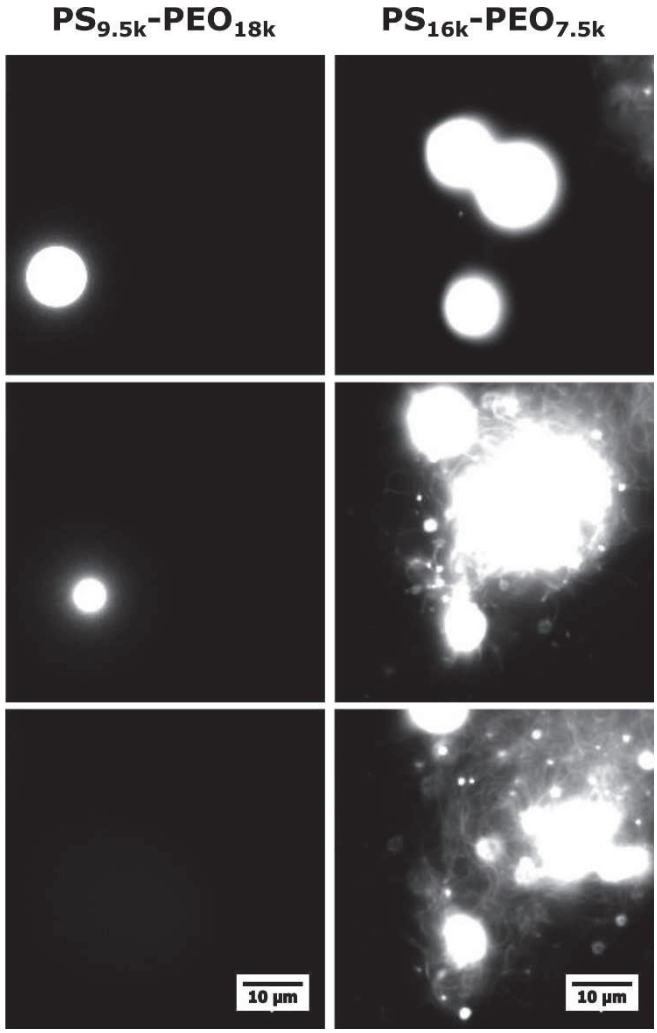

Figure 4 Morphologie des micelles formées à partir des gouttelettes en suspension. Le copolymère plus hydrophile (à gauche) forme des micelles sphériques. Le copolymère plus hydrophobe (à droite) forme des micelles allongées.

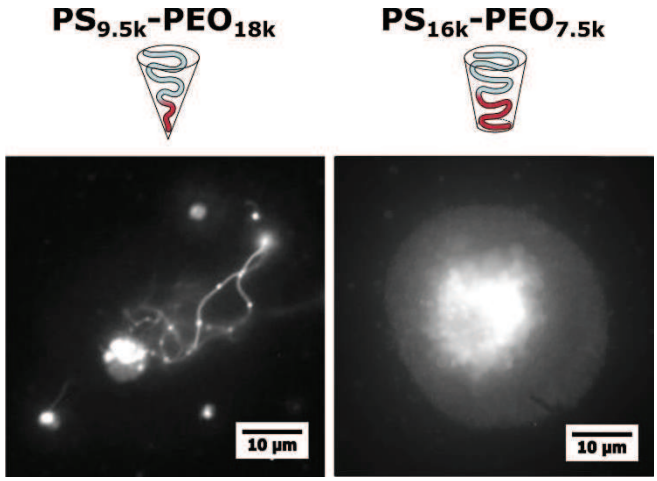

Figure 5 Morphologie des micelles formées à partir de gouttelettes adsorbées sur une surface en verre. Le copolymère plus hydrophile, qui normalement forme des micelles sphériques, forme des micelles allongées. Le copolymère plus hydrophobe, qui normalement doit former des micelles allongées, forme des vésicules.

Ces observations nous ont permis de développer une hypothèse pour expliquer la formation des différentes morphologies. On confirme ainsi qu'une émulsification spontanée des gouttelettes de chloroforme dans l'eau se produit lorsque les micelles sphériques sont formées. Par contre, lorsque les micelles allongées sont formées, l'émulsification spontanée provoque d'abord la formation de gouttelettes d'eau dans le chloroforme. C'est ensuite l'inversion de l'émulsion eau dans chloroforme qui provoque l'expulsion de micelles allongées (Figure 6).

Ce processus peut aussi expliquer l'observation des morphologies complexes, telles que des longues chaînes de vésicules, qui ne peuvent pas être formées par des instabilités interfaciales sans formation préalable d'une émulsion d'eau dans le chloroforme.

Nos résultats apportent un progrès dans la compréhension des mécanismes de formation impliqués dans les procédés d'évaporation de co-solvant et ils expliquent le polymorphisme des nanoparticules préparées de cette manière.

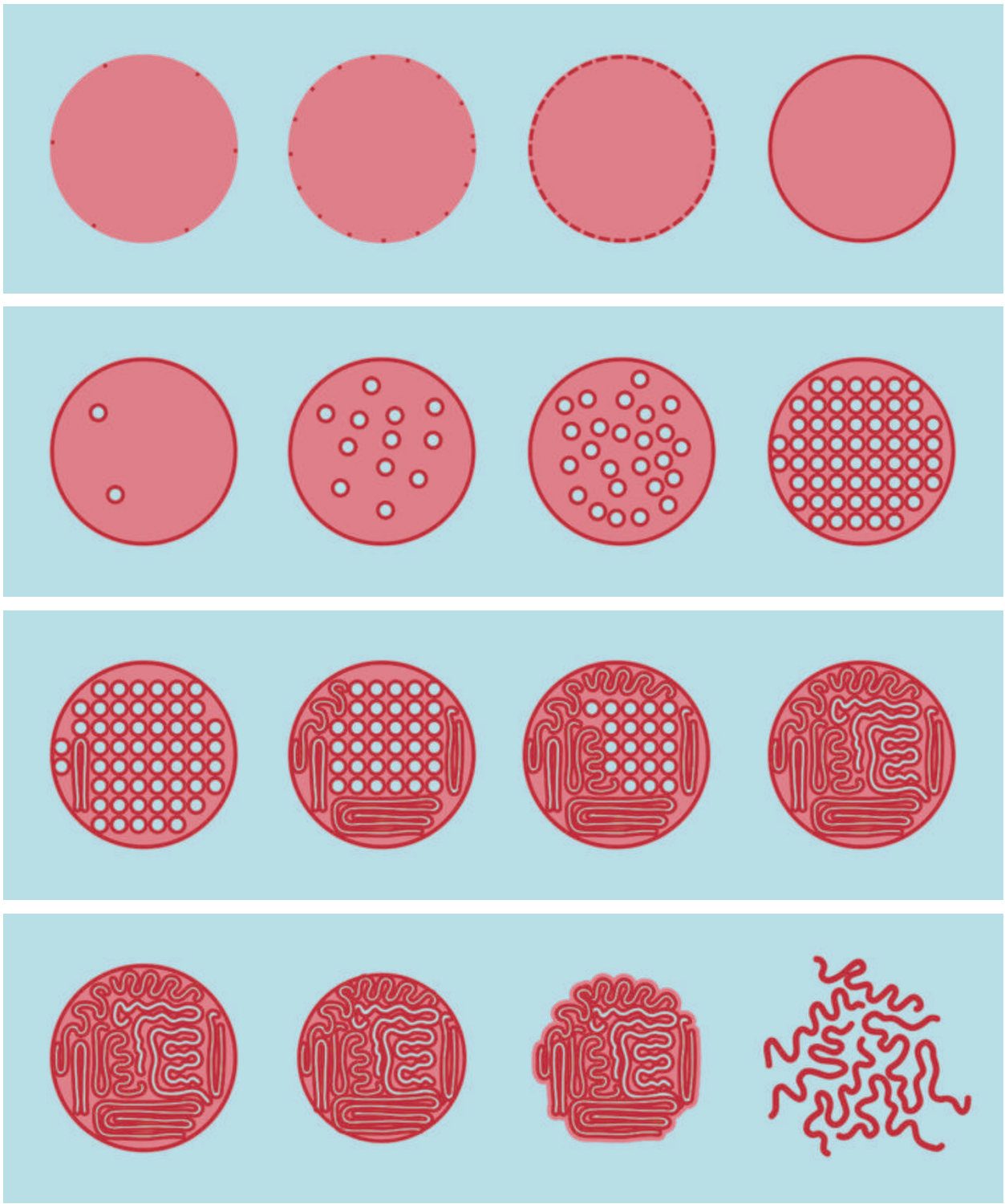

Figure 6 Vue schématique de l'hypothèse de formation des micelles allongées. Le copolymère s'accumule à l'interface entre la gouttelette de chloroforme et l'eau. Quand l'interface est densément peuplée, la création d'interfaces supplémentaires par des émulsions eau dans chloroforme est favorisée. Quand la quantité d'eau dans le chloroforme devient trop grande, il y aura une transition d'une émulsion à une phase éponge. Une évaporation ultérieure du solvant provoquera une inversion d'émulsion et la formation de micelles allongées.

7.3 Nouveau procédé de formation de micelles

Suite aux observations effectuées sur les émulsions, il était clair que l'utilisation d'une émulsion polydisperse comme point de départ pour la formation des nanoparticules ne pouvait pas être une situation idéale, car elle devait conduire à un polymorphisme dans l'échantillon final. Afin d'éviter une telle situation, une nouvelle technique a été développée pour la formation contrôlée de nanoparticules. Ceci a été réalisé par dépôt de la solution mère de copolymère séquencé à l'interface air-eau. Deux conditions expérimentales nouvelles sont ainsi obtenues : une interface chloroforme-air qui permet de régler la vitesse d'évaporation du solvant organique, et une interface de chloroforme et eau unique avec une courbure réglable.

La solution de chloroforme reste à l'interface air-eau grâce à l'équilibre entre les tensions de surface des trois solvants. Le taux d'évaporation du chloroforme a été réglé à l'aide d'une pompe péristaltique reliée à la fiole. En ajustant ce paramètre, il est possible d'obtenir des micelles de différentes morphologies indépendamment du paramètre d'empilement du copolymère utilisé (Figure 7).

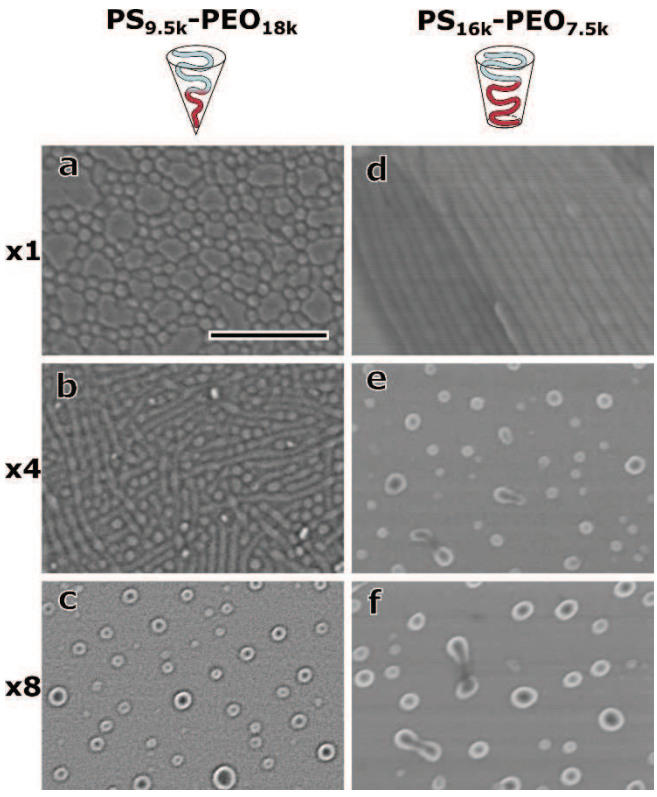

Figure 7 Vue d'ensemble des différentes morphologies obtenues en évaporant le solvant organique plus ou moins vite. A partir de copolymères dont le paramètre d'empilement prédirait des micelles sphériques ou allongées on obtient des micelles allongées ou des vésicules indépendamment du copolymère utilisé.

En outre, l'élimination des contraintes mécaniques intrinsèques à la formation de microémulsions en suspension permet la croissance de nanofils extrêmement longs de plusieurs centaines de micromètres, que l'on peut fonctionnaliser par inclusion de toute espèce soluble dans le chloroforme.

7.4 Module de flexion de micelles allongées

Afin de caractériser davantage les micelles allongées, leur module d'élasticité est déterminé en utilisant une technique originale. Nous déposons les micelles sur des substrats de polydiméthylsiloxane avec des micro-piliers régulièrement espacés. Nous obtenons des dépôts très ordonnés de micelles partiellement suspendues dont le module d'élasticité est caractérisé par des mesures de flexion faites avec un microscope à force atomique. Ce procédé de préparation de l'échantillon est un progrès rationnel par rapport aux techniques usuelles de dépôt de gouttes de solutions de nanofils sur des substrats poreux. L'obtention systématique de nanofils partiellement suspendus permet un degré beaucoup plus élevé de reproductibilité et simplifie l'acquisition de données. Une vue schématique de la technique utilisée est montrée en Figure 8.

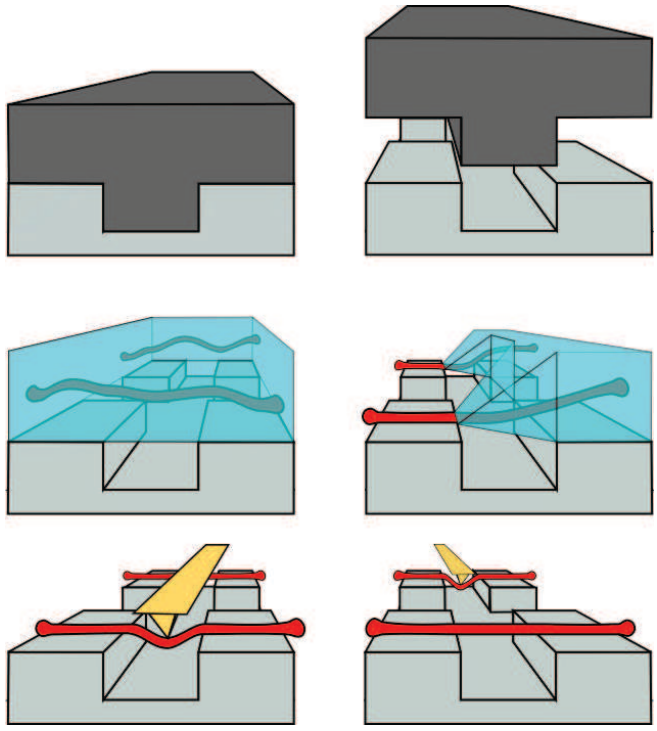

Figure 8 Vue schématique de l'expérience. Des substrats en PDMS sont préparés grâce à des moules en silicium. Les micelles sont déposées en solution sur les substrats et alignées. Avec l'AFM on fait des mesures de flexion.

Des micelles de différents diamètres ont été obtenues par addition d'homopolymère PS qui gonfle leur noyau et leurs modules ont été déterminés par cette méthode. Les modules mesurés montrent

une nette différence entre les micelles de copolymères séquencés purs et les micelles réalisées avec des mélanges homo- et copolymères (Figure 9).

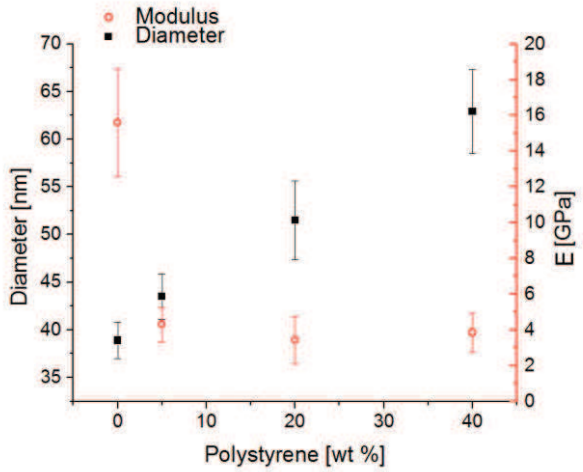

Figure 9 Module élastique et diamètre des micelles en fonction de la concentration en homopolymère dans le noyau.

La calorimétrie différentielle à balayage a révélé la présence de cristallites de POE dans les micelles de copolymères séquencés purs. Ces cristallites disparaissent très vite dès que les micelles sont gonflées avec de l'homopolymère (Figure 10).

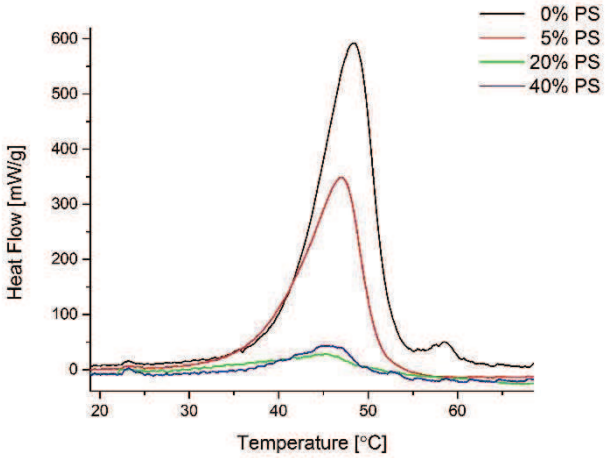

Figure 10 Thermogrammes normalisés des différentes micelles obtenus par calorimétrie différentielle à balayage. Les micelles contenant une plus grande quantité d'homopolymère montrent une décroissance de la contribution cristalline du PEO.

La présence d'une couronne cristalline affecte de deux façons le module des objets allongés. D'une part, la couronne cristalline est plus rigide que son homologue amorphe fournissant directement une rigidité supplémentaire. D'autre part, la cristallinité de la couronne va changer son énergie de surface qui contribue à l'énergie nécessaire pour effectuer la déformation associée à la mesure de rigidité.

7.5 Comportements *in vitro* et *in vivo*

Il a été montré que la morphologie des supports de médicament affecte fortement leur biocinétique *in vivo*. Les particules de forme allongée circulent plus longtemps et montrent une meilleure spécificité tumorale que les particules sphériques. Nos micelles PS-POE ont été utilisées comme système modèle pour étudier les différences de comportement des morphologies allongée et sphérique par rapport à la toxicité *in vitro*, l'absorption cellulaire et la biodistribution *in vivo* chez les souris saines.

Des cellules HeLa ont été utilisées pour étudier la cytotoxicité et l'internalisation des différentes micelles. Cela a été fait par incorporation d'un colorant fluorescent dans le cœur des micelles, et en les incubant avec les cellules pendant des temps variables. L'intensité de fluorescence moyenne par cellule a ensuite été mesurée à partir d'analyses de microscopie confocale. Au contraire des micelles sphériques, l'internalisation des micelles allongées semble se faire sur deux échelles de temps qui dépendent de leur rapport d'aspect.

Pour étudier la biodistribution des micelles dans des souris saines, un radio-isotope (^{111}In) a été incorporé dans le noyau en utilisant des interactions hydrophobes. La biodistribution a été déterminée en utilisant la tomographie d'émission monophotonique (SPECT). On s'attendait à ce que les micelles allongées circulent plus longtemps *in vivo* en raison de leur morphologie mais les résultats obtenus diffèrent de ce scénario. Deux échantillons de micelles sphériques avec un diamètre de 170 et 100 nm ont été testés et comparés avec des micelles allongées d'une longueur moyenne de 600 nm. Les particules ne sont pas éliminées par le système rénal et le radioisotope reste totalement conservé après 48 heures. Les micelles s'accumulent différemment entre la rate et le foie suivant leur taille et leur morphologie, les plus petites micelles sphériques étant les seules à rester en circulation 48 heures après l'injection. Une vue d'ensemble des résultats in vivo est montré en Figure 11.

Ces résultats préliminaires donnent les bases d'une étude future des effets de la morphologie sur la biocinétique des nanovéhicules.

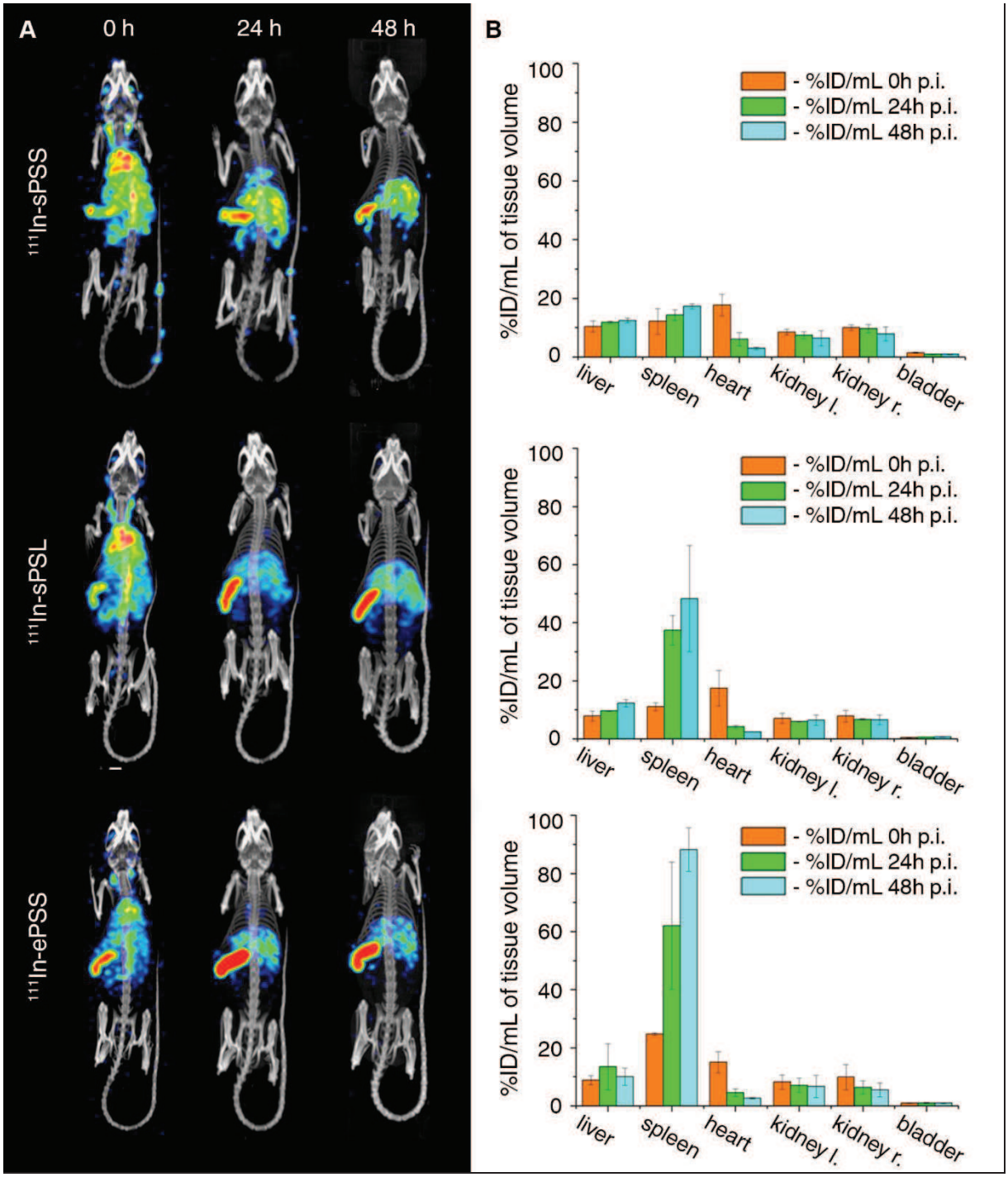

Figure 11 Vue d'ensemble des résultats in vivo. En haut, micelles sphériques de 100 nm de diamètre. Au centre, micelles sphériques de 170 nm de diamètre. En bas, micelles allongées de 90 nm de diamètre et 600 nm de longueur. L'accumulation dans la rate augmente sensiblement avec la taille, celle dans le foie est peu affectée, la circulation dans le sang n'est pas prolongée par la forme allongée des micelles.

7.6 Conclusions

L'objectif de cette thèse, la production et la caractérisation de nanovéhicules de morphologies différentes propres au traitement et au diagnostic par radio-isotopes, a conduit à une meilleure compréhension de la façon dont ces véhicules se forment. Les résultats ont permis de concevoir des méthodes de préparation novatrices qui permettent d'obtenir des échantillons de qualité supérieure à ce qui est actuellement l'état de l'art.

Cela a été fait grâce à des observations phénoménologiques des processus impliqués. L'émulsification spontanée en présence de copolymères amphiphiles a été étudiée sur une interface unique. Nous avons ainsi montré que la formation de nanoparticules sphériques exige une émulsification spontanée du solvant contenant le polymère vers celui qui est libre en polymère, tandis que la formation de micelles allongées nécessite le contraire : les micelles allongées sont formées par l'inversion d'une nano-émulsion d'eau dans du chloroforme.

Cette découverte a permis le développement d'une technique de préparation de micelles qui a deux avantages importants : elle permet d'ajuster la morphologie dominante des agrégats micellaires finaux et elle réduit la proportion de morphologies indésirables. En outre elle conserve la possibilité d'intégrer à volonté un composant hydrophobe dans le coeur hydrophobe des micelles.

Un nouveau procédé pour la préparation d'échantillons pour les essais de flexion de microscopie à force atomique a été développé. Cela a permis de mesurer le module d'élasticité de nanofils préparés avec des mélanges copolymère séquencé/homopolymère de composition variable. Les résultats obtenus montrent que la présence d'homopolymère diminue le module d'élasticité. Ceci est expliqué par la suppression de la cristallisation de la couronne par le gonflement du coeur.

Enfin, les nanoparticules de morphologies sphérique et allongée ont été comparées dans des études *in vivo* réalisées avec des souris saines. Les résultats montrent que leur temps de circulation et leur biodistribution peuvent être modulés par leur taille et leur morphologie, que le radio-isotope n'est pas éliminé par les reins. Ces nanoparticules constituent donc un système modèle flexible et adaptable pour étudier les effets de la taille et de la morphologie sur la circulation et la biodistribution de nanovéhicules.

Les résultats de cette thèse contribuent à une compréhension plus profonde de l'ingénierie et des propriétés mécaniques de particules de morphologie ajustable préparées à partir d'auto-assemblages de copolymères. Les méthodes de préparation développées permettent d'envisager l'obtention de nanovéhicules de morphologie, de taille et de rigidité variables, de surcroît fonctionnalisables par simple incorporation physique sans modification chimique.

7.7 References

[1] H. Maeda, J. Wu, T. Sawa, Y. Matsumura, K. Hori, *J. Control. Release* **2000**, *65*, 271–284.

[2] H. Maeda, *Adv. Enzyme Regul.* **2001**, *41*, 189–207.

[3] J. Fang, H. Nakamura, H. Maeda, *Adv. Drug Deliv. Rev.* **2011**, *63*, 136–151.

[4] S. Jain, F. S. Bates, *Macromolecules* **2004**, *37*, 1511–1523.

[5] T. Nicolai, O. Colombani, C. Chassenieux, *Soft Matter* **2010**, *6*, 3111–3118.

[6] K. Yu, A. Eisenberg, *Macromolecules* **1996**, *29*, 6359–6361.

[7] L. Zhang, K. Yu, a. Eisenberg, *Science (80-.).* **1996**, *272*, 1777–1779.

[8] L. Zhang, A. Eisenberg, *Science* **1995**, *268*, 1728–1731.

[9] J. Zhu, R. C. Hayward, *J. Am. Chem. Soc.* **2008**, *130*, 7496–7502.

[10] J. Zhu, R. C. Hayward, *J. Colloid Interface Sci.* **2012**, *365*, 275–279.

[11] R. Granek, R. C. Ball, M. E. Cates, *J. Phys. II* **1993**, *3*, 829–849.

Laurence JENNINGS

Micelles figées de copolymères séquencés: de l'auto-assemblage hors-équilibre aux comportements in vitro et in vivo

Résumé

L'objectif de cette thèse, la production et la caractérisation de nanovéhicules de morphologies différentes propres au traitement et au diagnostic par radio-isotopes, a conduit à une meilleure compréhension de la façon dont ces véhicules se forment. Les résultats ont permis de concevoir des méthodes de préparation novatrices qui permettent d'obtenir des échantillons de qualité supérieure à ce qui est actuellement l'état de l'art.

Un nouveau procédé pour la préparation d'échantillons pour les essais de flexion de microscopie à force atomique a été développé. Cela a permis de mesurer le module d'élasticité de nanofils préparés avec des mélanges copolymère séquencé/homopolymère de composition variable.

Enfin, les nanoparticules de morphologies sphérique et allongée ont été comparées dans des études in vivo réalisées avec des souris saines. Les résultats montrent que leur temps de circulation et leur biodistribution peuvent être modulés par leur taille et leur morphologie.

Nanovéhicules ; micelles ; morphologie allongée ; émulsification spontanée ; copolymères amphiphiles

Résumé en anglais

This thesis provides an overview of the formation, characterization and testing of micelles of different morphology for biological applications. One major aspect of this thesis is the understanding of the processes which lead to the formation of block copolymer micelles through the emulsion evaporation method. The results obtained made it possible to develop an innovative micelle formation technique which provides samples which are of superior quality to what the current state of the art.

A new method has been developed for the preparation of samples for three point bending tests experiments performed by atomic force microscopy. This has made it possible to determine the elastic modulus of elongated micelles formed with various blends of homopolymers and copolymers.

Finally, the behavior of spherical and elongated micelles was compared in vivo in healthy mice. The results have shown that the micelle size and morphology influences their biodistribution and circulation time.

Spontaneous emulsification ; Nanocarriers ; micelles ; elongated morphology ; amphiphilic block copolymers